ADDIS ABABA UNIVERSITY

ADDIS ABABA INSTITUTE OF TECHNOLOGY

AFRICAN RAILWAY CENTER OF EXCELLENCE

STUDY OF TRAIN OVERLOADING AND ITS IMPACT ON THE TRACTION MOTORS: Case of AA-LRT N-S line

A Thesis in Traction and Train Control

By: Yosef Berhan Jember

Supervisor: Dr.-Ing Getachew Biru

October 19, 2019

Addis Ababa

A Thesis

Submitted in Partial Fulfillment of the Requirements for the Degree of Master of Science in Railway Engineering (Traction and train control)

The undersigned have examined the thesis entitled '**STUDY OF TRAIN OVERLOADING AND ITS IMPACT ON THE TRACTION MOTORS: CASE OF ADDIS ABABA LIGHT RAIL TRANSIT NORTH-SOUTH LINE**' presented by **YOSEF BERHAN JEMBER**, a candidate for the degree of **Master of Science** and hereby certify that it is worthy of acceptance.

Dr.-Ing Getachew Biru		
Advisor	Signature	Date
Internal Examiner	Signature	Date
External Examiner	Signature	Date
Chair person	Signature	Date

UNDERTAKING

I certify that research work titled “STUDY OF TRAIN OVERLOADING AND ITS IMPACT ON THE TRACTION MOTORS: CASE OF ADDIS ABABA LIGHT RAIL TRANSIT NORTH-SOUTH LINE” is my own work. The work has not been presented elsewhere for assessment. Where material has been used from other sources it has been properly acknowledged / referred.

Yosef Berhan

ABSTRACT

The Addis Ababa Light Rail Transit (AA-LRT) trains are being subjected to a high volume of passenger overcrowding especially during peak hours of the day. Due to this, the traction motors are meeting a mechanical load that exceeds the designed overload capacity of the train. As per the vehicle specification of AA-LRT, a single train carries 254 passengers as a normal rating and 317 passengers with seats and standing in an overloaded condition. But, the operational scenario revealed that one train is carrying up to 60 passengers more than the permitted maximum number of passengers in the worst traffic scenario.

The improper passenger load on AA-LRT trains has various impacts on the traction motor while the train moving. Among those problems is that the traction motor is subjected to relatively high RMS current, higher copper loss, lower efficiency, and higher heating.

To evaluate the overloading of the drive, the train dynamics including the resistive forces acting on the traction motor has been modeled and analyzed. The dynamic model of the motor is simulated using MATLAB/Simulink. The North to South site of AA-LRT is selected as a case study due to its irregular track geometry, and frequent operational as well as system problem scenario on the line.

This study has indicated that passenger overcrowding has a considerable impact on the traction motor especially when the train is in acceleration. To quantify that impact, the value of traction motor parameters in improper train overloading is compared with the permissible train overload recommended by the designers. Based on that the following deviations are found due to improper passenger load. RMS current rise of about 36.5%, active power consumption increased by about 69.1%, reactive power consumption increased by about 15.93%, stator copper loss increased by about 32.25%, rotor copper loss increased by about 37.5%, and the efficiency dropped by about 77.7%, reduction in speed of the motor and the train speed. Particularly while carrying improper passenger load, when the train is about to start accelerating, speed reduction of about 56.65% is observed when compared with the speed of the motor when train has permissible passenger load.

The passenger overloading phenomena can also be followed by several operational and system problems like track gauge misalignment, train speed restriction, wear out of wheel flange, wheel-rail slip, passenger discomfort, and train body mechanical overloading.

Index terms: Traction motor, Track gauge, Wheel flange, Wheel rail slip, Traction motor overloading, Stator, Rotor.

ACKNOWLEDGMENTS

If I have not persistent consultation with my supervisor, Dr.-Ing Getachew Biru, it is been difficult to achieve this work. I want to thank AA-LRT staff from the general manager to the engineers for providing the required data as well as their experience based deep knowledge sharing. Particularly I need to express my sincere gratitude to power department staff, and rolling stock department staffs especially Mr. Endalkachew, for their unlimited cooperation. I heartedly appreciate all ARCE staff, for their big effort and facilitation to the research work. Mr. Zelalem Simuye, signaling manager at AA-LRT, deserves to get my recognition for his diligent attempt to help find valuable data for my research. Finally, I must express my love to my family and friends giving me precious thing i.e. Love, so as I stay happy all the time and give full attention to my research.

TABLE OF CONTENTS

LIST OF TABLES

LIST OF FIGURES

LIST OF ACRONYMS

AA-LRT – Addis Ababa Light Rail Transit

AC – Alternating Current

CREC - China Railway Group Limited

DC – Direct current

EMF – Electromotive force

EW – East to West

FDI – Fault Detection and Identification

FDI – Fault Detection and Isolation

HZ - Hertz

IGBT – Insulated Gate Bipolar Transistor

IM- Induction Motor

Km/hr – Kilometer per hour

KV - Kilovolt

Kw - Kilowatt

MCSA – Motor Current Signature Analysis

MV – Medium Voltage

NS – North to South

PI – Proportional Integral

PID – Proportional Integral Derivative

PMSM – Permanent Magnet Synchronous Motor

PPH – Passenger per Hour

PWM – Pulse Width Modulation
RMS – Root mean square
V – Volts
v/f – volts per hertz
vvvf – variable voltage variable frequency
WAP 5/7 – Wide or Broad Gauge AC Electric Passenger, Class 5/7

CHAPTER 1 INTRODUCTION

1.1 Background

Nowadays the demand for transportation is increasing with population growth. Air transport is quicker and comfortable, but particularly in developing countries, it is costly. While car transportation has lower passenger carrying capacity, and it relatively takes an extensive amount of travel time. So, with the advancement of electric vehicle technologies, electric railway transportation becomes preferably used to optimize both passenger carrying capacity and trip time. This kind of transportation is also pollution-free because of using clean energy.

There exists a different type of electric railway system like AC/DC and based on different voltage level classification. In urban areas, metros and modern tram using the DC traction power system are becoming popular. Metros and trams can be supplied DC traction power of different catenary voltage levels such as 750V and 1500V DC. This catenary feeds power to the trams via the pantograph structure to the traction motors built-in inside the train coupled with gearbox and wheel axle. The traction motors can be different in kind. DC series motors, DC shunt motors, compound motors, synchronous induction motors, asynchronous induction motors, and brushless DC motors can be used for electric propulsion purpose [1][2].

When compared to diesel engines, electric motors are rugged, and less loss, but there also exist various internal problems in electric motor operation for traction application. Traction motor overloading is one of the problems that can occur when the train is supplied power. The major cause for traction motor overloading is when the number of passengers onboard is exceeding the maximum designed capacity of a passenger train. Mainly in track geometrical structures with gradient, and areas having sharp curvatures, passenger overcrowding might cause a more severe effect on the operation and health of traction motor [3].

The main electrical loads in the traction power system are traction motors. There is also auxiliary equipment inside the train like door control system, lightings, air-conditioning

system, and cab controlling systems. Auxiliary systems are consuming a small amount of energy when compared to traction motors. Overloading conditions in traction motors can disturb the normal operation of the overall traction power network.

Factors contributing to traction motor overloading can be analyzed from the designed parameters of forces opposing train movement. The traction motors designed to produce a torque value that can carry and rotate the total mass of the train body with onboard passengers.

Wheel to rail friction and aerodynamic drag are the main resistive forces opposing train forward movement, by traction effort applied through motor inside. Force due to gravitation attraction, and centrifugal forces are additional resistive forces when the train is moving up a sloppy track, and on a curved track path respectively. There are also others like coupling force that needs to be considered when a transit operator is shunting two or more trains to work together [4].

Traction motor overloading mostly happens in sloppy areas of the track. At tracks with gradient, there is always a set of values that specify total axle load with the respective speed of travel to maximize the tractive effort at low friction and aerodynamic drag forces.

AA-LRT is an Electrified light rail transit (750 DC voltage overhead catenary system). It is inaugurated in September 2015. The case chosen to be studied in this paper is north to the south line of Addis Ababa Light Rail Transit (AA-LRT). AA-LRT has;

- ✓ Total length of **34.25 km** (North-South line 16.9 km and East-West line **17.35 km**).
- ✓ Two lines (i.e. North-South and East-West lines) use a common track of about **2.7km**.
- ✓ Standard Gauge (**1.435 meters**) and double track for the whole route.
- ✓ A capacity of **80,000 PPH** (Passenger/hr.) (Addis Ababa Light Rail Transit (AA-LRT) Project).

Recently collected data by the author revealed that AA-LRT (Addis Ababa Light Rail Transit) passenger trains mostly carry about 60 passengers more than the designed overload number of passengers in the worst traffic scenario. This paper is going to study

the impacts of passenger overcrowding/traction system overloading in AA-LRT tram's traction motor.

1.2 Statement of the problem

Addis Ababa Light Rail Transit (AA-LRT) is a project under Ethiopian Railways Corporation to minimize the transportation problem at the highly populated Ethiopian capital Addis Ababa. AA-LRT is a fully electrified urban railway system erected from North to South of Addis Ababa, and from East to West of Addis Ababa. It is using the 750V DC catenary system, but due to several reasons, AA-LRT trains are subjected to passenger overflow at most of its service hours every day. Since the trains that are actively working on the line are not proportional to the passengers in need of service, trains working now are over-utilized with no control of train safety. As per its design, one car of a train is rated to carry 254 passengers, and 317 passengers if overloaded [5]. Now practically one train is serving for 377 passengers especially at peak hours of the day. These phenomena are causing different operational problems like train door failure, speed restriction, track misalignment and internal problems on the traction motor. This paper is going to study and analyse the impacts of train overloading/passenger overflow on the asynchronous induction motor used for traction purposes by AA-LRT trains. Emphasis will explicitly be given for irregular areas on the track such as slopes and curves that might cause a considerable burden on the traction motor. Since track inconsistency and train stop is observed especially in the North to South line of AA-LRT, then this site is selected as a case to be studied in this paper.

For instance, on the North to South line from NS22 to around NS23 stations, from around Abnet to Sebategna the track geometry is designed with an average slope of 5.5% as per its design document. Since it is put on the asynchronous motor design that the maximum capacity of one train under the worst scenario is 317 people per car, but at peak times it is found that the train is carrying more than its maximum capacity of passengers. Keeping this figure in mind, particularly train movement around irregular tracks is sensitive to the operation of the traction motors. There is a design speed for the train when climbing slope, but this passenger overcrowding is not considered while determining the allowable train speed to safely pass over the track with gradient as well as curves.

Since train load data was collected in different ways so that an approximate number of passengers exceeding in a single train is found. Keeping all track topology design of AA-LRT to be correct, these non-estimated number of passengers correlated with the irregular track areas can be taken as uncalculated risk occurring in traction motors, trains as well as track parts.

1.3 Aim and scope of the study

1.3.1 Objective of the thesis

General objective

This thesis aims to study the various impacts of train overloading/passenger overcrowding on the traction motors when the train is traveling along North to South line of Addis Ababa Light Rail Transit.

Specific objectives

- ✓ Collect and analyze relevant load data of the train on the specified railway line.
- ✓ Develop a model of the train dynamics to calculate all the forces contributing to the movement of the train.
- ✓ Develop dynamic modeling of the traction motor.
- ✓ Analyze the effects of the overload on the induction motors.
- ✓ Simulate the traction drive system on MATLAB to assess the affected variables due to traction motor overloading.
- ✓ Draw relevant conclusions, and recommendations which can be of practical relevance to improve the performance of the railway network.

1.3.2 Scope of the Study and Limitations

Determination of train movement resistive forces with a tractive effort of the motor will be analyzed for AA-LRT North to south line. Analysis of the motor output variables particularly current, electromagnetic torque, and rotor speed alteration due to train overloading are performed from the dynamic model of the traction motor with the help of MATLAB simulation software. Three things can be raised under the limitations of this study. The first thing is the lack of every individual mechanical component-wise analysis of the effects of overloading. It is not done because of the unavailability of required data

from the AA-LRT department of rolling stock. The second limitation is that due to the matter of manufacturers' business the traction motor is a black box for the AA-LRT engineers other than some basic information provided by the manufacturer in documents. When traction motor is faulted, nobody knows why and what happens to it, it will just be packed and send back to the manufacturer for maintenance. This becomes a problem for getting the actual working conditions as well as fault type and another significant scenario as input for this research. A detailed document describing the whole nature of the motor is also not found with AA-LRT Company. Finally, the unavailability of free railway specific software can be taken as a limiting factor in this research.

1.4 Research methodology

The first step was problem identification. In September 2018 as part of the fulfillment of 'professional practice' course, the author was an internee at Addis Ababa Light Rail Transit (AA-LRT), Kality depot, for about one month. When having a visit on the various sections at AA-LRT, the author identified a number of technical problems happening in the operation. Among those problems the author gives priority to work on the one which does not get attention, but most problematic. That problem was overcrowding of passengers inside a train. Although this passenger overloading can cause a various problem, the impact of the overcrowding on the traction motor of the train has selected to be studied by the author regarding his affiliation. The next step was reading various literatures in relation with the stated problem area. Literatures related to passenger overloading effect, which particularly performed on AA-LRT case as well as any literature on induction motor overloading with respective impacts were researched. Literatures used for performing the research in each step were used till the end of thesis work.

The required information about the traction motor used by AA-LRT trains had gathered from the rolling stock department. The practical figure about the volume of passengers using the train service every hour of the day on North to South line has collected in various methods. Primary data are taken from a trainload sensor, three secondary data from the ticketing department, and two authors performing research on the area, used for comparison.

From the railway infrastructure department, the design data for the North to South line of AA-LRT has been taken to get exact information about the geometrical structure of North to South line of AA-LRT. Analysis of the data found from AA-LRT has been performed. Mathematical modeling of the train when moving along the track has been done with separate analysis on various track topologies, including a track with gradient and sloppy areas. Tractive effort is calculated using the train resistive force formula with the help of MATLAB/Simulink blocks. Formulas for resistive forces on train movement as air drag, friction, and forces due to gravitational attraction while the train is moving on sloppy tracks, plus centrifugal forces on curved track area are determined for computation. Then load torque per motored axle has been found while knowing the gear ratio.

For the asynchronous induction motor used as traction motor in AA-LRT trains, its torque-speed characteristics have been investigated. From the dynamic model equations of three-phase induction motor, the equations used for determining motor electrical quantities like current, voltage, power, torque and speed are deployed to observe the performance of traction motor when overloaded. Since the traction motor of AA-LRT train is vvvf controlled, a vvvf controller is modeled and its respective parameters are determined. The inverter feeding power to the motor is modeled using IGBT switches as found in the traction control unit of AALRT trams. For switching pattern control of IGBT switches, Sine triangular PWM is modeled because it is been mentioned in many kinds of literature that sine triangular PWM is oftentimes used with vvvf control of motors.

All the above components of the traction drive are modeled on MATLAB/Simulink software. And from the simulation result, the behavior of the selected motor parameters has seen to compare the result of normal traction load with overloading situation in terms of RMS current, the performance of traction motor, power consumption, copper loss in the motor, and efficiency of the traction motor.

1.4.1 Thesis Flow Chart

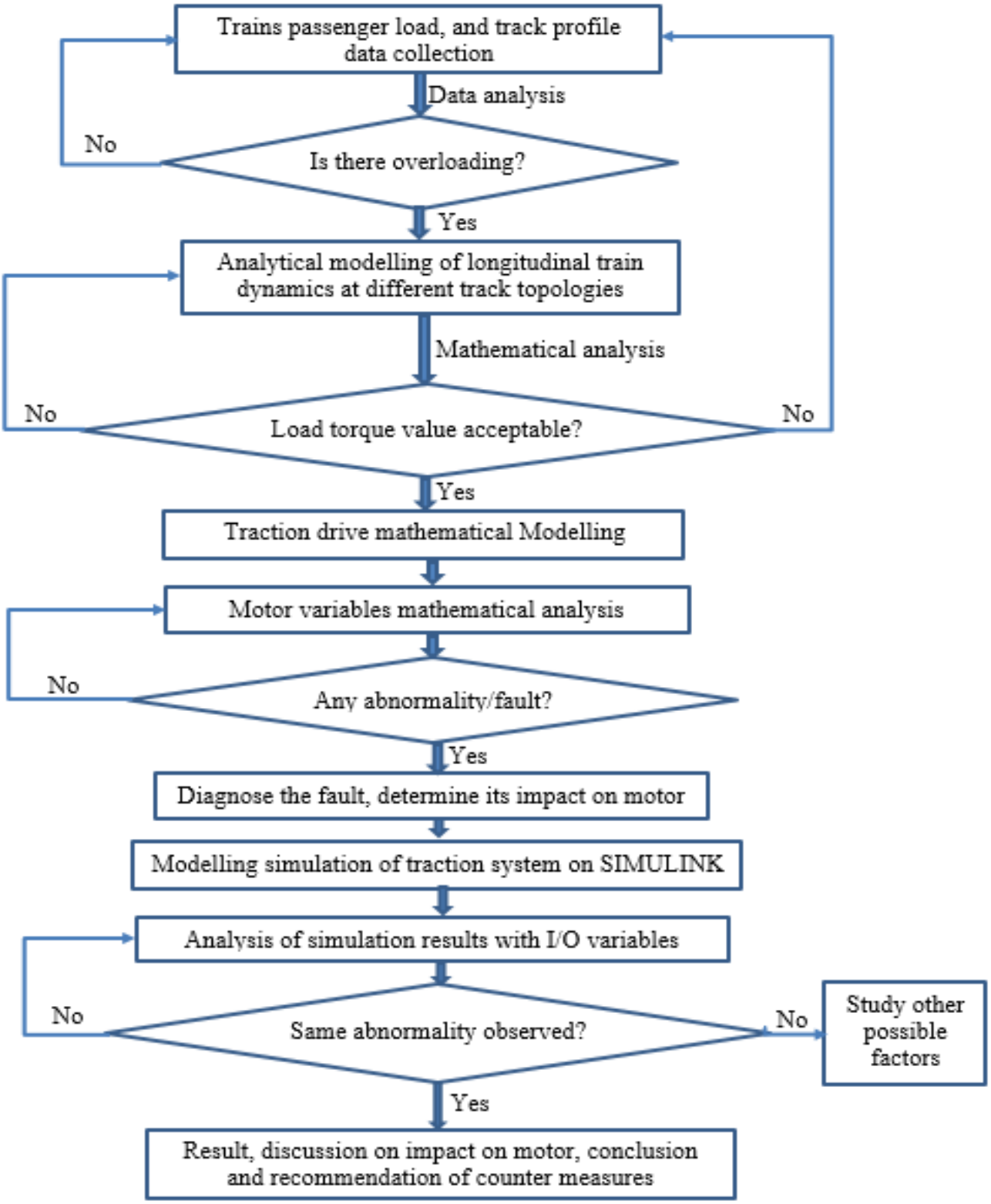

Figure 1-1 Thesis flowchart

1.5 Structure of the thesis

This thesis work consisted of five chapters. Chapter-One Introduction, Chapter-Two Theoretical background and Literature Review, Chapter-Three Data analysis and systems modelling, Chapter-Four Result analysis, and Discussion, and Chapter-Five Conclusion and Recommendation.

In the introduction part, the evolution and the current overall trends in electric railway systems have been assessed. The type of electric railway systems, comparison between electric motors when used for traction purposes, and other similar issues are discussed. AA-LRT is also well introduced in this section. Faults concerning operating with electrical motors are discussed in the introduction. Particularly the passenger overcrowding problem is picked and described in the point of view of motor overloading problem.

The second chapter, Theoretical background and Literature Review, was done starting from selecting literature in the criteria of their relevance to this research, based on the journal reputability as well as the credential of authors. This part has a compressed idea of many kinds of literature done in the area of longitudinal train dynamics development and analysis, induction motor modeling, and type of faults with their techniques of detection, isolation, and diagnosis.

Chapter Three is comprised of data analysis, modeling of train dynamics with analysis of train's forward movement resistive forces, induction motor dynamic modeling, modeling of traction converter and VVVF controller as well as simulation design of the traction drive has provided.

Chapters Four has the results that have found from the dynamic model of the traction drive when the train is traveling in North to south track areas of AA-LRT with various passenger loading scenarios. A brief discussion has provided to express the result. Possible remedies are recommended to eradicate passenger overloading on the North to South line of AA-LRT, as well as for minimizing its impact on the traction motor.

The Fifth chapter has a conclusion about the observed problems with the respective recommendation for future researchers.

CHAPTER 2 THEORETICAL BACKGROUND AND LITERATURE REVIEW

2.1 Introduction

In this section, a theoretical background of AA-LRT trams traction drive arrangement is provided. Description of main parts of the train regarding its main traction parts is included. Various scientific papers and books which have been written by authors of direct relevance and related affiliation to railway traction system, as well as electric drive technology, are reviewed. Particularly those research works which are focusing on asynchronous induction motor conditions, with mechanical overload problems and their respective responses in the change of current, electromagnetic torque and rotor speed, in turn, the consequences on the motor, are seen in different perspectives. To analyze the impact of the excess number of passengers on the train, it is known that the longitudinal dynamics of the train should be computed. For that matter, some literature related to the development of longitudinal train dynamics is revised. Impact of track trajectory i.e. Curves and gradients, on traction motors are assessed with some references. Indeed paper works related to analytical and software modeling of induction motor are included in this part.

2.2 Theoretical background

AA-LRT trams traction drive arrangement

AA-LRT project uses 6-axle double-articulated 70% low-floor Light Rail tramcar. Inside these trams, four traction motors are getting variable voltage variable frequency power supply from a two-step IGBT inverter. One motor drives one axle unit, so the two motor cars (Mc's) have two axles and two motors each. The trailer car (T) in the mid between the front and rear cars has two axles but no motor for either of the axles.

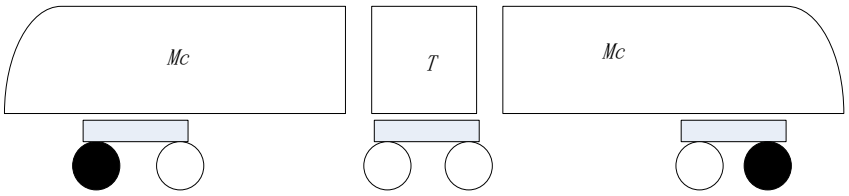

Figure 2-1 A Side view sketch of AA-LRT tram cars [5]

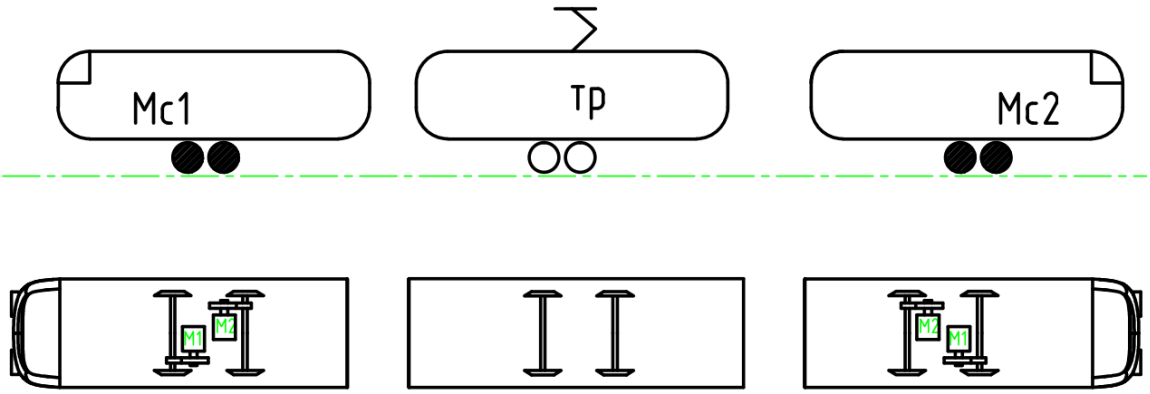

Figure 2-2 The Pantograph configuration and the motor configuration [6]

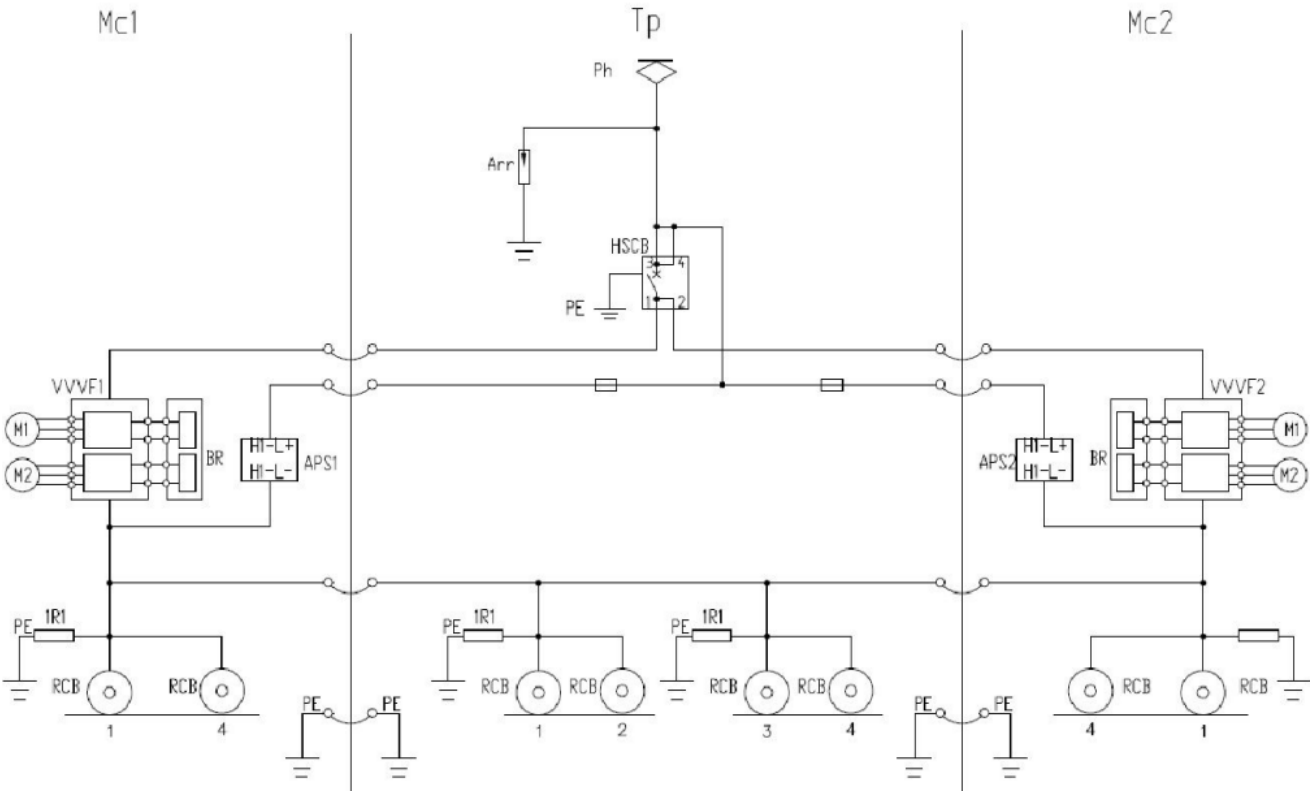

Figure 2-3 Schematic diagram showing circuit of traction feeding arrangement [5]

Since the tram can be driven in both side of Mc's, the motors can be controlled to be rotated clockwise and anti-clockwise direction.

Traction power supply

The train gets power via the overhead catenary system. Rated voltage of DC 750V is provided to the train from the catenary via the pantograph. A voltage variation range of 500V～900V is tolerable. The trailer is equipped with one pantograph to provide rated DC750V high voltage power from the catenary to the high-voltage equipment in vehicles. To ensure the safety of high-voltage system equipment in vehicles, the train is equipped with the surge absorbing high-pressure protection device (arrester) to protect the circuit equipment of high-voltage power supply by train.

Traction converter

Traction converter mainly consists of line contactor, IGBT inverter, and chopper power unit, logic control unit and filter capacitor. The role of it is to convert DC voltage into 3-phase AC voltage with variable voltage and variable frequency, which will drive the traction motor to put vehicles into operation (motoring), and will convert the 3-phase AC voltage of traction motors into DC voltage to be fed back to the catenary (regenerative braking). Provision should be taken that traction converter shall be able to withstand sudden variation to the input voltage and should be protected against input overvoltage, input under-voltage, output over-voltage, overheat failure, output overload, and overcurrent, open phase and short circuit.

Traction motor

Traction motor of AA-LRT trains is v/f controlled three-phase squirrel cage asynchronous induction motor and cooled by self-ventilation.

Table 2-1 Main performance parameters of traction motor

Number of Phases	3	Rated power	130Kw
Number of poles	6	Rated Voltage	AC 3*500V
Rs	0.01931ohm	Rated Current	210A
Ls	0.000183 H	Rated Frequency	71Hz
Rr’	0.009821 ohm	Rated rotational speed	1800 r/min
Lr’	0.000183 H	Maximum rotational speed	4377 r/min
Lm	0.00989 H		

2.3 Review of Literatures

Ehetaferaw [7] has done a research to investigate the effect of passenger overcrowding on the AA-LRT train. An analysis of the effects of overloading on under-frame steel structure are performed.

In [8], causes, effects, and magnitude of passenger overcrowding in AALRT lines have been comprehensively assessed. The author also shows passenger overcrowding and its effect on the platform area of the stations.

In [9], the author provides a broad explanation about electrical and electronic components of rolling stock. Traction systems are classified as concentrated and distributed kind based on the power distribution via each car of the train. The distributed type has many motors, whereas the concentrated only consists of few motors inside it. The distributed kind has the advantage of high hauling power, while the concentrated has better passenger comfort and ease of maintenance. DC electric motors were deployed for the propulsion of trains in the early times but later replaced by induction drives and synchronous motors having better performance as well as operational advantages over DC motors. Induction drives are comprised of asynchronous motors fed from power electronic converters. It also becomes a usual practice to feed two induction drives with a single inverter for balancing the

rotational speed of motors while wheel diameter difference exists. For traction purposes, PMSM (Permanent Magnet Synchronous Motors) is indicated to have low iron loss than IM (Induction Motor) drives.

In [10], medium voltage (MV) drive technology is assessed. The various difficulties facing on the deployment of MV drives are explained. For some of these problems possible countermeasures are indicated as well, research areas are identified. It is said that avoiding torsional vibration on the rotor, fault detection capability, and condition monitoring is among the requirements that MV drive needs to fulfill. Torsional vibration problem in MV drive happens due to large inertia of the motor and the mechanical load suspended on the rotor. An extra amount of torsional vibration while there is resonance, leads to high twisting torque in turn breakage of shafts and couplings will be the result. Pulse Width Modulation control with harmonic reduction is stated as a solution to withstand this problem. This paper outlined that MV's need to cope with appropriate fault detection and fault diagnosis as well as condition monitoring methods to avoid unnecessary halt followed by both economic loss and operational problem. Observer-based fault analysis of mechanical fault detection is listed as an instance of sensorless fault detection. It is deduced that the investigation of the quality of current and voltage waveforms at the input and output side can be a significant factor when analyzing MV drives.

Premature detection, diagnosis and condition monitoring of mechanical faults has been raised in [11] as a critical issue for the safety of induction motors. Since excessive load torque is one of the causes of mechanical failures like bearing faults, and eccentricity problems, mechanical faults are the most frequent failures in IM's. Several fault detection and analysis techniques such as mechanical vibration analysis and motor current signature analysis are brought in this paper. But wavelet analysis is said to be effective than MCSA (Motor Current Signature Analysis) for time-varying operating conditions. The problem with mechanical vibration fault analysis is its disability to detect early phenomena that might be below the noise threshold or hidden. Of those methods of fault detection and analysis are proposed to be used as per the context of the problem.

A review of many research works in the area of electrical motor fault detection with condition monitoring technique, including the author’s articulation is performed in [12]. Due emphasis is given for the incipient type of faults to be detected early, otherwise, it

may gradually cause severe impact followed by undesirable interruption of operation as well as an economic crisis. The main kind of faults happening in electrical machines are categorized into about seven groups. Among these faults, bearing fault, stator or armature faults, broken rotor bar, and end-ring faults, eccentricity related faults are the most prevalent ones that needs consideration. Increased torque pulsations, decreased average torque, increased losses, and reduction in efficiency, and excessive heating is some of the symptoms produced when the said faults are happening on the motor. Among the fault diagnosis methods, MCSA and Model-based detection are extensively used. Eccentricity problems and internal stress cause bearing faults. High stator core or winding temperature results in the armature of stator insulation failure. Broken rotor bar and end-ring faults can occur due to dynamic stresses arising from shaft torques, centrifugal forces, and cyclic stresses. Bent rotor shaft, bearing wear or misalignment, mechanical resonance at critical speed and the like factors causes eccentricity related faults. Eccentricity related faults can be identified by deploying a model-based approach to fault detection and diagnosis.

In [13], the numerous fault diagnosis techniques particularly model-based fault diagnosis, and Signal based fault diagnosis are distinguished. The authors divided fault diagnosis into a three-step process i.e. Fault detection, Fault isolation, and fault identification. "Generally, fault diagnosis methods can be categorized into Model-based methods, Signal-based methods, Knowledge-based methods, Hybrid methods (the combination method of at least two methods), and active fault diagnosis methods." The authors reviewed these fault detection methods by two parts (two papers). In this part one, model-based, and signal-based fault diagnosis methods are analyzed. The rest are investigated in the second part. Model-based fault diagnosis does a comparison value and behavior of output parameters between the real working system and the model of the system. Based on types of models used, model-based fault diagnosis is classified into four, namely "Deterministic fault diagnosis, stochastic fault diagnosis, Fault diagnosis for discrete events and hybrid systems, and fault diagnosis for networked and distributed systems." A measured/actual faulted parameter signal is taken to be analyzed in the signal-based method of fault diagnosis. "Signal based fault diagnosis methods have a wide application in real-time monitoring and diagnosis for induction motors power converters, and mechanical components in a system." Signal based fault diagnostics methods are further classified into three: Time-domain signal-based approach, frequency-domain signal-based approach, and

time-frequency signal based methods. A time-domain signal based method is the analysis of time-domain fault behaviors in a continuously varying system. Spectral analysis of the faulted signals to identify characteristics of the fault is what is called frequency domain signal based method of fault diagnosis. The time-frequency signal based method is used if the signal could be analyzed neither in time nor in the frequency domain. What happens in situations like when a motor is unloaded or unbalanced voltage supply, in varying loads, or unstable load torque, then the signals become difficult to be analyzed using only one of the said techniques of fault diagnosis.

The total stress and fatigue life of an electric motor rotor are determined to a large extent by centrifugal forces, tangential forces caused by torque, and the temperature gradient along with the rotor. A rapid increase in heat as a result of sudden variation in the electric current and the differing thermo-mechanical characteristics of the components leads to non-uniform stress in the assembly. A finite element method was utilized to solve the coupled thermal and mechanical problems. The mechanical durability of the rotor could be increased by sacrificing some of the electromagnetic performance. Therefore, it was emphasized that a comprehensive thermo-mechanical analysis is essential for the optimal design [14].

In [15], the longitudinal dynamics of a light rail vehicle was modeled and simulated in MATLAB-Simulink. The traction system consists of two parallel motor groups, each of which is composed of two separately-excited motors connected in series. The first simulation scenario represents how the traction system works in acceleration and braking modes for a given speed change profile. Within this scenario, the time-dependent responses of the motor armature and excitation currents, fluxes, motor traction moment, adhesion, resistance forces, and acceleration are evaluated, and the constant torque, field attenuation, operation zones, and vehicle traction force curve are described.

In [16], A description the various factors that resist the movement of the train is done. Methods like reducing the train mass, minimizing the aerodynamic drag by lowering maximum operational speed, and efficient driving strategy is mentioned as major solutions for maximization of the tractive effort.

An attempt was made to analyze the longitudinal dynamic model of the passenger train for the attainment of better vehicle ride quality and comfort. The modeling has been done in two phases: In the first phase, a mathematical model was analyzed which was further used for the evaluation of the longitudinal dynamic forces that appear on the buffer, draw gear and fastening devices during the braking process. The second phase includes simulation of longitudinal train dynamics considering the effects of forces like rolling resistance, brake force, coupler force and the gravitational force acting externally on a vehicle for better ride quality and comfort in comparison to the traction effort on WAP-5 and WAP-7 Indian locomotives [17].

Ohm [18] has comprehensively developed dynamic model equations for induction motors, by using a various reference frame.

A co-simulation method that combines longitudinal train simulation, locomotive traction control, and locomotive vehicle dynamics is presented. The modeling of other forces, braking propulsion resistance, curve drag, and grade forces are also discussed. As extensions to conventional longitudinal train dynamics, lateral forces and coupler impacts are examined in regards to interaction with wagon lateral and vertical dynamics. Various applications of longitudinal train dynamics are then presented. As an alternative to the tradition single wagon mass approach to longitudinal train dynamics, an example incorporating fully detailed wagon dynamics is presented for a crash analysis problem. Further applications of starting traction, air braking, distributed power, energy analysis, and tippler operation are also presented in [19].

CHAPTER 3 DATA ANALYSIS, AND SYSTEMS MODELLING

3.1 Prevalence of passenger overloading in AA-LRT

For predicting passenger overloading, the author has gathered primary source data and compare that data with other three sources of secondary data. The primary source is from the train's load sensor, the author has traveled round trips inside the cabin room, and recorded the instantaneous total train load variation reading from the cab display, for different hours of the day to about three days. The worst load scenario has been observed for a particular irregular track area, as well its variation with speed of train has been perceived. From that, about 7.5 tons has found in excess than the maximum possible carrying capacity of the train. i.e. about an average of 125 passengers in excess was boarding than the rated capacity of the train.

The other data is two months (1 December 2018 to 31 January 2019) passenger flow recording of AALRT Company for the North to South line, with daily passenger, trips and number of trains report. It has an explicit report of a flat hour and peak hour number of passengers, number of trips, number of trains (single or coupled), in an excel format, and indicates an average of about 368 passengers residing inside a single train (see appendix A). According to [7], after taking a count of the number of passengers in person, as well by taking a count from the CCTV camera of AALRT platform area, it is found that 408 passengers are using one train in the worst traffic scenario. In [8], the author conducted counting of the number of passengers in one train and revealed that the train is overloaded by 38.46% than its rated capacity, meaning 352 passengers are using one train at worst traffic cases of AALRT lines.

Keeping in mind that all the above data about passenger traffic of AALRT line have their shortcoming in terms of precision, the author decided to use the average of all the four sources of several passengers overloading. i.e. $\frac{379+368+408+352}{4} = 377$ Passengers,

Hence the above average value, 123 passengers above the rated capacity of the train, or about 60 passengers exceeding the overloaded capacity of the train is taken to conduct this research.

The Tables 3.1 and 3.2 shows the designed capacity of AA-LRT trains.

Table 3-1 Seating capacity of AALRT vehicles [5]

Number of passengers (persons)	Seated	Standing	Total
Seats	65	0	65
Seating capacity (standing: 6 persons/m^2)	65	189	254
Overload capacity (standing: 8 persons/m^2)	65	252	317

Table 3-2 Vehicle weight of AALRT train [5]

Loads	Car body weight	Passenger weight	Total weight
Empty vehicle (t)	44	0	44
Seating capacity (t)	44	15.24	59.24
Overload capacity (t)	44	19.02	63.02
Axle load		≤11（1+3%）t	

Note: Average weight of each passenger is taken 60kg

On the other hand, for exclusive analysis and study of the impact of track irregularity in correlation with the overloading, considerable track areas having a relatively higher magnitude of gradient and lower radius of curvature are identified and sampled by the author. The AUTOCAD design document is used for determining the radius of curvature, and the degree of the gradient. Besides the analysis of the overloading effect on level areas, investigation of the factor of the irregular track is mandatory, since often times an extra burden is imposed on traction motor due to slope and curves.

3.1.1 Curves and Gradients in AA-LRT North to South line

Gradient in North to South line

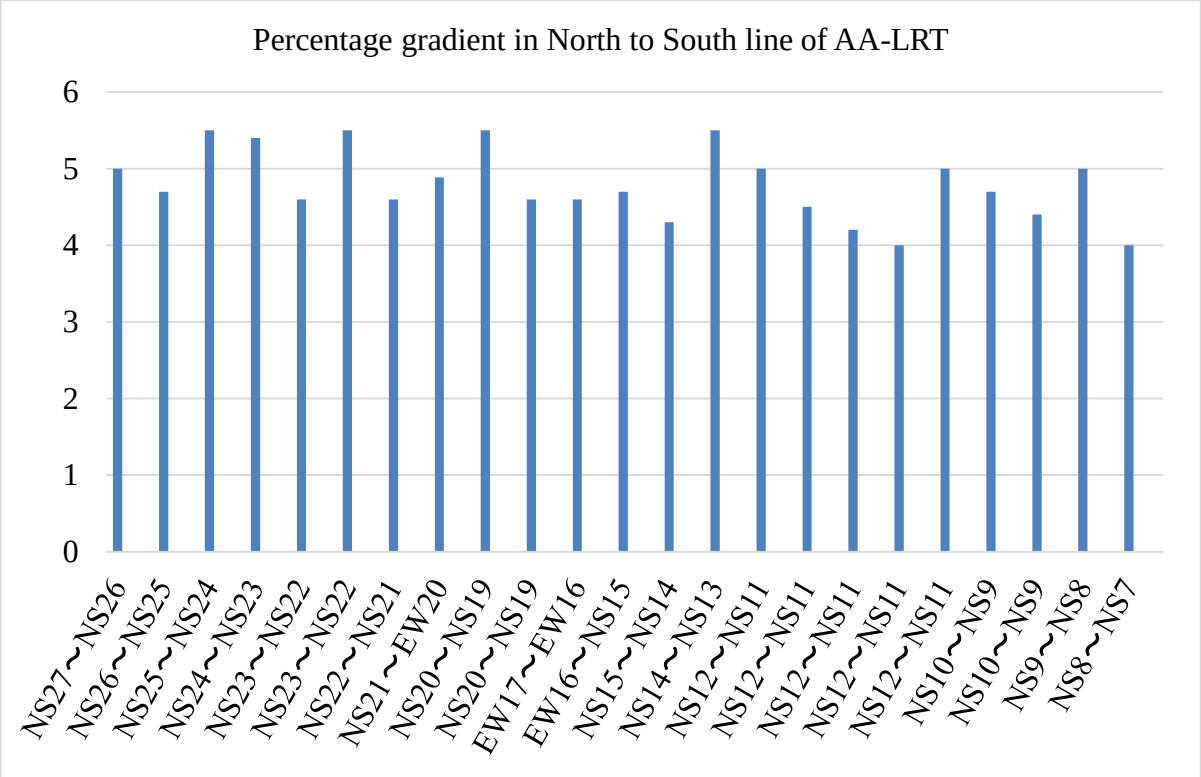

Figure 3-1 Gradient in North to South line of AA-LRT

The above chart shows a gradient of the North to South line of AA-LRT. Track areas with relatively higher percentage of gradient with longer distance are selected to this study. i.e NS21 (Darmar) to NS22 (Abnet), and NS22 (Abnet) to NS23 (Sebategna).

Curved paths in North-South line of AA-LRT

- ✓ Between NS-15 (Meshwalekia) and EW-16 (Stadium), Radius of curvature (R inner track = 50 m, R outer track =55 m)
- ✓ Between EW-20 (St. Lideda) and NS -21(Darmar), Radius of curvature (R inner track = 50 , R outer track = 55)
- ✓ Between NS- 23(Sebategna) and NS -24(Autobus Tera), Radius of curvature (R inner track = 50 , R outer track = 55)
- ✓ Between NS-26(Atikilit Tera) and NS – 27(Menelik Square), Radius of curvature (R inner track = 65 , R outer track = 70)

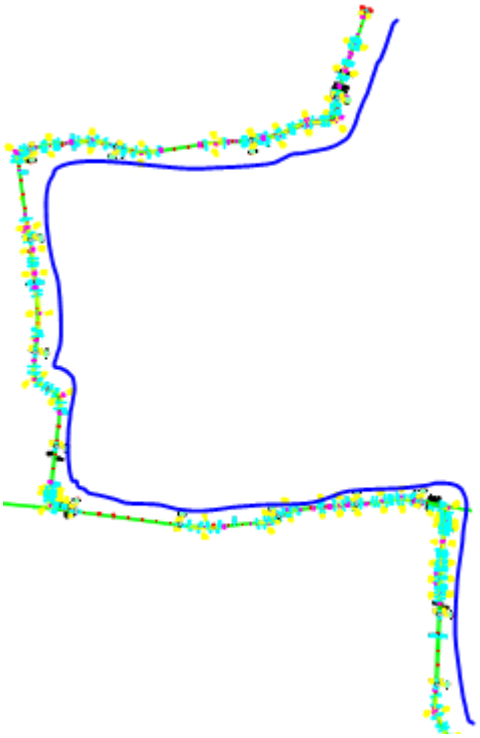

Figure 3-2 AutoCAD design of AA-LRT N-S line curved areas

For simulation and detail study of the effect of a curved track on this research, two curved paths in AA-LRT are sampled based on the location of the curves, the radius of curvature, and availability of gradient with the curve. Hence NS15 (Meshwalekia) to EW16 (Stadium), and NS23 (Sebategna) to NS24 (Autobus Tera) interstation track areas are selected.

The track areas NS11 to NS12 have been taken as a sample to study the overloading condition of the traction motor on level track while the train has improper passenger load.

3.2 Systems Modelling

This part provides analytical modeling of the various systems including:

- ✓ Modeling of longitudinal train dynamics
- ✓ Traction motor modeling
- ✓ Modeling of v/f speed controller
- ✓ Modeling of traction converter
- ✓ Overall model

The modeling is done and written here in an order that is convenient for finding variables and substituting in the next modeling process.

3.2.1 Longitudinal Train Dynamics Model

3.2.1.1 Train running resistance

The resistance force opposing train movement i.e. F is the summation of all individual forces opposed to train running direction, and those forces are mentioned as follows:

F_r - Rolling resistance

F_c - Resistance due to Curved track

F_g - Resistance due to Gradient

F_a - Force to accelerate train body

$$F_T = F_r + F_c + F_g + F_a \ , \tag{3-1}$$

Train rolling resistance

$$F_r = A + BV + CV^2 \quad , \tag{3-2}$$

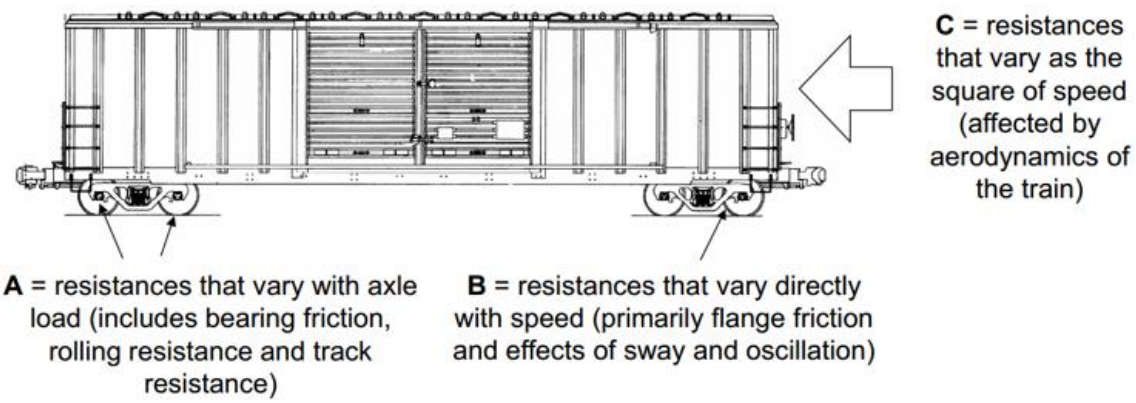

Figure 3-3 Running train rolling resistance factors [20]

For Chinese passenger coach (non-high-speed) the resistance due to rolling is ~~been~~ calculated with the following formula:

$$F_r = 9.81(1.82 + 0.01V + 0.000145V^2) \ , \tag{3-3}$$

where w_r is in Newton per $tonne$ mass

V- Speed of the train in Km/hr

MATLAB/Simulink model used to calculate the resistive force due to rolling is shown below. Operation blocks found in the Simulink library are used to construct the model according to the formula.

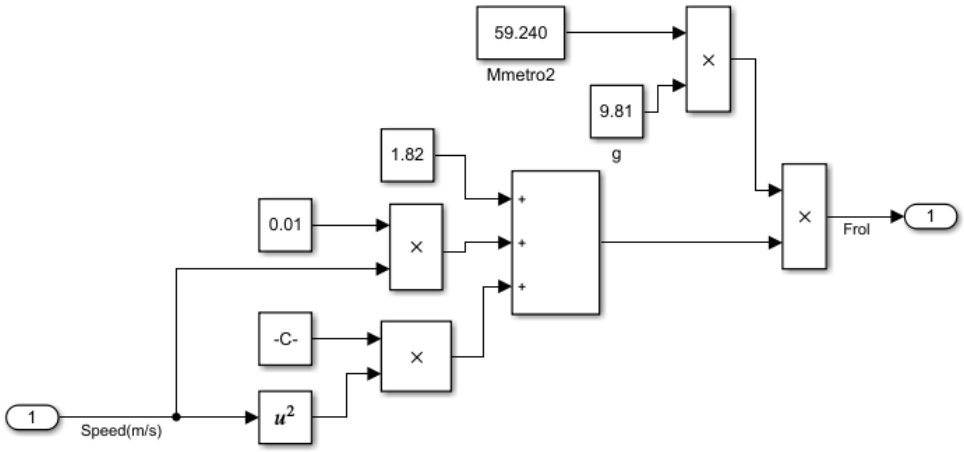

Figure 3-4 Simulink model of train resistive force due to rolling

Resistance due to Curved track

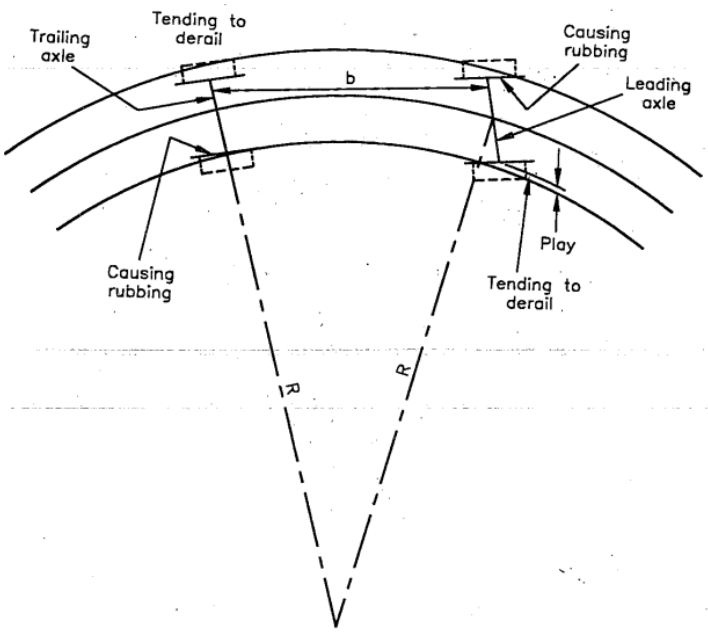

Figure 3-5 A Diagram showing radius of curvature

In Chinese railways trend, the train movement resistance due to track curves is computed using the formula:

$$F_c = 573/R \ , \tag{3-4}$$

Where F_c is measured in parts per thousand or $kgf/tonne$ ($Kilogram - force$).

Note: 1 Kgf= 9.806650$Newton$, and R- is radius of curvature in meters
Wheel diameter of AA-LRT trams is 660mm.

MATLAB/Simulink model used to calculate the resistive force due to curvature is shown as below.

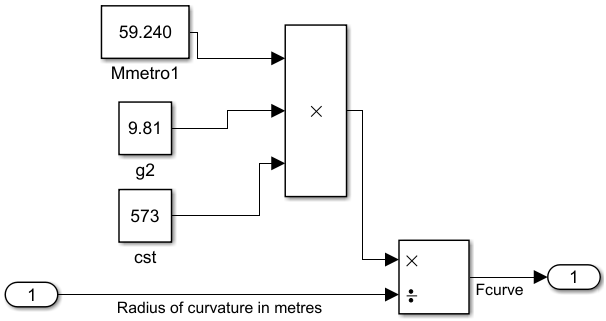

Figure 3-6 Simulink model of train resistive force due to curves

Resistance due to Gradient

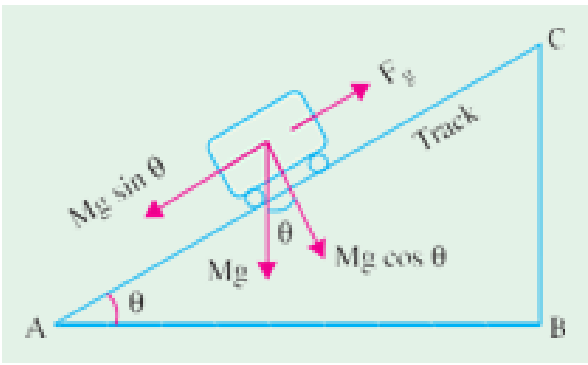

Figure 3-7 Geometric sketch showing train movement in a slope [21]

As seen from Fig. 3.5, $F_g = Wsin\theta = Mgsin\theta$

In railway practice, gradient is expressed as the rise (in metres) a track distance of 100 m and is called percentage gradient.

$$\%\, G = \frac{BC}{AC/100} = 100\frac{BC}{AC} = 100sin\theta\ , \tag{3-5}$$

Substituting the value of sin θ in the above equation, gives:

$$F_g = MgG/100 = 9.8 \times 10^{-2}MG\ , \tag{3-6}$$

- When M is in Kg,

$$F_g = 9.8 \times 10^{-2}MG\ newton\ , \tag{3-7}$$

- When M is given in $tonne$,

$$F_g = 9.8 \times 10^{-2}(1000M)G = 98MG\ newton\ , \tag{3-8}$$

MATLAB/Simulink model used to calculate the resistive force due to track gradient is shown as below.

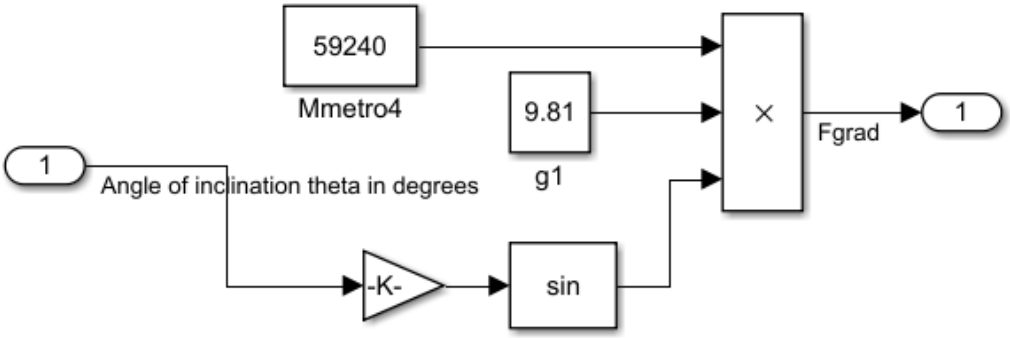

Figure 3-8 Simulink model of train resistive force due to gradient

Force to accelerate train body

If *M* is the dead (or stationary) mass of the train and a its linear acceleration, then

$$F_a = Ma\ , \tag{3-9}$$

Since a train has rotating parts like wheels, axles, motor armatures, and gearing, etc., it's *effective* (or accelerating) mass is more (about 6% – 8%) than its stationary mass [22].

These parts have to be given angular acceleration at the same time as the whole train is accelerated in the linear direction.

Therefore:

$$F_e = M_e a \ , \tag{3-10}$$

- If M_e is in Kg and α in m/s^2, then:

$$F_a = M_e a \ newton \ , \tag{3-11}$$

- If M_e is in tonne and α in $km/h/s$, then converting them into absolute units, results:

$$F_a = (1000M_e) \times (1000/3600)a = 277.8M_e a \ Newton \ , \tag{3-12}$$

The designer of the AA-LRT line has set the acceleration to be 1m/s^2 while the speed of the train is 0 to 40km/hr, and 0.5m/s^2 for speed beyond 40km/hr.

The force required to accelerate the train is calculated using MATLAB/Simulink model and shown in figure 3.7 below.

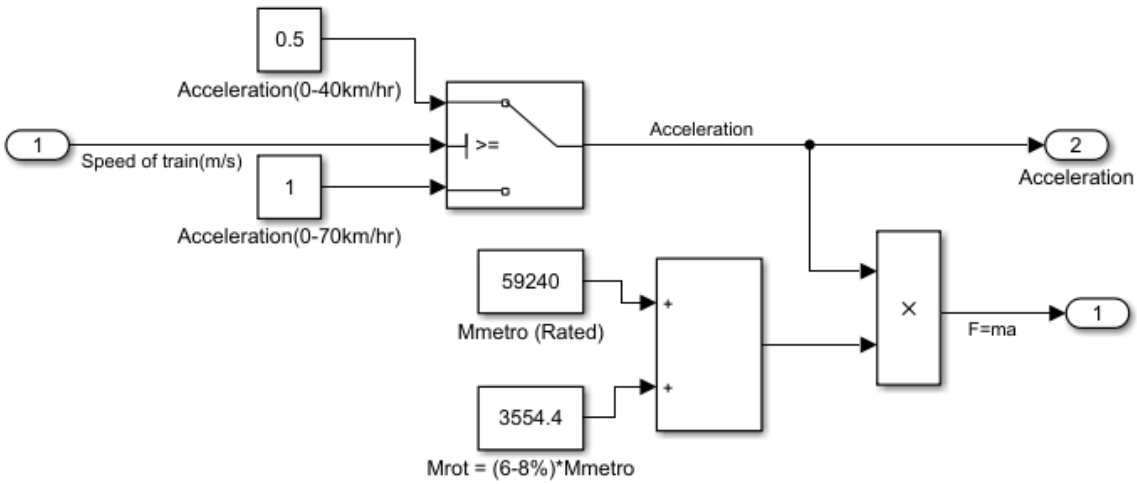

Figure 3-9 Simulink model of force to accelerate train

Power Transmission System from Motor to Axle and vice versa

After finding the train movement resistive forces, the force exerted on the axle of the train can be calculated from the summation of the individual forces. Then the load torque

imposed on the traction motor via the gear system, can be computed by multiplying the force with radius of the wheel and dividing to the gear ration.

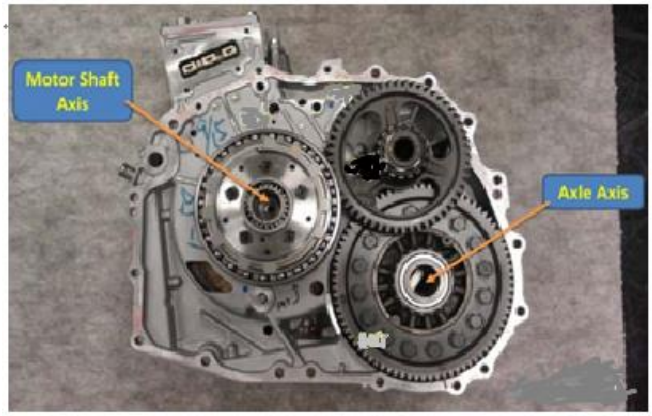

Figure 3-10 An image of traction motor to wheel axle gear box mechanism [23]

- 70% low floor tram gearbox has a Final Drive Ratio of (G_r) of $8.2{:}\,1$ [24], [25].

Load Torque per axle = Resistive Force per axle × Radius of wheel, mathematically:

$$T_m = (F_T \times r_{wheel})/8.2\ , \qquad (3\text{-}13)$$

Where: T_m- Load Torque per axle, in $N-m$

F_T - Total resistive force per axle, in N, and

r_{wheel}- Radius of the wheel, in $Meter$

- AALRT trams wheel diameter is 660mm for new wheel, 580mm for full wear [5].

For a traction motor to be operating at a steady speed, the electromagnetic torque generated by the motor should be equal and opposite of the load torque imposed on it. If the torque produced by the motor is less than load torque, the motor will decelerate, or if the electromagnetic torque is greater than load torque, then the motor will be accelerating. The load torque is the controlling factor for the motor current to be increasing or decreasing. The value of the motor electromechanical quantities is dependent on motor current [26].

3.2.2 Traction motor modelling

The traction motor used by AA-LRT trams is a constant v/f (volts by hertz) controlled asynchronous induction motor of squirrel cage kind rotor. So traction motor modeling will be all about three-phase induction motor modeling. Mathematical modeling plays a very important role in the design, exploitation, and control of electric drives [27].

The mathematical model of the three-phase induction motor is important to formulate equations that hold the relationship between electromagnetic torque and other electrical and mechanical quantities of the motor [28]. Even if the per-phase equivalent circuit model is used to evaluate the steady-state performance of induction motors, it will not be correct to deploy this model for assessing the dynamic performance of the motor [29]. In this paper, for modeling the traction motor the dynamic model equations will be developed to show how the various electrical quantities of the motor can be related while the motor is in real-time operation. These dynamic modeling equations are also the basis for working with and, better understanding the properties of three-phase induction motor which has been simulated with the help of MATLAB/Simulink in this study. The per-phase equivalent circuit model of induction motors can be used to compute electrical and mechanical parameters of the induction motor while in steady-state.

3.2.2.1 *Dynamic model of traction motor/three phase induction motor voltage equations*

As shown in Figure 3.8 below, three-phase induction motor has three input terminals in the stator to supply power from the source to its internal stator windings surrounding the iron core, and the other three terminals of the stator are short-circuited. Similarly, the rotary part of the motor is composed of an iron core with short-circuited three-phase windings (for Wound type), or iron core with a cylinder of steel laminations, with aluminum or copper conductors embedded in its surface (Squirrel cage rotor). The squirrel cage rotor type induction motor is mostly used for traction applications [30]. The induction motor used in AA-LRT trams has also squirrel cage kind rotor. For electromechanical energy conversion process to happen in induction motor such that the rotor will rotate while an MMF (Magneto-motive force) is created in the air-gap between stator and rotor structures. To comprehensively analyze the input-output values of the various electromechanical quantities, it needs a mathematical model in the dynamic situation of the motor.

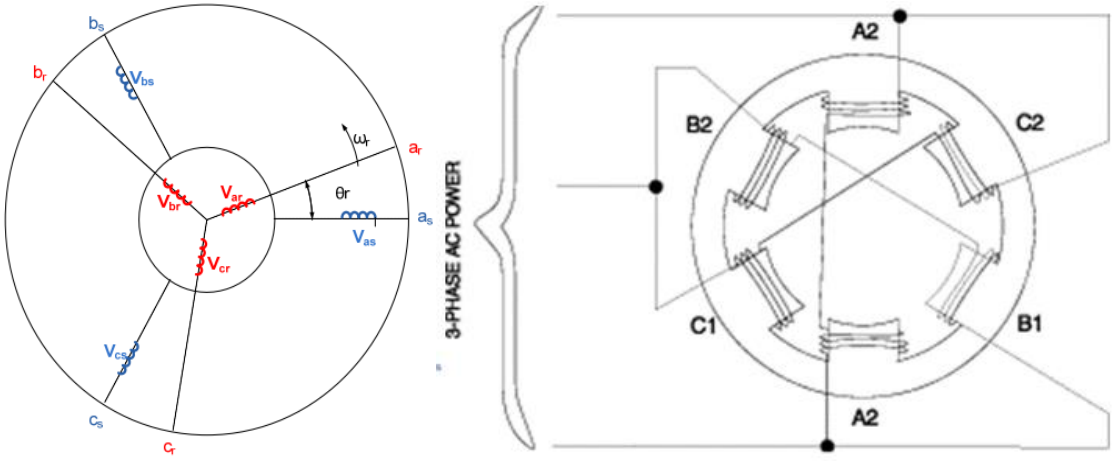

Figure 3-11 a. Three phases winding arrangement of an induction motor b. Three phase power connected to 6-pole stator

The voltage equations for the induction motor shown in Figure 3.12 above are:

$$v_{as} = r_s i_{as} + \frac{d\lambda_{as}}{dt} \ , \tag{3-14}$$

$$v_{bs} = r_s i_{bs} + \frac{d\lambda_{bs}}{dt} \ , \tag{3-15}$$

$$v_{cs} = r_s i_{cs} + \frac{d\lambda_{cs}}{dt} \ , \tag{3-16}$$

$$v_{ar} = r_r i_{ar} + \frac{d\lambda_{ar}}{dt} \ , \tag{3-17}$$

$$v_{br} = r_r i_{br} + \frac{d\lambda_{br}}{dt} \ , \tag{3-18}$$

$$v_{cr} = r_r i_{cr} + \frac{d\lambda_{cr}}{dt} \ , \tag{3-19}$$

r_s is stator resistance for each phase
r_s is rotor resistance for each phase
v is phase voltage
i is phase current
λ is linkage flus

$$\lambda = Li \ , \tag{3-20}$$

So the flux linkage along each winding between stator and stator, rotor and rotor, and stator and rotor can be rewritten as:

$$\lambda_{as} = L_{asas} i_{as} + L_{asbs} i_{bs} + L_{ascs} i_{cs} + L_{asar} i_{ar} + L_{asbr} i_{br} + L_{ascr} i_{cr} \ , \tag{3-21}$$

$$\lambda_{bs} = L_{bsas} i_{as} + L_{bsbs} i_{bs} + L_{bscs} i_{cs} + L_{bsar} i_{ar} + L_{bsbr} i_{br} + L_{bscr} i_{cr} \ , \tag{3-22}$$

$$\lambda_{cs} = L_{csas} i_{as} + L_{csbs} i_{bs} + L_{cscs} i_{cs} + L_{csar} i_{ar} + L_{csbr} i_{br} + L_{cscr} i_{cr} \ , \tag{3-23}$$

$$\lambda_{ar} = L_{aras}i_{as} + L_{arbs}i_{bs} + L_{arcs}i_{cs} + L_{arar}i_{ar} + L_{arbr}i_{br} + L_{arcr}i_{cr}\ , \quad (3\text{-}24)$$

$$\lambda_{br} = L_{bras}i_{as} + L_{brbs}i_{bs} + L_{brcs}i_{cs} + L_{brar}i_{ar} + L_{brbr}i_{br} + L_{brcr}i_{cr}\ , \quad (3\text{-}25)$$

$$\lambda_{cr} = L_{cras}i_{as} + L_{crbs}i_{bs} + L_{crcs}i_{cs} + L_{crar}i_{ar} + L_{crbr}i_{br} + L_{crcr}i_{cr}\ , \quad (3\text{-}26)$$

$$\frac{d\lambda}{dt} = L\frac{di}{dt}\ , \quad (3\text{-}27)$$

To simplify the voltage equation by substituting the time-varying values of the linkage flux between each and every of the stator winding and rotor windings (circuits in relative motion) is a complicated task to perform due to the fact that the rotor is always in relative motion with the stator, for fixing that, a change of variables eliminates the time-varying inductances resulting in voltage equations which are still nonlinear but converted to a manageable form [31]. For fixing this issue many scholars at different times developed their equations to substitute the time-varying inductance for ease of analyzing the dynamic behavior of three-phase induction motors. Those stator and rotor variables transformation theory formulated by various scholars is called a frame of reference. Most of those reference frame theories brought conversion of the motor parameters from three-dimensional analysis to its two-dimensional equivalent by:

- Referring the stator parameters to rotor side (Rotor reference frame),
- Rotor parameters referred to stator side (Stator reference frame) and,
- Both stator and rotor variables referred to a reference frame rotating in synchronism with the rotating magnetic field (Synchronous frame of reference),

A study has been done to formulate an equation that makes all transformations able to convert one another by using an independently rotating frame, which eliminates all time-varying inductances by referring the stator and rotor variables to a frame of reference which may rotate at any angular velocity or remain stationary [31]. i.e.

- Both stator and rotor parameters referred to an arbitrary frame (Arbitrary frame of reference).

In [31], a summary of the frame of references is put in table as below. A generalized methodology for converting to and from one type of reference frame has also been developed.

Table 3-3 Summary of reference frame theories [31]

Reference frame speed	Interpretation
ω (unspecified)	Stationary and circuit variables referred to the arbitrary reference frame (by Krause).
0	Stationary circuit variables referred to the stationary reference frame (by Stanley, Clarke).
ω_r or ω_m	Stationary circuit variables referred to a reference frame fixed in the rotor (by Park, Brereton).
ω_{Re}	Stationary circuit variables referred to the synchronously rotating reference frame (by Kron).

Based on that, the author of this paper adopted a dynamic model of AA-LRT trams traction motor/three-phase asynchronous motor in the popularly used Park's transformation by transforming stationary a-b-c variables to rotating q-d-0 (direct-quadrature-zero) axis, and rotor a-b-c quantities to those rotating q-d-0 coordinates as follows.

Before performing dynamic and steady-state modeling for three-phase induction motor, the following assumptions made for better handling of the equations [32]:

- The air-gap has constant area in all its circumference.
- The three phases of the motor are symmetrical.
- Distribution of phase windings is perfectly sinusoidal
- Saturation in ferromagnetic iron core is neglected, means flux density stays linear
- Hysteresis and Eddy current losses are neglected.
- There happens no variation with temperature in values of winding resistances and inductances.

Keeping the above assumptions, the dynamic modelling is performed in the following sections .Park's transformation in three-phase induction machine is written;

$$\begin{bmatrix} X_{qd0} \\ X_{qds} \\ X_{qdr} \end{bmatrix} = \begin{bmatrix} 0 & 0 \\ P & 0 \\ 0 & Pr \end{bmatrix} \times \begin{bmatrix} X_{abcs} \\ X_{abcr} \end{bmatrix}, \tag{3-28}$$

Where X stands for Voltage, Current or Flux linkage quantities.

Ps is Park's transformation factor for stator quantities and,

Pr is Park's transformation factor for rotor quantities

$$P_s = \sqrt{\frac{2}{3}}\begin{bmatrix} \frac{1}{\sqrt{2}} & \frac{1}{\sqrt{2}} & \frac{1}{\sqrt{2}} \\ \cos\theta & \cos(\theta-120) & \cos(\theta+120) \\ \sin\theta & \sin(\theta-120) & \sin(\theta+120) \end{bmatrix}, \quad (3\text{-}29)$$

And inverse Park's transformation is:

$$P_s^{-1} = \sqrt{\frac{2}{3}}\begin{bmatrix} \frac{1}{\sqrt{2}} & \cos(\theta) & \sin(\theta) \\ \frac{1}{\sqrt{2}} & \cos(\theta-120) & \sin(\theta-120) \\ \frac{1}{\sqrt{2}} & \cos(\theta+120) & \sin(\theta+120) \end{bmatrix}, \quad (3\text{-}30)$$

where θ is the angle between rotating d-q reference frame and a-axis of the stator, and θ can be defined in accordance with the rotational speed of d-q frame as;

$$\theta = \int_0^t \omega(\gamma)dy + \theta(0), \quad (3\text{-}31)$$

where ω is the rotational speed of the d-q coordinate axes, i.e., the synchronous speed.

Park's transformation also needed to be applied to the rotor a-b-c windings in order to obtain the rotor circuit voltage equation in q-d-0 co-ordinates. To do so, it can be observed that the stator phase-a winding (and thus its a-axis) is fixed, the rotor phase-a winding (and thus its a-axis) rotates. If P transformation is applied to the rotor, its rotation should not be accounted, i.e. it will be treated as if it is fixed. More elaboration is provided in figure below for better understanding.

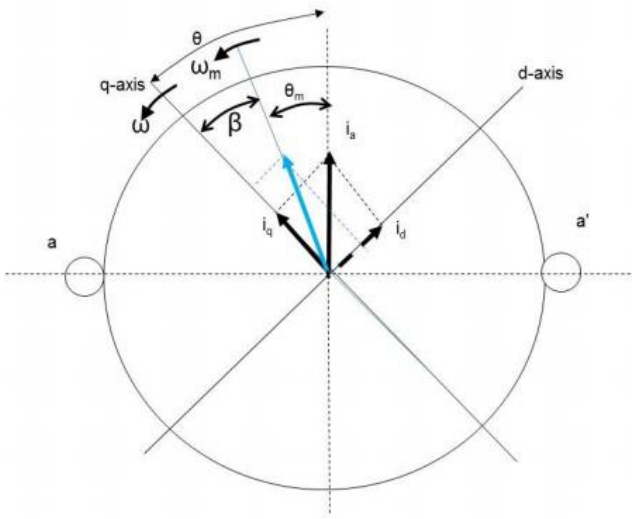

Figure 3-12 Graphical representation of a-b-c axis and q-d-0 axis of motor

As shown in Figure above, θ is the angle between the stator a-axis and the q-axis of the synchronously rotating reference frame;

- ✓ θ_m, the angle between the stator a-axis and the rotor a-axis and,
- ✓ β, the angle between the rotor a-axis and the q-axis of the synchronously rotating reference frame.

Hence the stator a-axis is stationary, the q-d axis rotates at ω, and the rotor a-axis rotates at ω_m. Observe that $\beta=\theta-\theta_m$.

When the i_{ar} vector (between i_a and i_q) is considered, which is coincident with the rotor a-axis. It can be observed that it could be decomposed into the q-d reference frame, but angle β can be taken as it is instead of θ. If so, the transformation that is needed for the rotor is exactly like the transformation used for the stator, except substituting β for θ, and account for the fact that, to the rotor windings, the q-d coordinate system appears to be moving at $\omega-\omega_m$. Then Park's transformation for the rotor winding can be rewritten as;

$$P_r = \sqrt{\frac{2}{3}}\begin{bmatrix} \frac{1}{\sqrt{2}} & \frac{1}{\sqrt{2}} & \frac{1}{\sqrt{2}} \\ cos\,\beta & cos(\beta-120) & cos(\beta+120) \\ sin\,\beta & sin(\beta-120) & sin(\beta+120) \end{bmatrix}, \quad (3\text{-}32)$$

$$\beta = \int_0^t \omega\,(\gamma) - \omega_m(\gamma)dy + \theta(0) - \theta_m(0)\,, \quad (3\text{-}33)$$

where $\omega(\gamma) - \omega_m(\gamma)dy$ is the ω_r term, and $\theta(0) - \theta_m(0)$ is for $\beta(0)$.
And its inverse transform as;

$$\underline{P_r}^{-1} = \sqrt{\frac{2}{3}}\begin{bmatrix} \frac{1}{\sqrt{2}} & cos(\beta) & sin(\beta) \\ \frac{1}{\sqrt{2}} & cos(\beta - 120) & sin(\beta - 120) \\ \frac{1}{\sqrt{2}} & cos(\beta + 120) & sin(\beta + 120) \end{bmatrix}, \quad (3\text{-}34)$$

Afterwards, the transformation of a-b-c quantities to their qd0 equivalent for both stator and rotor of the three phase induction motor can be performed starting from the voltage equations of three phase asynchronous motor as follows;

$$\begin{bmatrix} v_{as} \\ v_{bs} \\ v_{cs} \\ v_{ar} \\ v_{br} \\ v_{cr} \end{bmatrix} = \begin{bmatrix} r_s & 0 & 0 & 0 & 0 & 0 \\ 0 & r_s & 0 & 0 & 0 & 0 \\ 0 & 0 & r_s & 0 & 0 & 0 \\ 0 & 0 & 0 & r_r & 0 & 0 \\ 0 & 0 & 0 & 0 & r_r & 0 \\ 0 & 0 & 0 & 0 & 0 & r_r \end{bmatrix}\begin{bmatrix} i_{as} \\ i_{bs} \\ i_{cs} \\ i_{ar} \\ i_{br} \\ i_{cr} \end{bmatrix} + \frac{d}{dt}\begin{bmatrix} \lambda_{as} \\ \lambda_{bs} \\ \lambda_{cs} \\ \lambda_{ar} \\ \lambda_{br} \\ \lambda_{cr} \end{bmatrix}, \quad (3\text{-}35)$$

Where;

$$\begin{bmatrix} \lambda_{sa} \\ \lambda_{sb} \\ \lambda_{sc} \\ \lambda_{ra} \\ \lambda_{rb} \\ \lambda_{rc} \end{bmatrix} = \begin{bmatrix} \underline{L_s} & \underline{L_{sr}} \\ \underline{L_{rs}} & \underline{L_r} \end{bmatrix}\begin{bmatrix} i_{sa} \\ i_{sb} \\ i_{sc} \\ i_{ra} \\ i_{rb} \\ i_{rc} \end{bmatrix}, \quad (3\text{-}36)$$

In induction machine, the rotor to rotor self and mutual terms, and the stator to stator self and mutual terms, are all constants (independent of rotor position and therefore independent of time). The rotor-rotor and stator-stator matrices are therefore stated as;

$$\underline{\boldsymbol{L_r}} = \begin{bmatrix} l_r + L_{mr} & -\frac{1}{2}L_{mr} & -\frac{1}{2}L_{mr} \\ -\frac{1}{2}L_{mr} & l_r + L_{mr} & -\frac{1}{2}L_{mr} \\ -\frac{1}{2}L_{mr} & -\frac{1}{2}L_{mr} & l_r + L_{mr} \end{bmatrix} \underline{L_s} = \begin{bmatrix} l_s + L_{ms} & -\frac{1}{2}L_{ms} & -\frac{1}{2}L_{ms} \\ -\frac{1}{2}L_{ms} & l_s + L_{ms} & -\frac{1}{2}L_{ms} \\ -\frac{1}{2}L_{ms} & -\frac{1}{2}L_{ms} & l_s + L_{ms} \end{bmatrix}, \quad (3\text{-}37)$$

l_r is rotor leakage inductance, L_{mr} is rotor magnetizing inductance and,

l_s is stator leakage inductance, L_{ms} is stator magnetizing inductance

As can be seen from the above equation, diagonal elements of the matrix are the self-inductance of each winding comprised of leakage and mutual inductances. Whereas off-diagonal components express mutual inductance (magnetizing only).

Off-diagonal elements are mutual inductances between windings and are negative because 120° axis offset between any pair of windings results in flux contributed by one winding to have negative component along the main axis of another winding as shown in Figure 3-9 above.

The "1/2" in off-diagonals results from definition of self and mutual inductances [31].

It is different for the rotor to stator mutual inductances, however, because the positions of the rotor to stator windings change with rotor movement. Thus, the mutual inductance between any pair of rotor to stator windings is a function of rotor position, as written below;

$$\underline{L}_{rs} = L_{sr}\begin{bmatrix} cos\theta_m & cos(\theta_m - 120) & cos(\theta_m + 120) \\ cos(\theta_m + 120) & cos\theta_m & cos(\theta_m - 120) \\ cos(\theta_m - 120) & cos(\theta_m + 120) & cos\theta_m \end{bmatrix} = \underline{L}_{sr}^{T}\,, \qquad (3\text{-}38)$$

And the matrix of stator to rotor mutual inductance will be the transpose:

$$\underline{L}_{sr} = L_{sr}\begin{bmatrix} cos\theta_m & cos(\theta_m + 120) & cos(\theta_m - 120) \\ cos(\theta_m - 120) & cos\theta_m & cos(\theta_m + 120) \\ cos(\theta_m + 120) & cos(\theta_m - 120) & cos\theta_m \end{bmatrix}, \qquad (3\text{-}39)$$

$L_{ms} = L_{mr} = L_{sr}$ as a result of referring all quantities to the stator [31].

The voltage equations above can be rewritten in compacted form as;

$$\begin{bmatrix} \underline{v}_{abcs} \\ \underline{v}_{abcr} \end{bmatrix} = \begin{bmatrix} \underline{r}_s & \underline{0} \\ \underline{0} & \underline{r}_r \end{bmatrix}\begin{bmatrix} \underline{i}_{abcs} \\ \underline{i}_{abcr} \end{bmatrix} + \begin{bmatrix} \dot{\underline{\lambda}}_{abcs} \\ \dot{\underline{\lambda}}_{abcr} \end{bmatrix}, \qquad (3\text{-}40)$$

Applying the d-q transformations to the voltage equation will be;

$$\begin{bmatrix} \underline{P}_s & \underline{0} \\ \underline{0} & \underline{P}_r \end{bmatrix}\begin{bmatrix} \underline{v}_{abcs} \\ \underline{v}_{abcr} \end{bmatrix} = \begin{bmatrix} \underline{P}_s & \underline{0} \\ \underline{0} & \underline{P}_r \end{bmatrix}\begin{bmatrix} \underline{r}_s & \underline{0} \\ \underline{0} & \underline{r}_r \end{bmatrix}\begin{bmatrix} \underline{i}_{abcs} \\ \underline{i}_{abcr} \end{bmatrix} + \begin{bmatrix} \underline{P}_s & \underline{0} \\ \underline{0} & \underline{P}_r \end{bmatrix}\begin{bmatrix} \dot{\underline{\lambda}}_{abcs} \\ \dot{\underline{\lambda}}_{abcr} \end{bmatrix}, \qquad (3\text{-}41)$$

After multiplication of the matrix results;

$$\begin{bmatrix} \underline{v}_{0dqs} \\ \underline{v}_{0dqr} \end{bmatrix} = \begin{bmatrix} \underline{P_s} r_s & \underline{0} \\ \underline{0} & \underline{P_r} r_r \end{bmatrix} \begin{bmatrix} \underline{i}_{abcs} \\ \underline{i}_{abcr} \end{bmatrix} + \begin{bmatrix} \underline{P_s} \dot{\underline{\lambda}}_{abcs} \\ \underline{P_r} \dot{\underline{\lambda}}_{abcr} \end{bmatrix}, \tag{3-42}$$

By inverse Park's transformation the current can be written like;

$$\begin{bmatrix} \underline{i}_{abcs} \\ \underline{i}_{abcr} \end{bmatrix} = \begin{bmatrix} \underline{P_s}^{-1} & \underline{0} \\ \underline{0} & \underline{P_r}^{-1} \end{bmatrix} \begin{bmatrix} \underline{i}_{0dqs} \\ \underline{i}_{0dqr} \end{bmatrix}, \tag{3-43}$$

Substituting eqn. (3-43) in to eqn. (3-42) gives;

$$\begin{bmatrix} \underline{v}_{0dqs} \\ \underline{v}_{0dqr} \end{bmatrix} = \begin{bmatrix} \underline{P} r_s & \underline{0} \\ \underline{0} & \underline{P_r} r_r \end{bmatrix} \begin{bmatrix} \underline{P_s}^{-1} & \underline{0} \\ \underline{0} & \underline{P_r}^{-1} \end{bmatrix} \begin{bmatrix} \underline{i}_{0dqs} \\ \underline{i}_{0dqr} \end{bmatrix} + \begin{bmatrix} \underline{P_s} \dot{\underline{\lambda}}_{abcs} \\ \underline{P_r} \dot{\underline{\lambda}}_{abcr} \end{bmatrix}, \tag{3-44}$$

Multiplying the matrix for the current term;

$$\begin{bmatrix} \underline{v}_{0dqs} \\ \underline{v}_{0dqr} \end{bmatrix} = \begin{bmatrix} \underline{P} r_s \underline{P_s}^{-1} & \underline{0} \\ \underline{0} & \underline{P_r} r_r \underline{P_r}^{-1} \end{bmatrix} \begin{bmatrix} \underline{i}_{0dqs} \\ \underline{i}_{0dqr} \end{bmatrix} + \begin{bmatrix} \underline{P_s} \dot{\underline{\lambda}}_{abcs} \\ \underline{P_r} \dot{\underline{\lambda}}_{abcr} \end{bmatrix}, \tag{3-45}$$

The term two matrix elements collapse to r_s and r_r, respectively, because $KRK^{-1}=R$ if R is diagonal having equal diagonal elements.

This follows from $KRK^{-1} = KrUK^{-1} = rKUK^{-1} = rKK^{-1} = rU = R$, where r is the scalar value of each element in R, and U is the identity matrix. Accordingly, eqn. (3-45) will be;

$$\begin{bmatrix} \underline{v}_{0dqs} \\ \underline{v}_{0dqr} \end{bmatrix} = \begin{bmatrix} \underline{r_s} & \underline{0} \\ \underline{0} & r_r \end{bmatrix} \begin{bmatrix} \underline{i}_{0dqs} \\ \underline{i}_{0dqr} \end{bmatrix} + \begin{bmatrix} \underline{P_s} \dot{\underline{\lambda}}_{abcs} \\ \underline{P_r} \dot{\underline{\lambda}}_{abcr} \end{bmatrix}, \tag{3-46}$$

Taking out term three vector, consider the transformation of stator flux linkages according to;

$$\underline{\lambda}_{0dqs} = \underline{P_s} \underline{\lambda}_{abcs} \ , \tag{3-47}$$

Differentiating both sides using chain rule;

$$\dot{\underline{\lambda}}_{0dqs} = \underline{P} \dot{\underline{\lambda}}_{abcs} + \underline{\lambda}_{abcs} \dot{\underline{P}_s} \ , \tag{3-48}$$

Solve for the first term on the right-hand side;

$$\underline{P} \dot{\underline{\lambda}}_{abcs} = \dot{\underline{\lambda}}_{0dqs} - \underline{\lambda}_{abcs} \dot{\underline{P}_s} \ , \tag{3-49}$$

And using Park's transformation;

$$\underline{\lambda}_{abcs} = \underline{P}_s^{-1}\underline{\lambda}_{qd0s}\ , \tag{3-50}$$

Then;

$$\underline{P}_s\dot{\underline{\lambda}}_{abcs} = \dot{\underline{\lambda}}_{0dqs} - \underline{\lambda}_{0dqs}\underline{P}_s^{-1}\dot{\underline{P}}_s\ , \tag{3-51}$$

The same procedure for the rotor quantities results in;

$$\underline{P}_r\dot{\underline{\lambda}}_{abcr} = \dot{\underline{\lambda}}_{0dqr} - \underline{\lambda}_{0dqr}\underline{P}_r^{-1}\dot{\underline{P}}_r\ \ , \tag{3-52}$$

Now substituting eqn. (3-51) and eqn. (3-52) into eqn.(3-46) gives;

$$\begin{bmatrix}\underline{v}_{0dqs}\\ \underline{v}_{0dqr}\end{bmatrix} = \begin{bmatrix}\underline{r}_s & \underline{0}\\ \underline{0} & r_r\end{bmatrix}\begin{bmatrix}\underline{i}_{0dqs}\\ \underline{i}_{0dqr}\end{bmatrix} + \begin{bmatrix}\dot{\underline{\lambda}}_{0dqs}\\ \dot{\underline{\lambda}}_{0dqr}\end{bmatrix} - \begin{bmatrix}\underline{\lambda}_{0dqs}\underline{P}_s^{-1}\dot{\underline{P}}_s\\ \underline{\lambda}_{0dqr}\underline{P}_r^{-1}\dot{\underline{P}}_r\end{bmatrix}, \tag{3-53}$$

The above equation provides the relation between stator and rotor equations expressed in terms of qd0 quantities instead of abc quantities.

From the above equation, both currents and flux linkages are as state variables. It is better if flux linkages expressed in terms of currents, resulting in a state-space equation in current variables.

$$\begin{bmatrix}\lambda_{as}\\ \lambda_{bs}\\ \lambda_{cs}\\ \lambda_{ar}\\ \lambda_{br}\\ \lambda_{cr}\end{bmatrix} = \begin{bmatrix}\underline{L}_s & \underline{L}_{sr}\\ \underline{L}_{rs} & \underline{L}_r\end{bmatrix}\begin{bmatrix}i_{as}\\ i_{bs}\\ i_{cs}\\ i_{ar}\\ i_{br}\\ i_{cr}\end{bmatrix} \Rightarrow \begin{bmatrix}\underline{\lambda}_{abcs}\\ \underline{\lambda}_{abcr}\end{bmatrix} = \begin{bmatrix}\underline{L}_s & \underline{L}_{sr}\\ \underline{L}_{rs} & \underline{L}_r\end{bmatrix}\begin{bmatrix}\underline{i}_{abcs}\\ \underline{i}_{abcr}\end{bmatrix}, \tag{3-54}$$

Applying Park's transformation to replace abc currents to their dq0 equivalent will be;

$$\begin{bmatrix}\underline{\lambda}_{abcs}\\ \underline{\lambda}_{abcr}\end{bmatrix} = \begin{bmatrix}\underline{L}_s & \underline{L}_{sr}\\ \underline{L}_{rs} & \underline{L}_r\end{bmatrix}\begin{bmatrix}\underline{P}_s^{-1} & 0\\ 0 & \underline{P}_r^{-1}\end{bmatrix}\begin{bmatrix}\underline{i}_{0dqs}\\ \underline{i}_{0dqr}\end{bmatrix}, \tag{3-55}$$

Then the equation for the flux linkage in terms of current can be rewritten as;

$$\begin{bmatrix}\underline{\lambda}_{0dqs}\\ \underline{\lambda}_{0dqr}\end{bmatrix} = \begin{bmatrix}\underline{P}_s & 0\\ 0 & \underline{P}_r\end{bmatrix}\begin{bmatrix}\underline{L}_s & \underline{L}_{sr}\\ \underline{L}_{rs} & \underline{L}_r\end{bmatrix}\begin{bmatrix}\underline{P}_s^{-1} & 0\\ 0 & \underline{P}_r^{-1}\end{bmatrix}\begin{bmatrix}\underline{i}_{0dqs}\\ \underline{i}_{0dqr}\end{bmatrix}, \tag{3-56}$$

Multiplication of the right hand side matrix gives;

$$\begin{bmatrix} \underline{\lambda}_{0dqs} \\ \underline{\lambda}_{0dqr} \end{bmatrix} = \begin{bmatrix} \underline{P}_s \underline{L}_s \underline{P}_s^{-1} & \underline{P}_s \underline{L}_{sr} \underline{P}_r^{-1} \\ \underline{P}_r \underline{L}_{rs} \underline{P}_s^{-1} & \underline{P}_r \underline{L}_r \underline{P}_r^{-1} \end{bmatrix} \begin{bmatrix} \underline{i}_{0dqs} \\ \underline{i}_{0dqr} \end{bmatrix}, \tag{3-57}$$

Recalling the equations for $\underline{L}_r$ $\underline{L}_s$ $\underline{L}_{rs}$and $\underline{L}_{sr}$the inductance matrices to substitute into back to eqn.(3-57), and evaluating the product will be;

$$\underline{P}_s \underline{L}_s \underline{P}_s^{-1} = \begin{bmatrix} l_s + M & 0 & 0 \\ 0 & l_s + M & 0 \\ 0 & 0 & l_s \end{bmatrix} \equiv \underline{L}_{s0dq} \ , \tag{3-58}$$

$$\underline{P}_s \underline{L}_{sr} \underline{P}_r^{-1} = \underline{P}_r \underline{L}_{rs} \underline{P}_s^{-1} = \begin{bmatrix} M & 0 & 0 \\ 0 & M & 0 \\ 0 & 0 & 0 \end{bmatrix} \equiv \underline{L}_{m0dq} \ , \tag{3-59}$$

$$\underline{P}_r \underline{L}_r \underline{P}_r^{-1} = \begin{bmatrix} l_r + M & 0 & 0 \\ 0 & l_r + M & 0 \\ 0 & 0 & l_r \end{bmatrix} \equiv \underline{L}_{r0dq} \ , \tag{3-60}$$

In [31], it is stated that L_M =3/2(Lms) = 3/2(Lmr), and L_M here after will be written like M for ease of writing it.

Now substituting the expressions of (3-60), as denoted by the right-hand side nomenclature, into (3-57), gives;

$$\begin{bmatrix} \underline{\lambda}_{0dqs} \\ \underline{\lambda}_{0dqr} \end{bmatrix} = \begin{bmatrix} \underline{L}_{s0dq} & \underline{L}_{m0dq} \\ \underline{L}_{m0dq} & \underline{L}_{r0dq} \end{bmatrix} \begin{bmatrix} \underline{i}_{0dqs} \\ \underline{i}_{0dqr} \end{bmatrix}, \tag{3-61}$$

From (3-60) the inductance matrix is constant, (3-61) can be differentiated to yield;

$$\begin{bmatrix} \underline{\dot{\lambda}}_{0qds} \\ \underline{\dot{\lambda}}_{0qdr} \end{bmatrix} = \begin{bmatrix} \underline{L}_{s0qd} & \underline{L}_{m0qd} \\ \underline{L}_{m0qd} & \underline{L}_{r0qd} \end{bmatrix} \begin{bmatrix} \underline{i}_{0qds} \\ \underline{i}_{0qdr} \end{bmatrix}, \tag{3-62}$$

Now (3-62) can be substituted for flux linkage derivatives into our voltage equation in (3-53) will give;

$$\begin{bmatrix} \underline{v}_{0dqs} \\ \underline{v}_{0dqr} \end{bmatrix} = \begin{bmatrix} \underline{r}_s & \underline{0} \\ \underline{0} & \underline{r}_r \end{bmatrix} \begin{bmatrix} \underline{i}_{0dqs} \\ \underline{i}_{0dqr} \end{bmatrix} + \begin{bmatrix} \underline{L}_{s0dq} & \underline{L}_{m0dq} \\ \underline{L}_{m0dq} & \underline{L}_{r0dq} \end{bmatrix} \begin{bmatrix} \underline{i}_{0dqs} \\ \underline{i}_{0dqr} \end{bmatrix} - \begin{bmatrix} \underline{\dot{P}}_s \underline{P}_s^{-1} \underline{\lambda}_{0dqs} \\ \underline{\dot{P}}_r \underline{P}_r^{-1} \underline{\lambda}_{0dqr} \end{bmatrix}, \tag{3-63}$$

Still the last term of eqn.(3-63) is in terms of flux linkage, it will be managed to substitute these term with current in the coming section as follows;

For Solving $\underline{\dot{P}}_s \underline{P}_s^{-1}$ and $\underline{\dot{P}}_r \underline{P}_r^{-1}$, recalling Park's transformation;

$$\underline{P} = \sqrt{\frac{2}{3}}\begin{bmatrix} \frac{1}{\sqrt{2}} & \frac{1}{\sqrt{2}} & \frac{1}{\sqrt{2}} \\ \cos\theta & \cos(\theta-120) & \cos(\theta+120) \\ \sin\theta & \sin(\theta-120) & \sin(\theta+120) \end{bmatrix},$$

$$\underline{P}^{-1} = \sqrt{\frac{2}{3}}\begin{bmatrix} \frac{1}{\sqrt{2}} & \cos(\theta) & \sin(\theta) \\ \frac{1}{\sqrt{2}} & \cos(\theta-120) & \sin(\theta-120) \\ \frac{1}{\sqrt{2}} & \cos(\theta+120) & \sin(\theta+120) \end{bmatrix},$$

To find $\dot{\underline{P}}_s$, the derivative of θ is needed, it's again worth recalling expression of θ in terms of angular speed;

$$\theta = \int_0^t \omega(\gamma)dy + \theta(0),$$

From fundamental theorem of calculus, it can be rewritten as;

$$\dot{\theta}(t) = \omega, \tag{3-64}$$

Hence;

$$\dot{\underline{P}}_s = \sqrt{\frac{2}{3}}\omega\begin{bmatrix} 0 & 0 & 0 \\ -\sin\theta & -\sin(\theta-120) & -\sin(\theta+120) \\ cos\theta & \cos(\theta-120) & \cos(\theta+120) \end{bmatrix},$$

Similarly from the expression of $\dot{\underline{P}}_r\underline{P}_r^{-1}$ the second product can be found;

$$\underline{P}_r = \sqrt{\frac{2}{3}}\begin{bmatrix} \frac{1}{\sqrt{2}} & \frac{1}{\sqrt{2}} & \frac{1}{\sqrt{2}} \\ \cos\beta & \cos(\beta-120) & \cos(\beta+120) \\ \sin\beta & \sin(\beta-120) & \sin(\beta+120) \end{bmatrix},$$

$$\underline{P}_r^{-1} = \sqrt{\frac{2}{3}}\begin{bmatrix} \frac{1}{\sqrt{2}} & \cos(\beta) & \sin(\beta) \\ \frac{1}{\sqrt{2}} & \cos(\beta-120) & \sin(\beta-120) \\ \frac{1}{\sqrt{2}} & \cos(\beta+120) & \sin(\beta+120) \end{bmatrix},$$

Recalling that;

$$\beta = \int_0^t \omega(\gamma) - \omega_m(\gamma)dy + \theta(0) - \theta_m(0),$$

$$\dot{\beta}(t) = \omega - \omega_m, \tag{3-65}$$

Therefore;

$$\dot{\underline{P}}_r = \sqrt{\frac{2}{3}}(\omega-\omega_m)\begin{bmatrix} 0 & 0 & 0 \\ -sin\beta & -sin(\beta-120) & -sin(\beta+120) \\ cos\beta & cos(\beta-120) & cos(\beta+120) \end{bmatrix}, \tag{3-66}$$

Now $\dot{P}_s P_s^{-1}$and $\dot{P}_r P_r^{-1}$ can be computed as;

$$\dot{P}_s P_s^{-1} = \sqrt{\frac{2}{3}}\omega \begin{bmatrix} 0 & 0 & 0 \\ -sin\theta & -sin(\theta-120) & -sin(\theta+120) \\ cos\theta & cos(\theta-120) & cos(\theta+120) \end{bmatrix} \sqrt{\frac{2}{3}} \begin{bmatrix} \frac{1}{\sqrt{2}} & cos\theta & sin\theta \\ \frac{1}{\sqrt{2}} & cos(\theta-120) & sin(\theta-120) \\ \frac{1}{\sqrt{2}} & cos(\theta+120) & sin(\theta+120) \end{bmatrix} \quad (3\text{-}67)$$

$$= \frac{2}{3}\omega \begin{bmatrix} 0 & 0 & 0 \\ 0 & 0 & -\frac{3}{2} \\ 0 & \frac{3}{2} & 0 \end{bmatrix} = \begin{bmatrix} 0 & 0 & 0 \\ 0 & 0 & -\omega \\ 0 & \omega & 0 \end{bmatrix}$$

$$\dot{P}_s P_s^{-1} = \sqrt{\frac{2}{3}}(\omega-\omega_m) \begin{bmatrix} 0 & 0 & 0 \\ -sin\beta & -sin(\beta-120) & -sin(\beta+120) \\ cos\beta & cos(\beta-120) & cos(\beta+120) \end{bmatrix} \sqrt{\frac{2}{3}} \begin{bmatrix} \frac{1}{\sqrt{2}} & cos\beta & sin\beta \\ \frac{1}{\sqrt{2}} & cos(\beta-120) & sin(\beta-120) \\ \frac{1}{\sqrt{2}} & cos(\beta+120) & sin(\beta+120) \end{bmatrix} \quad (3\text{-}68)$$

$$= \frac{2}{3}(\omega-\omega_m) \begin{bmatrix} 0 & 0 & 0 \\ 0 & 0 & -\frac{3}{2} \\ 0 & \frac{3}{2} & 0 \end{bmatrix} = \begin{bmatrix} 0 & 0 & 0 \\ 0 & 0 & -(\omega-\omega_m) \\ 0 & (\omega-\omega_m) & 0 \end{bmatrix}$$

Then substitution of (3-67) and (3-68) into the last term of the voltage equations (3-63),

$$\begin{bmatrix} \underline{v}_{0dqs} \\ \underline{v}_{0dqr} \end{bmatrix} = \begin{bmatrix} \underline{r}_s & \underline{0} \\ \underline{0} & \underline{r}_r \end{bmatrix} \begin{bmatrix} \underline{i}_{0dqs} \\ \underline{i}_{0dqr} \end{bmatrix} + \begin{bmatrix} \underline{L}_{s0dq} & \underline{L}_{m0dq} \\ \underline{L}_{m0dq} & \underline{L}_{r0dq} \end{bmatrix} \begin{bmatrix} \underline{i}_{0dqs} \\ \underline{i}_{0dqr} \end{bmatrix} - \begin{bmatrix} \underline{\dot{P}_s P_s^{-1}} \underline{\lambda}_{0dqs} \\ \underline{\dot{P}_r P_r^{-1}} \underline{\lambda}_{0dqr} \end{bmatrix},$$

Fully expansion of (3-63) matrix gives;

$$\begin{bmatrix} v_{0s} \\ v_{ds} \\ v_{qs} \\ v_{0r} \\ v_{dr} \\ v_{qr} \end{bmatrix} = \begin{bmatrix} r_s & 0 & 0 & 0 & 0 & 0 \\ 0 & r_s & 0 & 0 & 0 & 0 \\ 0 & 0 & r_s & 0 & 0 & 0 \\ 0 & 0 & 0 & r_r & 0 & 0 \\ 0 & 0 & 0 & 0 & r_r & 0 \\ 0 & 0 & 0 & 0 & 0 & r_r \end{bmatrix} \begin{bmatrix} i_{0s} \\ i_{ds} \\ i_{qs} \\ i_{0r} \\ i_{dr} \\ i_{qr} \end{bmatrix} + \begin{bmatrix} l_s & 0 & 0 & 0 & 0 & 0 \\ 0 & l_s+M & 0 & 0 & M & 0 \\ 0 & 0 & l_s+M & 0 & 0 & M \\ 0 & 0 & 0 & l_r & 0 & 0 \\ 0 & M & 0 & 0 & l_r+M & 0 \\ 0 & 0 & M & 0 & 0 & l_r+M \end{bmatrix} \begin{bmatrix} i_{0s} \\ i_{ds} \\ i_{qs} \\ i_{0r} \\ i_{dr} \\ i_{qr} \end{bmatrix} -$$

$$\begin{bmatrix} 0 & 0 & 0 & 0 & 0 & 0 \\ 0 & 0 & \omega & 0 & 0 & 0 \\ 0 & -\omega & 0 & 0 & 0 & 0 \\ 0 & 0 & 0 & 0 & 0 & 0 \\ 0 & 0 & 0 & 0 & 0 & \omega-\omega_m \\ 0 & 0 & 0 & 0 & -(\omega-\omega_m) & 0 \end{bmatrix} \begin{bmatrix} \lambda_{0s} \\ \lambda_{ds} \\ \lambda_{qs} \\ \lambda_{0r} \\ \lambda_{dr} \\ \lambda_{qr} \end{bmatrix}, \quad (3\text{-}69)$$

There exist “Speed voltages” in the expression that are $\omega\lambda_{qs}$, $-\omega\lambda_{\mathrm{ds}}$, $(\omega - \omega_{\mathrm{m}})\lambda_{\mathrm{qr}}$, and $-(\omega - \omega_{\mathrm{m}})\,\lambda_{\mathrm{ds}}$,

These speed voltages represent the fact that a rotating flux wave will create voltages in windings that are stationary relative to that flux wave.

From the last voltage equation above, collapsing the last matrix-vector product by performing the multiplication, resulting in:

$$\begin{bmatrix} v_{0s} \\ v_{ds} \\ v_{qs} \\ v_{0r} \\ v_{dr} \\ v_{qr} \end{bmatrix} = \begin{bmatrix} r_s & 0 & 0 & 0 & 0 & 0 \\ 0 & r_s & 0 & 0 & 0 & 0 \\ 0 & 0 & r_s & 0 & 0 & 0 \\ 0 & 0 & 0 & r_r & 0 & 0 \\ 0 & 0 & 0 & 0 & r_r & 0 \\ 0 & 0 & 0 & 0 & 0 & r_r \end{bmatrix} \begin{bmatrix} i_{0s} \\ i_{ds} \\ i_{qs} \\ i_{0r} \\ i_{dr} \\ i_{qr} \end{bmatrix} + \begin{bmatrix} l_s & 0 & 0 & 0 & 0 & 0 \\ 0 & l_s + M & 0 & 0 & M & 0 \\ 0 & 0 & l_s + M & 0 & 0 & M \\ 0 & 0 & 0 & l_r & 0 & 0 \\ 0 & M & 0 & 0 & l_r + M & 0 \\ 0 & 0 & M & 0 & 0 & l_r + M \end{bmatrix} \begin{bmatrix} i_{0s} \\ i_{ds} \\ i_{qs} \\ i_{0r} \\ i_{dr} \\ i_{qr} \end{bmatrix} - \begin{bmatrix} 0 \\ \omega\lambda_{qs} \\ -\omega\lambda_{ds} \\ 0 \\ (\omega - \omega_m)\lambda_{qr} \\ -(\omega - \omega_m)\lambda_{dr} \end{bmatrix} \quad (3\text{-}70)$$

An equivalent circuit found in [31] is provided and can fit these above equations:

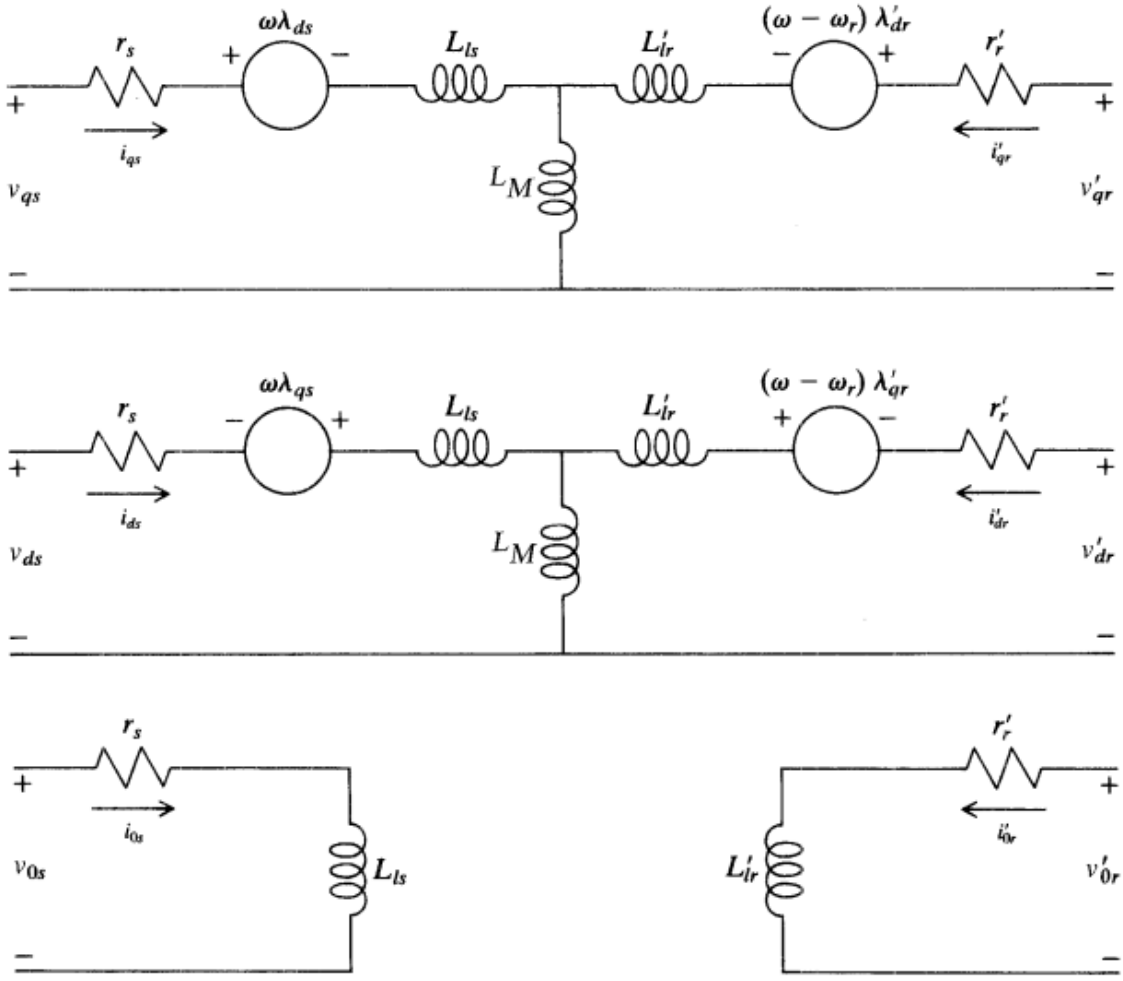

Figure 3-13 Arbitrary reference frame equivalent circuits for a three phase symmetrical induction motor [31]

It is worth notice that there are some symbols in the above equivalent circuit differ with the ones used in this study i.e. L_M=M, and L_{ls} and L_{lr} are ls and lr, respectively, and the primed notation indicates quantities referred to the stator, which are assumed in the previous dynamic modelling.

The above dynamic model equivalent circuit in arbitrary frame can be converted into many forms by varying the selection of ω. For $\omega = \omega_{Re}$, it can be equivalent circuit model in synchronous frame, while $\omega = \omega_r$, it can represent dynamic equivalent circuit in rotor frame of reference, and equivalent circuit model in a stationary frame of reference can be get when ω = 0, [18].

The other task left is expressing individual 0dq elements of λ_{0dqs} and λ_{0dqr} in terms of 0dq currents, will be performed next;

Recalling eqn.(3-62);

$$\begin{bmatrix} \underline{\lambda}_{0dqs} \\ \underline{\lambda}_{0dqr} \end{bmatrix} = \begin{bmatrix} \underline{L}_{s0dq} & \underline{L}_{m0dq} \\ \underline{L}_{m0dq} & \underline{L}_{r0dq} \end{bmatrix} \begin{bmatrix} \underline{i}_{0dqs} \\ \underline{i}_{0dqr} \end{bmatrix},$$

And it can be expanded as;

$$\begin{bmatrix} \lambda_{0s} \\ \lambda_{ds} \\ \lambda_{qs} \\ \lambda_{0r} \\ \lambda_{dr} \\ \lambda_{qr} \end{bmatrix} = \begin{bmatrix} l_s & 0 & 0 & 0 & 0 & 0 \\ 0 & l_s + \mathrm{M} & 0 & 0 & \mathrm{M} & 0 \\ 0 & 0 & l_s + M & 0 & 0 & M \\ 0 & 0 & 0 & l_r & 0 & 0 \\ 0 & \mathrm{M} & 0 & 0 & l_r + \mathrm{M} & 0 \\ 0 & 0 & M & 0 & 0 & l_r + M \end{bmatrix} \begin{bmatrix} i_{0s} \\ i_{ds} \\ i_{qs} \\ i_{0r} \\ i_{dr} \\ i_{qr} \end{bmatrix},$$

From the above equation it can be observed that;

$$\begin{aligned} \lambda_{qs} &= (l_s + M)i_{qs} + Mi_{qr} & \lambda_{qr} &= Mi_{qs} + (l_r + M)i_{qr} \\ \lambda_{ds} &= (l_s + M)i_{ds} + Mi_{dr} & \lambda_{dr} &= Mi_{ds} + (l_r + M)i_{dr} \end{aligned}, \qquad (3\text{-}71)$$

Substitution of these terms into (3-70) results the following;

$$\begin{bmatrix} v_{0s} \\ v_{ds} \\ v_{qs} \\ v_{0r} \\ v_{dr} \\ v_{qr} \end{bmatrix} = \begin{bmatrix} r_s & 0 & 0 & 0 & 0 & 0 \\ 0 & r_s & 0 & 0 & 0 & 0 \\ 0 & 0 & r_s & 0 & 0 & 0 \\ 0 & 0 & 0 & r_r & 0 & 0 \\ 0 & 0 & 0 & 0 & r_r & 0 \\ 0 & 0 & 0 & 0 & 0 & r_r \end{bmatrix} \begin{bmatrix} i_{0s} \\ i_{ds} \\ i_{qs} \\ i_{0r} \\ i_{dr} \\ i_{qr} \end{bmatrix} + \begin{bmatrix} l_s & 0 & 0 & 0 & 0 & 0 \\ 0 & l_s + M & 0 & 0 & M & 0 \\ 0 & 0 & l_s + M & 0 & 0 & M \\ 0 & 0 & 0 & l_r & 0 & 0 \\ 0 & M & 0 & 0 & l_r + M & 0 \\ 0 & 0 & M & 0 & 0 & l_r + M \end{bmatrix} \begin{bmatrix} i_{0s} \\ i_{ds} \\ i_{qs} \\ i_{0r} \\ i_{dr} \\ i_{qr} \end{bmatrix} - \begin{bmatrix} 0 \\ \omega[(l_s + M)i_{qs} + Mi_{qr}] \\ -\omega[(l_s + M)i_{ds} + Mi_{dr}] \\ 0 \\ (\omega - \omega_m)[Mi_{qs} + (l_r + M)i_{qr}] \\ -(\omega - \omega_m)[Mi_{ds} + (l_r + M)i_{dr}] \end{bmatrix} \qquad (3\text{-}72)$$

Then expanding back out the last vector so that it is a product of a matrix and a current vector, and changing the sign of the last matrix by multiplying it by the negative sign gives;

$$\begin{bmatrix} v_{0s} \\ v_{ds} \\ v_{qs} \\ v_{0r} \\ v_{dr} \\ v_{qr} \end{bmatrix} = \begin{bmatrix} r_s & 0 & 0 & 0 & 0 & 0 \\ 0 & r_s & 0 & 0 & 0 & 0 \\ 0 & 0 & r_s & 0 & 0 & 0 \\ 0 & 0 & 0 & r_r & 0 & 0 \\ 0 & 0 & 0 & 0 & r_r & 0 \\ 0 & 0 & 0 & 0 & 0 & r_r \end{bmatrix} \begin{bmatrix} i_{0s} \\ i_{ds} \\ i_{qs} \\ i_{0r} \\ i_{dr} \\ i_{qr} \end{bmatrix} + \begin{bmatrix} l_s & 0 & 0 & 0 & 0 & 0 \\ 0 & l_s + M & 0 & 0 & M & 0 \\ 0 & 0 & l_s + M & 0 & 0 & M \\ 0 & 0 & 0 & l_r & 0 & 0 \\ 0 & M & 0 & 0 & l_r + M & 0 \\ 0 & 0 & M & 0 & 0 & l_r + M \end{bmatrix} \begin{bmatrix} i_{0s} \\ i_{ds} \\ i_{qs} \\ i_{0r} \\ i_{dr} \\ i_{qr} \end{bmatrix}$$

$$+ \begin{bmatrix} 0 & 0 & 0 & 0 & 0 & 0 \\ 0 & 0 & -\omega(l_s + M) & 0 & 0 & -\omega M \\ 0 & 0 & 0 & 0 & \omega M & 0 \\ 0 & \omega(l_s + M) & 0 & 0 & 0 & 0 \\ 0 & 0 & -(\omega - \omega_m)M & 0 & 0 & -(\omega - \omega_m)(l_r + M) \\ 0 & (\omega - \omega_m)M & 0 & 0 & (\omega - \omega_m)(l_r + M) & 0 \end{bmatrix} \begin{bmatrix} i_{0s} \\ i_{ds} \\ i_{qs} \\ i_{0r} \\ i_{dr} \\ i_{qr} \end{bmatrix}$$

Notice that in the right hand side of the above matrix, the matrices are multiplying the same vector (the current vector); therefore, these two matrices can be combined. i.e collecting of same terms results in;

$$\begin{bmatrix} v_{0s} \\ v_{ds} \\ v_{qs} \\ v_{0r} \\ v_{dr} \\ v_{qr} \end{bmatrix} = \begin{bmatrix} r_s & 0 & 0 & 0 & 0 & 0 \\ 0 & r_s & -\omega(l_s+M) & 0 & 0 & -\omega M \\ 0 & 0 & r_s & 0 & \omega M & 0 \\ 0 & \omega(l_s+M) & 0 & r_r & 0 & 0 \\ 0 & 0 & -(\omega-\omega_m)M & 0 & r_r & -(\omega-\omega_m)(l_r+M) \\ 0 & (\omega-\omega_m)M & 0 & 0 & (\omega-\omega_m)(l_r+M) & r_r \end{bmatrix} \begin{bmatrix} i_{0s} \\ i_{ds} \\ i_{qs} \\ i_{0r} \\ i_{dr} \\ i_{qr} \end{bmatrix} + \begin{bmatrix} l_s & 0 & 0 & 0 & 0 & 0 \\ 0 & l_s+M & 0 & 0 & M & 0 \\ 0 & 0 & l_s+M & 0 & 0 & M \\ 0 & 0 & 0 & l_r & 0 & 0 \\ 0 & M & 0 & 0 & l_r+M & 0 \\ 0 & 0 & M & 0 & 0 & l_r+M \end{bmatrix} \begin{bmatrix} i_{0s} \\ i_{ds} \\ i_{qs} \\ i_{0r} \\ i_{dr} \\ i_{qr} \end{bmatrix} \quad (3\text{-}73)$$

Finally, the above equations are the complete transformed three phase induction motor voltage equations in terms of "current".

3.2.2.2 *Electromagnetic torque equation for the three phase induction motor*

In relation with the above equations of three phase induction motor modelled while in a dynamic condition, its respective electromagnetic torque produce at any given rotor angle of rotation can be expressed as;

$$T_{em} = \frac{\partial W_c}{\partial \theta_m}, \quad (3\text{-}74)$$

where Wc is the co-energy of the coupling fields associated with the various windings, Θm is the angle in mechanical degrees between the main rotor axis and fixed reference. As stated in the initial steps of this modelling, linear flux-current relation is considered, i.e. no saturation, so that the co-energy Wc of the coupling field equals its energy, W_f; that:

$$T_{em} = \frac{\partial W_f}{\partial \theta_m}, \quad (3\text{-}75)$$

Θm (degrees) = θm/p rad/sec

Where p is number of pole pairs.

$$T_{em} = p\frac{\partial W_f}{\partial \theta_m}, \quad (3\text{-}76)$$

For a linear electromagnetic system with J electrical inputs (windings), the total field energy is given by [31];

$$W_f = \frac{1}{2}\sum_{p=1}^{J}\sum_{q=1}^{J} L_{pq}\, i_p\, i_q\ , \tag{3-77}$$

Where Lpq is the winding's self-inductance when p=q and when p ≠ q, it is the mutual inductance between the two windings (the energy stored in the leakage inductances is not a part of the energy stored in the coupling field).

Now back to the previous equations for self and mutual inductances both in the stator and rotor, and between the stator and rotor, substituting it into the energy equation above results in;

$$W_f = \frac{1}{2}\underline{i}_{abcs}^{T}(\underline{L}_s - l_s\underline{U})\underline{i}_{abcs} + \underline{i}_{abcs}^{T}\underline{L}_{sr}\underline{i}_{abcr} + \frac{1}{2}\underline{i}_{abcr}^{T}(\underline{L}_r - l_r\underline{U})\underline{i}_{abcr}\ , \tag{3-78}$$

Substituting (3-76) into (3-77), and observing that dependence on θm only occurs in the middle term, will be;

$$\frac{\partial W_f}{\partial \theta_m} = \frac{\partial}{\partial \theta_m}\underline{i}_{abcs}^{T}\underline{L}_{sr}\underline{i}_{abcr}, \tag{3-79}$$

Then;

$$T_{em} = p\,\frac{\partial}{\partial \theta_m}\underline{i}_{abcs}^{T}\underline{L}_{sr}\underline{i}_{abcr}\ , \tag{3-80}$$

But only Lsr depends on θm, so;

$$T_{em} = p\underline{i}_{abcs}^{T}\frac{\partial \underline{L}_{sr}}{\partial \theta_m}\underline{i}_{abcr}\ , \tag{3-81}$$

When the above differentiation is performed, and with the associated matrix multiplication to show;

$$\begin{aligned} T_{em} = -pL_m\Big\{\Big[i_{as}\Big(i_{ar} - \tfrac{1}{2}i_{br} - \tfrac{1}{2}i_{cr}\Big) + i_{bs}\Big(i_{br} - \tfrac{1}{2}i_{ar} - \tfrac{1}{2}i_{cr}\Big) + i_{cs}\Big(i_{cr} - \tfrac{1}{2}i_{br} - \tfrac{1}{2}i_{ar}\Big)\Big]\, sin\theta_m \\ + \tfrac{\sqrt{3}}{2}[i_{as}(i_{br} - i_{cr}) + i_{bs}(i_{cr} - i_{ar}) + i_{cs}(i_{ar} - i_{br})]cos\theta_m\Big\} \end{aligned} \tag{3-82}$$

When the abc model completed, relation of torque to rotor speed according to:

$$T_{em} = \frac{J}{p}\frac{d\omega_m}{dt} + T_m\ , \tag{3-83}$$

Where J is the inertia of the rotor in kg-m^2 (or joule-sec^2), the first term on the right is the inertial torque, and the second term is the mechanical torque (and has a negative value for generation).

For any purpose, if the torque needs to be expressed in terms of the qd0 quantities, the above equation can be transformed from abc to qd0 axis as follows;

$$\begin{aligned} \underline{i}_{abcs} &= \underline{P}_s^{-1}\underline{i}_{0dqs} \\ \underline{i}_{abcr} &= \underline{P}_r^{-1}\underline{i}_{0dqr} \end{aligned}, \tag{3-84}$$

Substituting the above transformation into the torque equation;

$$T_{em} = p\underline{i}_{abcs}^{T}\frac{\partial}{\partial\theta_m}\underline{L}_{sr}\underline{i}_{abcr} = p\left(\underline{P}_s^{-1}\underline{i}_{0dqs}\right)^{T}\frac{\partial}{\partial\theta_m}\underline{L}_{sr}\underline{P}_r^{-1}\underline{i}_{0dqr}\,, \tag{3-85}$$

$$\underline{P}_s = \sqrt{\frac{2}{3}}\begin{bmatrix} \frac{1}{\sqrt{2}} & \frac{1}{\sqrt{2}} & \frac{1}{\sqrt{2}} \\ \cos\theta & \cos(\theta-120) & \cos(\theta+120) \\ \sin\theta & \sin(\theta-120) & \sin(\theta+120) \end{bmatrix},$$

$$\underline{P}_s^{-1} = \sqrt{\frac{2}{3}}\begin{bmatrix} \frac{1}{\sqrt{2}} & \cos(\theta) & \sin(\theta) \\ \frac{1}{\sqrt{2}} & \cos(\theta-120) & \sin(\theta-120) \\ \frac{1}{\sqrt{2}} & \cos(\theta+120) & \sin(\theta+120) \end{bmatrix},$$

$$\underline{L}_{sr} = L_{sr}\begin{bmatrix} \cos\theta_m & \cos(\theta_m+120) & \cos(\theta_m-120) \\ \cos(\theta_m-120) & \cos\theta_m & \cos(\theta_m+120) \\ \cos(\theta_m+120) & \cos(\theta_m-120) & \cos\theta_m \end{bmatrix},$$

$$T_{em} = p\left(\sqrt{\frac{2}{3}}\begin{bmatrix} \frac{1}{\sqrt{2}} & cos\theta & sin\theta \\ \frac{1}{\sqrt{2}} & cos(\theta-120) & sin(\theta-120) \\ \frac{1}{\sqrt{2}} & cos(\theta+120) & sin(\theta+120) \end{bmatrix}\begin{bmatrix} i_{0s} \\ i_{ds} \\ i_{qs} \end{bmatrix}\right)^{T} \times$$

$$\frac{\partial}{\partial\theta_m}\left\{L_{sr}\begin{bmatrix} cos\theta_m & cos(\theta_m+120) & cos(\theta_m-120) \\ cos(\theta_m-120) & cos\theta_m & cos(\theta_m+120) \\ cos(\theta_m+120) & cos(\theta_m-120) & cos\theta_m \end{bmatrix}\sqrt{\frac{2}{3}}\begin{bmatrix} \frac{1}{\sqrt{2}} & cos\beta & sin\beta \\ \frac{1}{\sqrt{2}} & cos(\beta-120) & sin(\beta-120) \\ \frac{1}{\sqrt{2}} & cos(\beta+120) & sin(\beta+120) \end{bmatrix}\begin{bmatrix} i_{0r} \\ i_{dr} \\ i_{qr} \end{bmatrix}\right\} \tag{3-86}$$

Substituting M = (3/2)L_{sr}, and solving the above equation gives;

$$T_{em} = \frac{3}{2}pM\left(i_{qs}i_{dr} - i_{ds}i_{qr}\right), \tag{3-87}$$

Recalling that;

$$\lambda_{qs} = (l_s + M)i_{qs} + Mi_{qr} \qquad \lambda_{qr} = Mi_{qs} + (l_r + M)i_{qr}$$
$$\lambda_{ds} = (l_s + M)i_{ds} + Mi_{dr} \qquad \lambda_{dr} = Mi_{ds} + (l_r + M)i_{dr}$$

Substituting the flux linkage expressions into (3-87), and then performing algebraic manipulations, some other expressions may be derived from the above, as follows:

$$T_{em} = \frac{3}{2}p\left(\lambda_{qr}i_{dr} - \lambda_{dr}i_{qr}\right), \quad (3\text{-}88)$$

$$T_{em} = \frac{3}{2}p\left(\lambda_{ds}i_{qs} - \lambda_{qs}i_{ds}\right), \quad (3\text{-}89)$$

$$T_{em} = \frac{3}{2}\frac{L_m}{l_s+L_m}p\left(\lambda_{dr}i_{qs} - \lambda_{qr}i_{ds}\right), \quad (3\text{-}90)$$

$$T_{em} = \frac{3}{2}\frac{L_m}{l_s+L_m}p\left(\lambda_{qs}i_{dr} - \lambda_{ds}i_{qr}\right), \quad (3\text{-}91)$$

Lm here could be replaced by (2/3)M.

3.2.2.3 *Power equations of three phase induction motor*

The real and reactive powers can also be expressed in terms of qd0 quantities by integrating space vector representations of the currents with the qd0 formulas as follows;

For three-phase induction motors, the space vector $Y_s{}^s$ of the stator voltage, current and flux linkage is defined from its phase quantities [18] by;

$$Y_s^s = (\frac{2}{3})(Y_a + \alpha Y_b + \alpha^2 Y_c), \quad (3\text{-}92)$$

where $\alpha = exp(j\ 2\pi/3)$. The above transform is reversible and each phase quantities can be calculated from the space vector by,

$$I_a = Re(Y_s^s),\ I_b = Re(\alpha^2 Y_s^s),\ I_c = Re(\alpha Y_s^s), \quad (3\text{-}93)$$

So that;

$$\bar{\imath}_s = i_a + \frac{j}{\sqrt{3}}(i_b - i_c), \quad (3\text{-}94)$$

This space vector came about as a result of a scaling choice that made, of 2/3. The following expressions can clarify the reason of making this scaling;

Three phase currents can be expressed as;

$$i_a = I_p cos\omega t; \qquad i_b = I_p cos(\omega t - 120); \qquad i_c = I_p cos(\omega t + 120) \quad (3\text{-}95)$$

Where I_p is the peak amplitude of the waveform.

Substitution into the space vector expression above yields:

$$\bar{\imath}_s = I_p cos\omega t + \frac{j}{\sqrt{3}}\Big(I_p cos(\omega t - 120) - I_p cos(\omega t + 120)\Big), \quad (3\text{-}96)$$

Factor out the I_p and also multiply and divide the second term by 2 (to get it to a form recognizable as a trig identity) results in:

$$\bar{\imath}_s = I_p\left[cos\omega t + \frac{2j}{\sqrt{3}}\frac{1}{2}\big(cos(\omega t - 120) - cos(\omega t + 120)\big)\right], \quad (3\text{-}97)$$

Recalling that sin(u)sin(v) = (1/2)[cos(u-v) - cos(u+v)], we can write the above as:

$$\bar{\imath}_s = I_p\left[cos\omega t + \frac{2j}{\sqrt{3}}\big(sin(\omega t)sin(120)\big)\right] = I_p\left[cos\omega t + \frac{2j}{\sqrt{3}}\Big(sin(\omega t)\frac{\sqrt{3}}{2}\Big)\right] = I_p\big[cos\omega t + j\big(sin(\omega t)\big)\big] \quad (3\text{-}98)$$

Taking magnitudes: $|\bar{\imath}_s| = I_p[\cos^2\omega t + \sin^2\omega t] = I_p = |i_a|$

Therefore, we can write: $\bar{\imath}_s = I_p e^{j\omega t} e^{j\theta_i}$

Now expression of power in qd0 quantities can be derived as follows;

$$P = 3V_{rms}I_{rms}cos\varphi\ , \quad (3\text{-}99)$$

$$Q = 3V_{rms}I_{rms}sin\varphi\ , \quad (3\text{-}100)$$

Where $\varphi=\theta_v - \theta_i$, and with $\theta_v=0$ (the reference), $\varphi = -\theta_i$.

Changing rms values to peak values, and rewriting the equation;

$$P = 3\frac{V_p}{\sqrt{2}}\frac{I_p}{\sqrt{2}}Re\{cos\varphi + jsin\varphi\}\ , \quad (3\text{-}101)$$

$$Q = 3\frac{V_p}{\sqrt{2}}\frac{I_p}{\sqrt{2}}Im\{cos\varphi + jsin\varphi\}\ , \quad (3\text{-}102)$$

Changing the rectangular to exponential and solving the denominator;

$$P = \frac{3}{2}V_pI_pRe\{e^{j\varphi}\}\ , \quad (3\text{-}103)$$

$$Q = \frac{3}{2}V_pI_pIm\{e^{j\varphi}\}\ , \quad (3\text{-}104)$$

Bring the peak magnitudes inside the Re and Im operator; multiply by $e^{j\omega t}$ and by $e^{-j\omega t}$;

$$P = \frac{3}{2}Re\{V_pe^{j\omega t}I_pe^{-j\omega t}e^{j\varphi}\}, \quad (3\text{-}105)$$

$$Q = \frac{3}{2}Im\{V_pe^{j\omega t}I_pe^{-j\omega t}e^{j\varphi}\}, \quad (3\text{-}106)$$

Replace φ by $-\theta_i$.

$$P = \frac{3}{2} Re\left\{ V_p \underbrace{e^{j\omega t}}_{\bar{v}_s} I_p \underbrace{e^{-j\omega t}}_{\bar{\imath}_s^*} e^{-j\theta_i} \right\} , \tag{3-107}$$

$$Q = \frac{3}{2} Im\left\{ V_p \underbrace{e^{j\omega t}}_{\bar{v}_s} I_p \underbrace{e^{-j\omega t}}_{\bar{\imath}_s^*} e^{-j\theta_i} \right\} , \tag{3-108}$$

When the space vectors inside the curly brackets are observed. Therefore:

$$P = \frac{3}{2} \mathrm{Re}\{\bar{v}\bar{\imath}^*\} ,$$

$$Q = \frac{3}{2} \mathrm{Im}\{\bar{v}\bar{\imath}^*\} ,$$

(Note: The 3/2 is because the transformations are all amplitude invariant but not power invariant.)

Finally a task of substituting qd0 quantities into space-vector power expressions will be performed. A space vector may be decomposed into q-d transformation variables according to;

$$\bar{x}^a = x_d + jx_q , \tag{3-109}$$

Applying this into the stator voltage and current electrical quantities;

$$\bar{\imath}_s = i_{ds} + ji_{qs} , \tag{3-110}$$

$$\bar{v}_s = v_{ds} + jv_{qs} , \tag{3-111}$$

Substituting these current and voltage expressions to the above power equations;

$$P_s = \frac{3}{2} Re\{\bar{v}_s \bar{\imath}_s^*\} = \frac{3}{2} Re\{(v_{ds} + jv_{qs})(i_{ds} - ji_{qs})\} , \tag{3-112}$$

$$Q_s = \frac{3}{2} Im\{\bar{v}_s \bar{\imath}_s^*\} = \frac{3}{2} Im\{(v_{ds} + jv_{qs})(i_{ds} - ji_{qs})\} , \tag{3-113}$$

After algebraic simplification;

$$P_s = \frac{3}{2} Re\{(v_{ds} i_{ds} - jv_{ds} i_{qs} + jv_{qs} i_{ds} + v_{qs} i_{qs})\} , \tag{3-114}$$

$$Q_s = \frac{3}{2} Im\{(v_{ds} i_{ds} - j v_{ds} i_{qs} + j v_{qs} i_{ds} + v_{qs} i_{qs})\}, \quad (3\text{-}115)$$

Collecting real and imaginary terms gives;

$$P_s = \frac{3}{2} Re\{(v_{ds} i_{ds} + v_{qs} i_{qs}) + j(v_{qs} i_{ds} - v_{ds} i_{qs})\}, \quad (3\text{-}116)$$

$$Q_s = \frac{3}{2} Im\{(v_{ds} i_{ds} + v_{qs} i_{qs}) + j(v_{qs} i_{ds} - v_{ds} i_{qs})\}, \quad (3\text{-}117)$$

Hence the real and reactive powers of the motor in terms of qd0 quantities will have a form of;

$$P_s = \frac{3}{2} (v_{ds} i_{ds} + v_{qs} i_{qs}), \quad (3\text{-}118)$$

$$Q_s = \frac{3}{2} (v_{qs} i_{ds} - v_{ds} i_{qs}), \quad (3\text{-}119)$$

All the previous equations holding for the dynamic operation of a three phase induction motor are implemented to develop block diagram of an induction motor on a simulation software like MATLAB/Simulink. Although there can exist a number of arrangements to construct the software diagram of an induction motor, the following block diagram in figure 3.14 is popularly used to do so, and it becomes a standard of simulation [33], [34], [31].

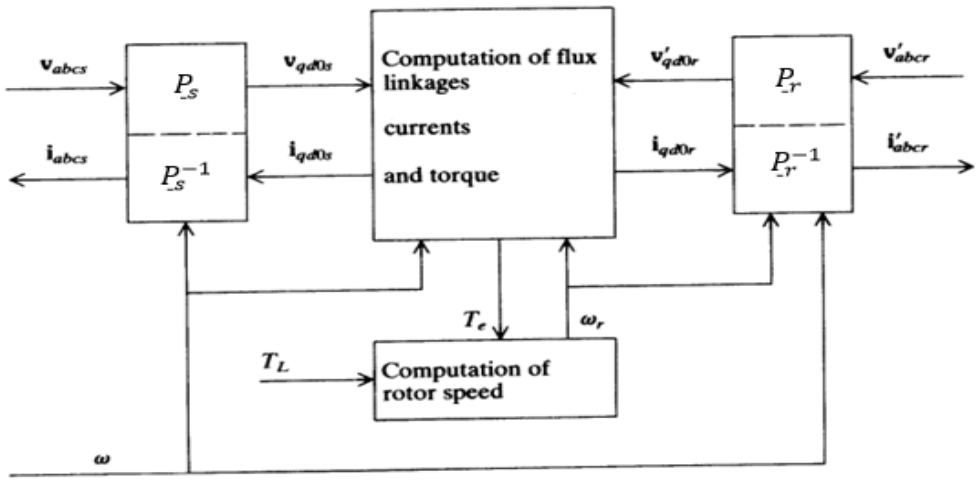

Figure 3-14 Block diagram for simulation of a symmetrical 3-phase induction machine in the arbitrary reference frame [31]

The next figure 3.15 shows the MATLAB/Simulink built in three phase induction motor whose block diagram is expanded above in figure 3.14.

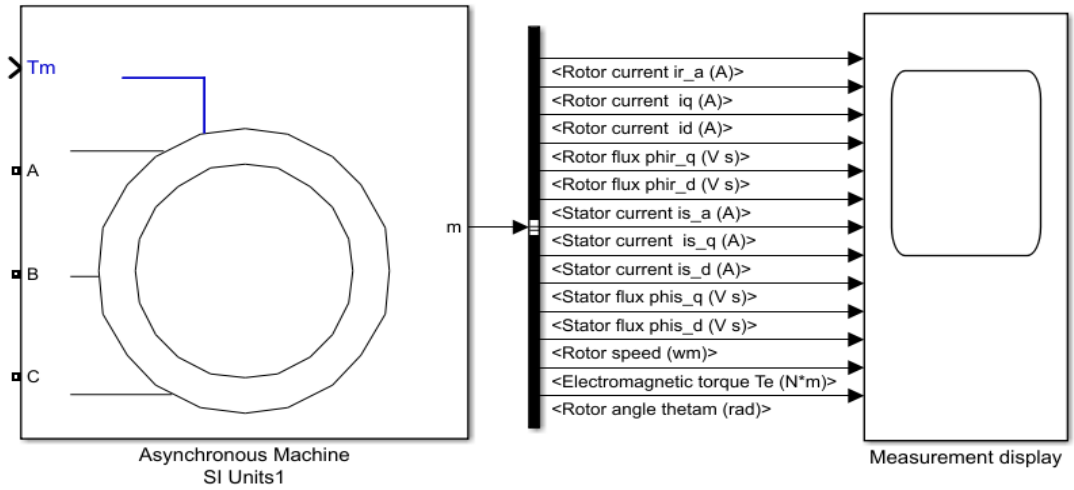

Figure 3-15 Simulink built in model of three phase induction motor

3.2.2.4 *Steady state equations of traction motor/three phase induction motor*

Although the dynamic modelling equations formulated in the previous section are the ones which can appropriately indicate the performance of traction motor, the steady condition of the motor can also be analyzed from its per-phase equivalent circuit model as shown in fig below. Steady state analysis is done by taking an assumption of constant values for rotor angle theta, motor torque, current and voltage.

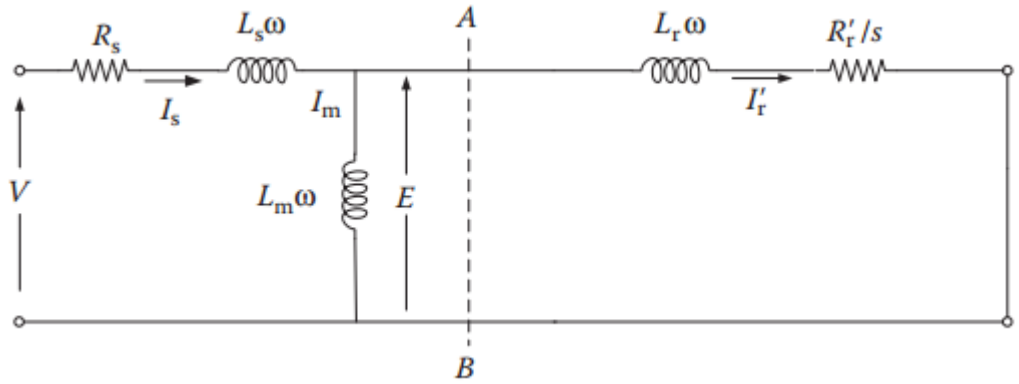

Figure 3-16 Per-phase equivalent circuit model of an induction motor [30]

Where: R_S – Stator resistance,

R_r' – Rotor resistance referred to stator side

L_m – Magnetizing inductance of the motor

L_S – Stator inductance

L_r – Rotor inductance

ω – Angular frequency
S – Slip of the motor

Ls and *Lr* are defined by:

$$Ls = Lls + Lm,\ Lr = Llr + Lm\ , \tag{3-120}$$

Where: L_{ls}- Stator leakage inductance
L_{rs} - Rotor leakage inductance

As in transformers case, for convenience of circuit analysis the stator parameters can be referred to rotor side , or the rotor parameters referred to stator side using the factor of turn ratio, n. The later one is what has done in this modelling. The conversion of referred values to actual values is as follows:

$$\begin{gathered} r_{r(referred)} = \frac{r_r}{n^2} \\ x_{r(referred)} = \frac{x_r}{n^2} \\ I_{r(referred)} = nI_r \\ r_{Load(referred)} = \frac{r_{Load}}{n^2} = \frac{r_r}{n^2}(\frac{1}{s} - 1) = r_{r(referred)}(\frac{1}{s} - 1) \end{gathered} \quad , \tag{3-121}$$

But in the name plate of motors, the referred values of the rotor quantities are directly given for analysis.

From the motor equivalent circuit, the various electrical quantities at steady condition can be calculated by applying laws in circuit analysis as follows;

The impedances of stator, field, and rotor can be expressed as;

$$Z_s = R_s + jL_s\omega, \tag{3-122}$$

$$Z_m = jL_m\omega, \tag{3-123}$$

$$Z_r = \frac{R_r'}{s} + jL_r\omega, \tag{3-124}$$

The driving-point impedance of the circuit is;

$$Z = Z_s + \frac{Z_m Z_r}{Z_m + Z_r}\ , \tag{3-125}$$

The current I_s and I_r' can be calculated as;

$$I_s = \frac{V}{Z} \ , \tag{3-126}$$

And,

$$I_r' = \frac{Z_m}{Z_m + Z_r} I_s \ , \tag{3-127}$$

The total electrical power supplied to the motor for three phases is;

$$P_{elec} = 3I_r'^2 \frac{R_r'}{s} \ , \tag{3-128}$$

The mechanical power of the rotor can be obtained by subtracting the total power loss in the stator as;

$$P_{mech} = P_{elec} - 3I_r'^2 R_r' \ , \tag{3-129}$$

The angular velocity of the rotor, ω_m, is;

$$\omega_m = \frac{2}{P}\omega(1 - s) \ , \tag{3-130}$$

The torque developed by the motor can be determined by;

$$T = \frac{P_{mech}}{\omega_m} \ , \tag{3-131}$$

Figure 3-18 below illustrate torque–slip characteristics of an induction motor with fixed voltage and frequency. s_m is the rated slip of the motor [3].

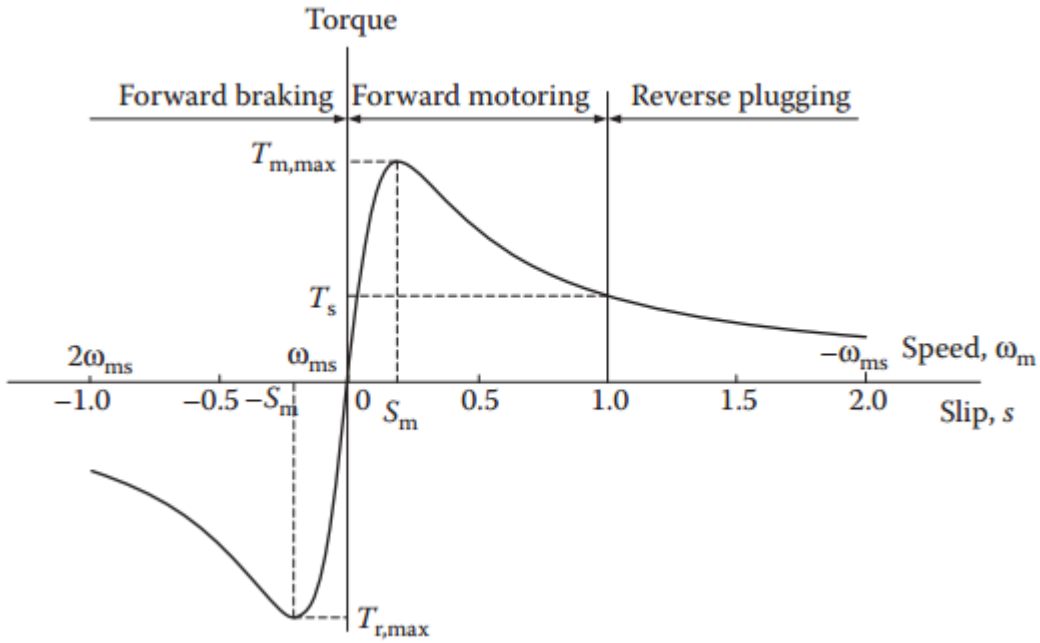

Figure 3-17 Torque–slip characteristics of an induction motor with fixed stator frequency and voltage.

The above speed torque behavior of conventional uncontrolled induction motor cannot be applicable to train traction applications. That is because of having low starting torque, limited speed range, and unstable operation. The high slips corresponding to the maximum torque value are also able to cause high current flowing through windings and that can cause a catastrophe on the motor. Hence, when an induction motor is going to be used for traction purpose, it must be controlled in a way of providing desired speed-torque characteristics [3].

3.2.3 Modelling of v/f speed controller

The traction motor/three phase asynchronous motor used in AA-LRT trams has a scalar speed controller called constant volts by hertz or v/f. This control approach is easy to implement, has relatively low cost, and it works using variables that do not depend each other, however it is taken as poor performance control system when compared to other advanced control techniques [32], [33], [35]. Although simpler kind, the v/f controller has the following advantages [32];

- ✓ Small starting currents.
- ✓ Constant torque in all operation range.

- ✓ Controlling supply voltage can keep the motor in the desired condition whether to accelerate or decelerate.
- ✓ Stability and smoothness of control.

The v/f controller is works by adjustment of the supply voltage to supply frequency ratio in order to keep constant air-gap flux, and avoid flux saturation [32], [36].

The uncontrolled torque – speed curve of induction motor is steeper that the rotor speed and synchronous speed have closer value to the electrical frequency. So, controlling the frequency will control the speed. And based on a phase voltage equation [31];

$$v_{as} = r_s i_{as} + \dot{\lambda}_{as} \,, \tag{3-132}$$

For steady conditions at intermediate to high speeds where in the flux linkage term dominates the resistive term in the voltage equation, the magnitude of the applied voltage is related to the magnitude of the stator flux linkage by;

$$V_s = \omega_e \Lambda_s \,, \tag{3-133}$$

Which suggests that in order to maintain constant flux linkage, the stator voltage magnitude should be proportional to frequency [31].

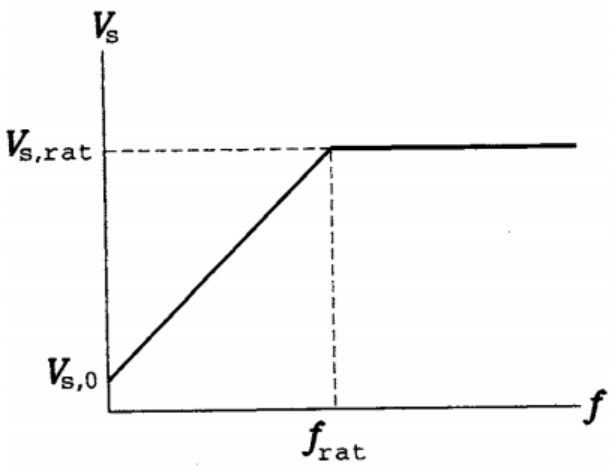

Figure 3-18 Voltage versus frequency relation [35]

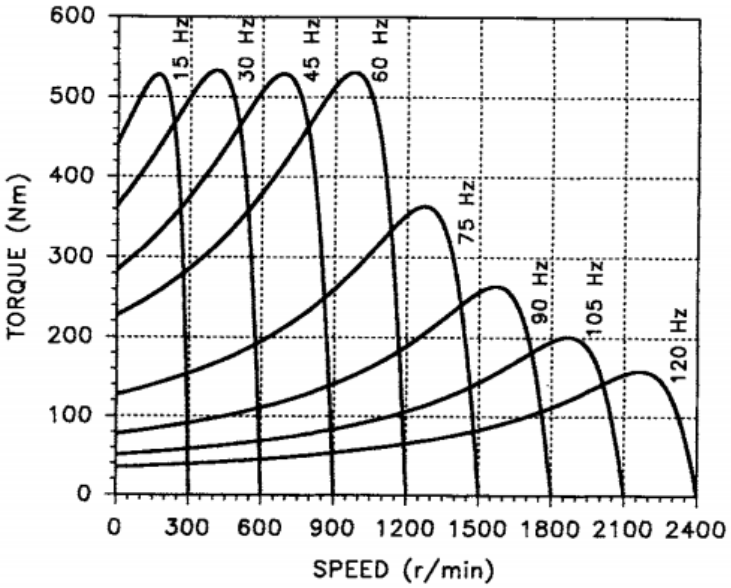

Figure 3-19 Torque speed characteristics of induction motor with v/f control [35].

For traction application, the torque–speed characteristic of an induction motor can be varied by simultaneously controlling the voltage and frequency, by constant volt/hertz control [3].

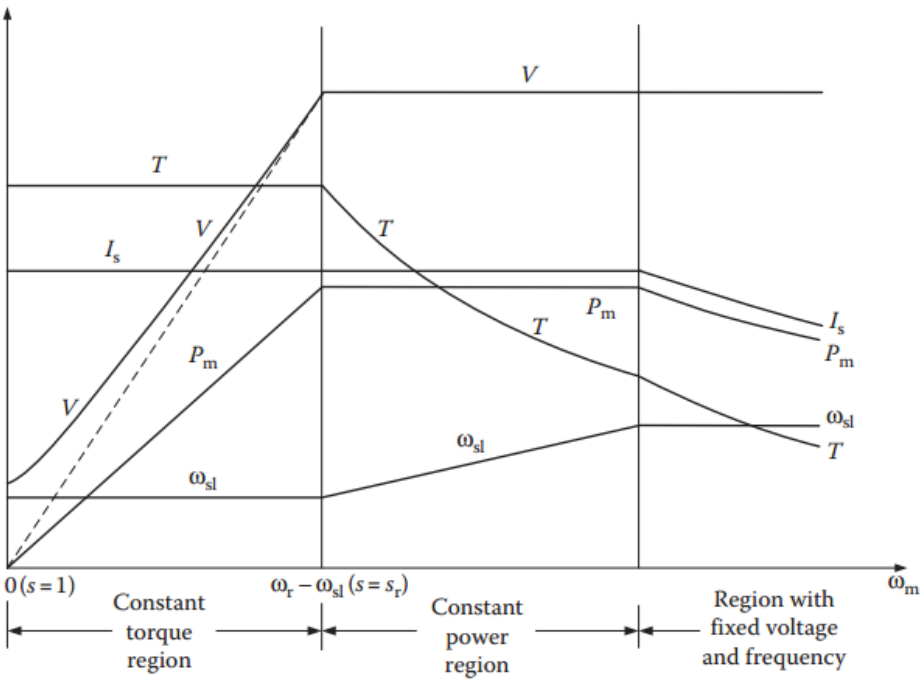

Figure 3-20 Characteristics of induction motors for electric vehicles [37], [3]

It is to mean from the equivalent circuit in Figure 3-16, the field current I_m should be kept constant and equal to its rated value. i.e.

$$I_{mr} = \frac{E}{X_m} = \frac{E_{rated}}{\omega_r L_m}, \tag{3-134}$$

Where I_{mr} is the rated field current, and E_{rated} and ωr are the rated mmf and frequency of the stator, respectively. To maintain a constant flux, the E/ω should be kept constant and equal to E_{rated}/ω_r. Ignoring the voltage drop in the stator impedance Z_S results in a constant V/ω until the frequency and voltage reach their rated values [3].

From the per-phase equivalent circuit, the rotor current can be calculated as;

$$I'_r = \frac{(\omega/\omega_r)E_{rated}}{jL_r\omega + R'_r/s}, \tag{3-135}$$

The torque produced can be computed by;

$$T = \frac{3}{\omega} I'^2_r \, R'_r/s = \frac{3}{\omega}\left[\frac{(\omega/\omega_r)^2 E^2_{rated} R'_r/s}{(R'_r/s)^2 + (L_r\omega)^2}\right], \tag{3-136}$$

The slip s_m corresponding to the maximum torque will be;

$$s_m = \pm\frac{R'_r}{L_r\omega}, \tag{3-137}$$

The maximum torque will be;

$$T_{max} = \frac{3}{2}\frac{E^2_{rated}}{L_r\omega^2_r}, \tag{3-138}$$

While realization of v/f controller, simulation or implementation, for keeping the ratio of voltage to frequency value constant C ($C = V_{rated}/f_{rated}$), an intelligent controller is needed taking the speed error input and generating appropriate output value to make sure that the voltage to frequency ratio is kept. The following block diagram illustrates these method;

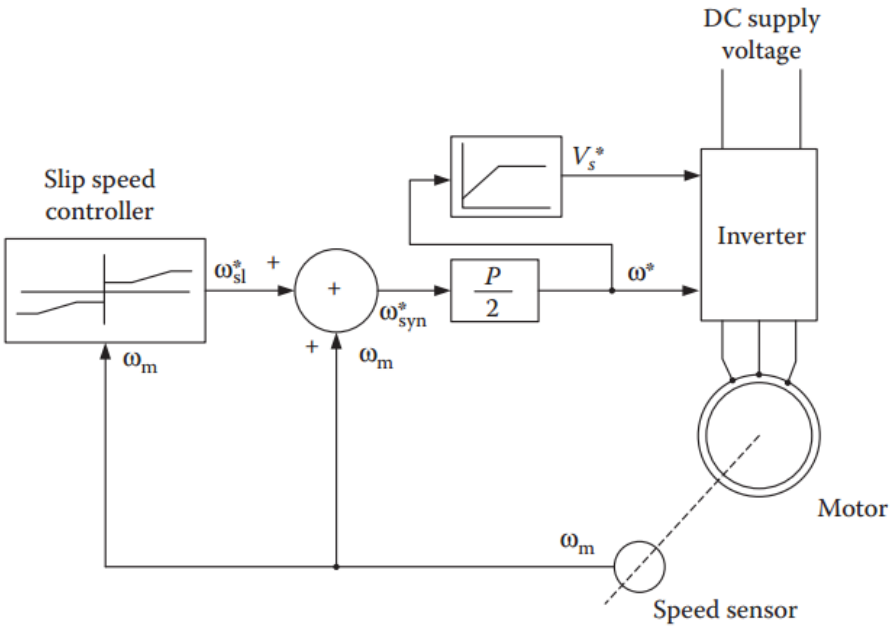

Figure 3-21 General configuration of constant V/f control [38].

As can be seen from the above block diagram the v/f controlling can be implemented with the help of an intelligent controller. The controller does its task in a way that;

- ✓ If the desired speed is less than the measured speed, the controller reduces the command signal to the amplifier or inverter.
- ✓ If the desired speed is greater than measured, the controller increases the command signal.

The command signal can be the amplitude of sine wave in sine triangle modulation inverter.

There are different controllers possibly used for speed control purpose, but the PID (Proportional Integral Derivative) family is most usual kind of controller used for feedback systems. PID controller's best performance, its intuitiveness and relatively simplicity makes it to be used in a wide range of process, and eventually be used like a standard controller in industries [39]. More than 90% of all feedback controllers are PID. Among P, PI, and PID, PI is used in most control loops, because derivative action is not used very often, since computational cost as well as system complexity can be reduced. PI controller is also preferable for systems desiring zero steady state error [40],[32],[39].

As said above, the PI (Proportional Integral) controller is performing its control action by maintaining proportional value of the error in comparison with its past value. The present (Proportional) and Past (Integral) values are computed by the following formula;

$$y(t) = k_p e(t) + k_i \int_0^t e(t)dt \,, \tag{3-139}$$

Where Kp is the proportional gain, Ki is the integral gain, e(t) is the error input to the PI controller and y(t) is the corrected output of the controller. Based on the above equation the PI controller can have the following block diagram.

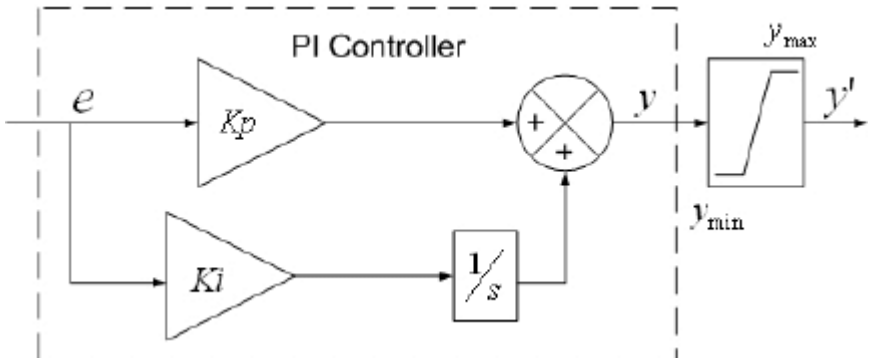

Figure 3-22 Block diagram representation of a PI controller [41].

PI controller can be utilized by varying the proportional and integral gains of the controller until getting the desired control behavior of the system. Although there are automatic control options of tuning the gains, there is are also many laws of tuning set by scholars for getting the appropriate operating point of a PI controller [42], [39], [43].

The PI controller is then selected by the author of these paper for MATLAB/Simulink simulation of speed control of the traction motor using v/f control. The values of the Proportional and Integral controller gain are set at **Kp = 0.1**, and **Ki = 0.01**, a series of simulation in MATLAB/Simulink is conducted to specify their initial point and for tuning the values up to achieving better control action.

3.2.4 Modelling of Traction Converter

With the growth of semiconductor devices technology, it is been possible to manufacture power electronic switches which can pass a high power with large frequency. The advancement of these high power switches is followed by the ease of controlling speed, position and torque control of high power machines including traction motors, fans,

elevators etc. The following figure shows schematics of the signal processing on machines to vary their input parameters amplitude and the frequency of input signal to the machine.

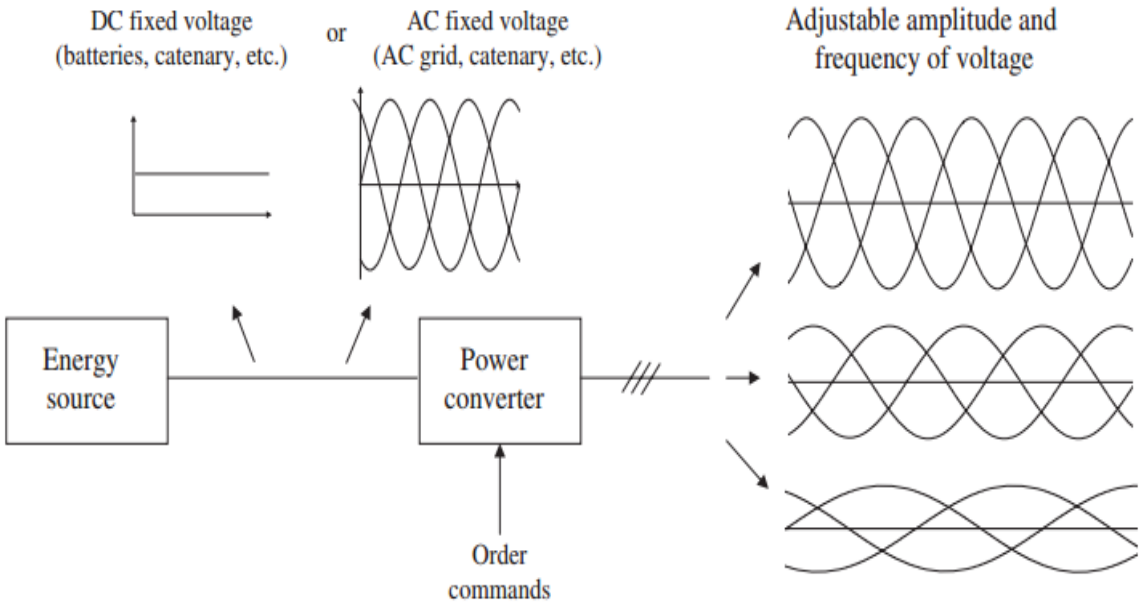

Figure 3-23 Interaction between the energy source and the power converter, to supply the electric machine [30]

These power electronic switches are different in kind according to their material composition, polarity, controllability, triggering strategy, and their respective ratings. In AA-LRT trams, the variable voltage variable frequency input power to traction motors is fed through a three phase two level inverter. An inverter has basically has a function of converting fixed DC signal to variable AC signal. These inverter supplying AC power to AA-LRT trams traction motor is designed using IGBT (Insulated Gate Bipolar Transistors) switches as follows;

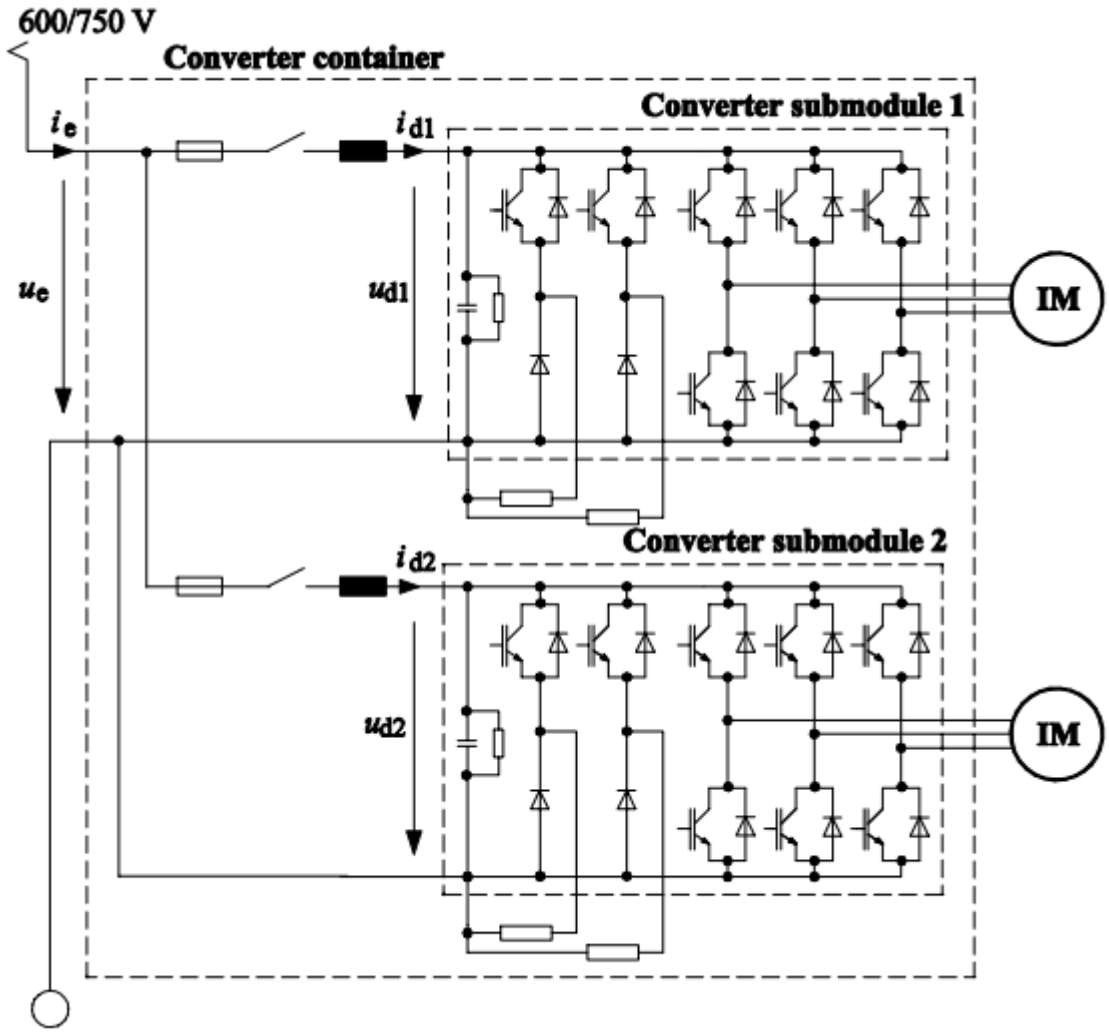

Figure 3-24 Main circuit diagram of a drive unit of a low-floor tramway vehicle (Bombardier Transportation) [44]

AA-LRT trams are using this kind of inverter configuration for traction purpose. This inverter is a two-step bidirectional converter which can allow flow of power both from grid to motor and from motor to grid while braking the train. When the train is braking or when power is transferred from the traction motor to the grid there may happen overvoltage in the DC lines feeding the train unless a storage device is found onboard. By now, there is no storage device onboard of AA-LRT trains so that due to the backed power from the traction motor, if the voltage on the catenary (overhead DC line feeding power to the train) is beyond 900V, it will start dissipating on a resistor (38.4Watts) via the chopper unit as shown in the figure above [6].

The IGBT is a three terminal, voltage controlled power electronic switch used for controlling a signal passing through it by applying a control command via one of its terminals which is the gate terminal. The following figure shows symbol of an IGBT with antiparallel diode.

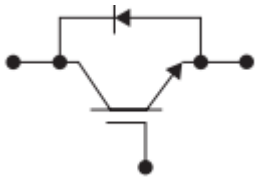

Figure 3-25 Schematic representation of a diode and an IGBT [30]

$\frac{\Delta V}{\Delta t}$, change of voltage with time across the IGBT switch can cause a voltage spike of very high magnitude due to the high switching frequency of the switch. To protect the switch from damaging by these high voltage, an antiparallel diode (1000V, 6A) is used with the IGBT switch [6]. The standard module sizes of an IGBT switch suitable for Light Rail Transit with 750V DC applications are 1700 V, 2400 A [44]. An IGBT switch generally has the following operating specifications [45];

Table 3-4 Ratings of an IGBT semiconductor switch

Device	Voltage/Current Rating	Upper frequency, (Hz)	Switching time (μs)	On-State Resistance (Ω)
IGBTs	2500V/2400A	100K	5-10	2.3m
	1200V/52A	100K	5-10	0.13
	1200V/25A	100K	5-10	0.14
	1200V/80A	100K	5-10	44m
	1800V/2200A	100K	5-10	1.76m

A practical power electronics switch has the following kind of V/I characteristics while it is switching ON and switching OFF [45].

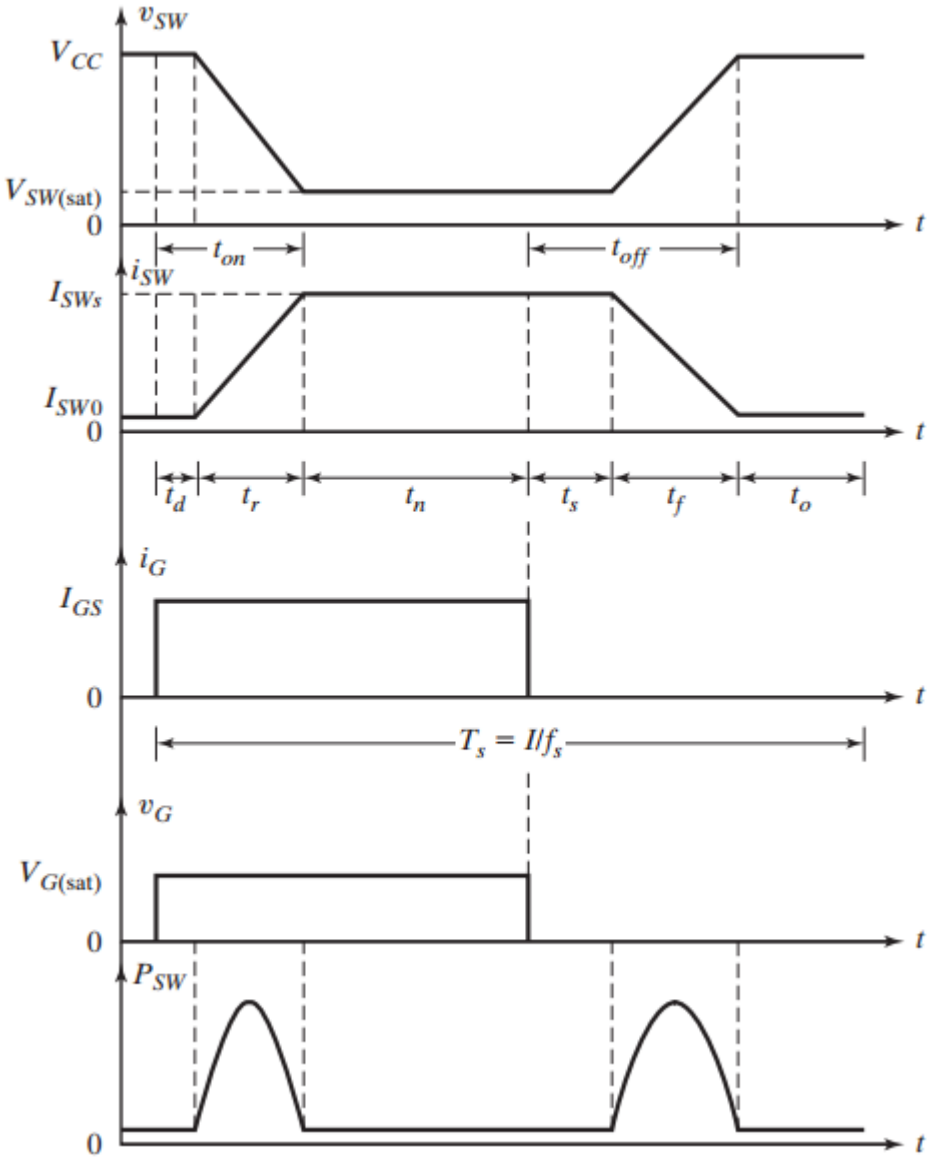

Figure 3-26 Typical waveforms of device voltages and currents [45]

Where V is voltage drop on the switch, I is current flowing through the switch, and P is power dissipated by the switch.

As said in the previous paragraphs, an IGBT switches of the converter needs to be controlled via their gate terminal in order for getting the desired output AC wave form.

The strategy of control may be different based on the application, converter topology, machine topology, nature of the energy source, etc. but the most popular or commonly employed control algorithms are divided into two, namely the Control strategy and the Modulation. The control strategy part does generate voltage references of AC output according to basic control theories, and inputted for the next step, i.e Modulation. The modulation create the switching pattern for the switches based on the voltage references it received from the control strategy. Despite the various switch pattern controlling techniques, sine triangular pulse width modulation (PWM) is exclusively used for volt/hertz controlled induction motor [30], [3].

PWM works triggering of the switches by generating a pattern of switching. The pattern of switching is commanded from the comparator circuit which compares the sine wave from the v/f controller, with the triangular input signal. Then when the sine wave is greater than the triangular wave the upper switch will be ON, when the sine wave is less than the triangular wave the lower switch is ON, as shown in figures below [3], [30], [31], [45].

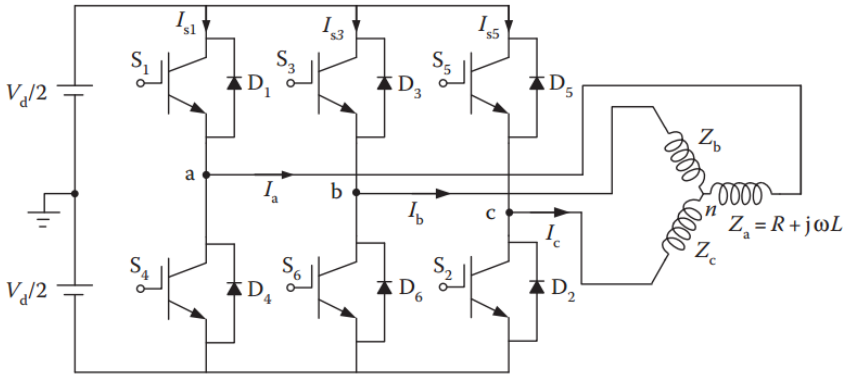

Figure 3-27 Two level inverter connected to load [3]

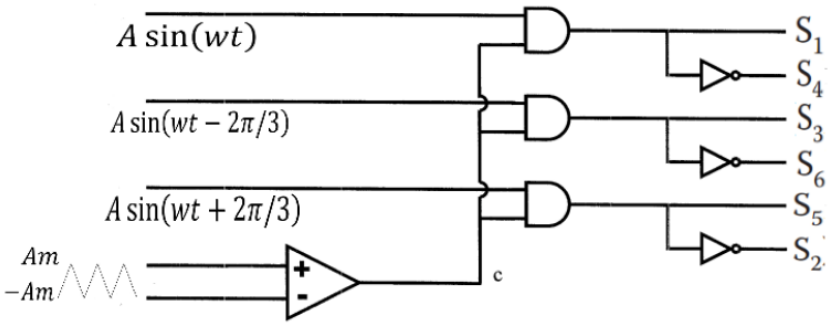

Figure 3-28 Sine triangular PWM [3], [31]

The reference sine wave is called the message signal, and the triangular wave signal is a carrier wave signal of the modulation.

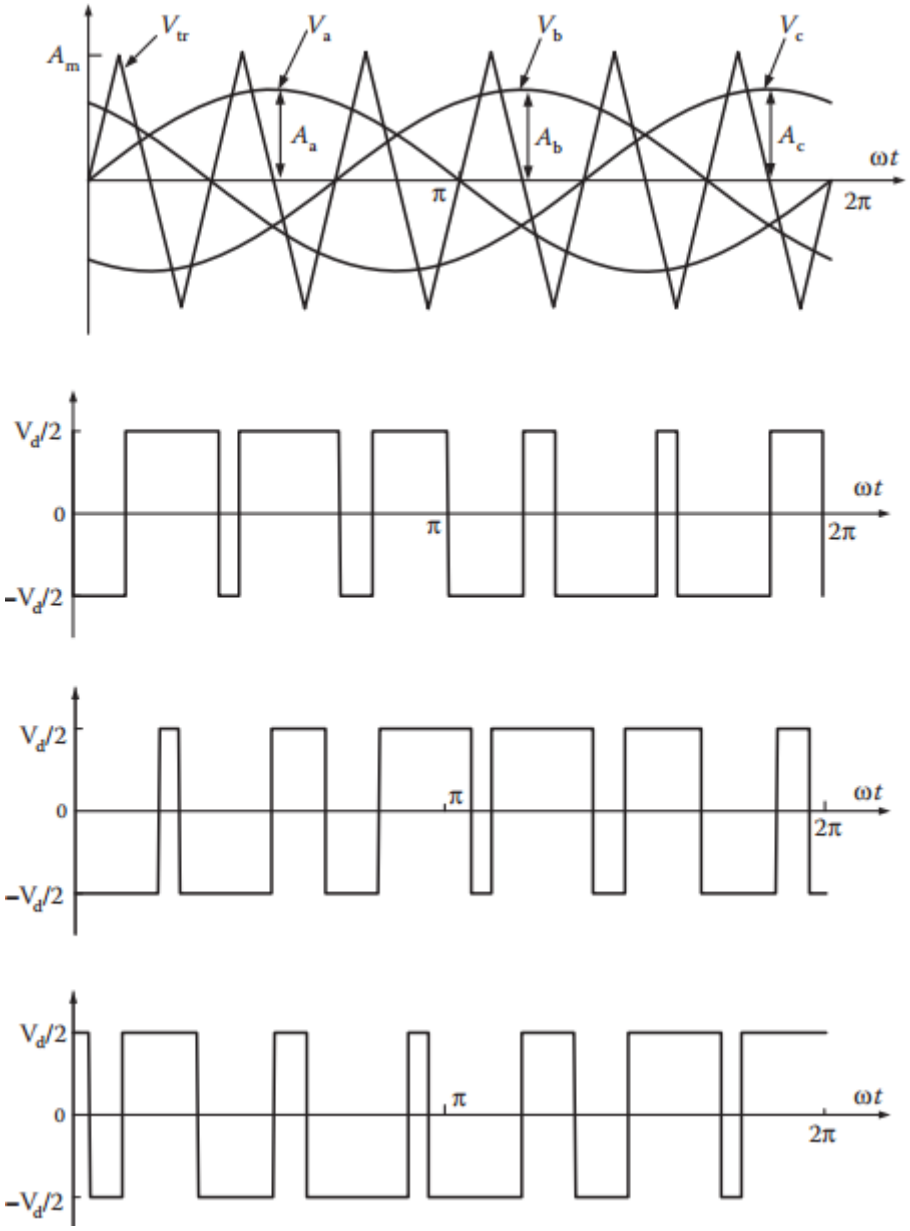

Figure 3-29 Inverter output voltage of phase a, b, c respectively from up to down [3].

The ratio of the amplitude of the reference sine wave (i.e A) to the amplitude of the triangular signal (i.e Am) is called modulation index m.

$$m = \frac{A}{Am} \quad [36], \tag{3-140}$$

The modulation index, m lies always between 0 and 1. It becomes 1 when the motor is allowed to be operating at rated voltage and frequency. If m becomes greater than 1, it is over modulation and causes distortion in the output AC waveform.

The output phase voltage waveform from the inverter, Vao, Vbo, or Vco can be;

$$Vao = m(V_d/2)sin(\omega t)\ , \tag{3-141}$$

The fundamental (rms) component in the phase waveform V_{ao}, V_{bo}, or V_{co} is given by;

$$Vao = m\frac{Vd}{2\sqrt{2}}, \tag{3-142}$$

Note: For modulation index greater than 1 the above formula no longer be valid, and the output will just be [45];

$$Vao = (V_d/2)sin(\omega t)\ \ , \tag{3-143}$$

The inverter used in AA-LRT trams has input of 750V fixed DC, and output of 0 to 500V rms with 0 to 71Hz variable voltage variable frequency output.

3.2.5 Simulation model of AA-LRT trams v/f controlled traction drive

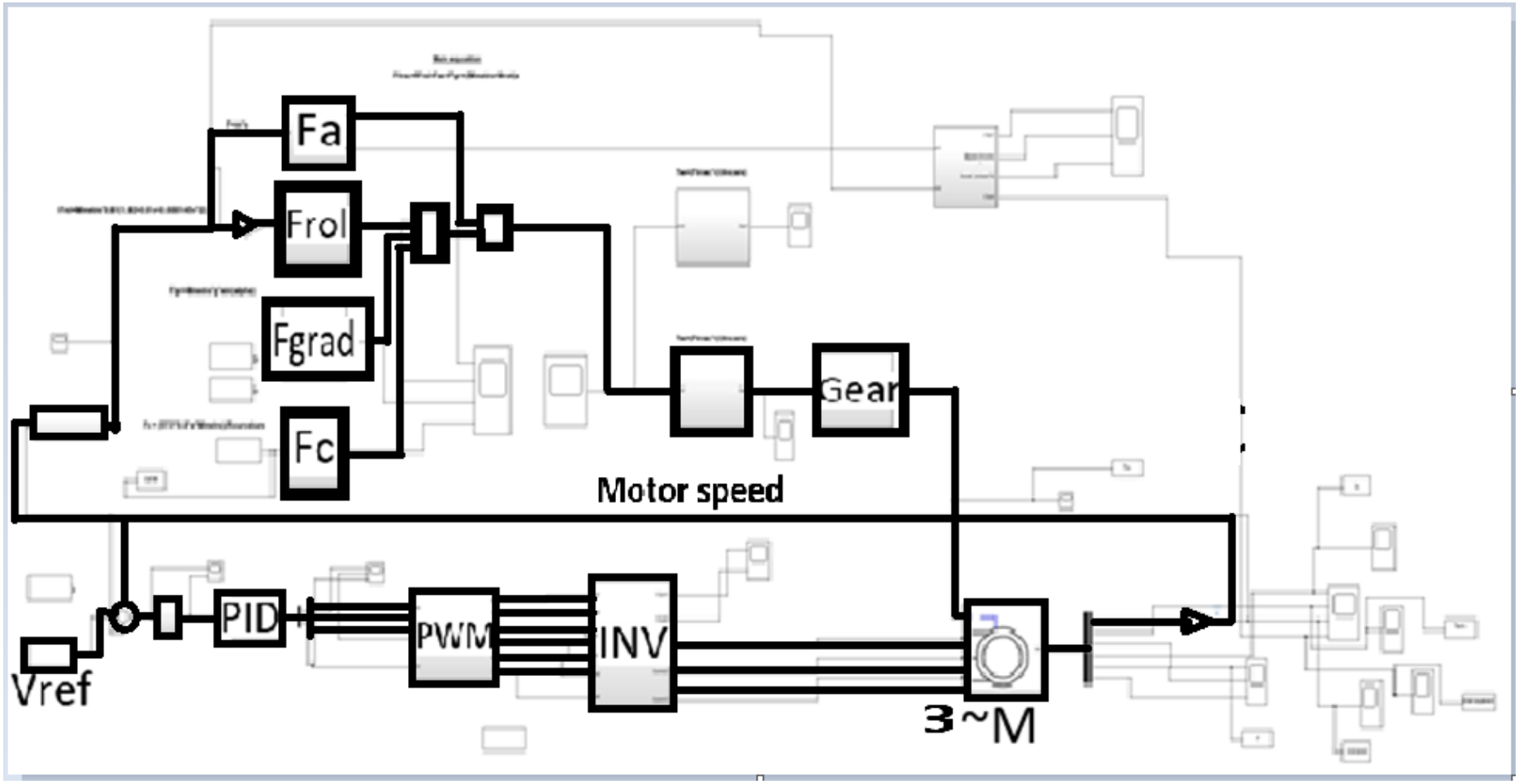

Figure 3-30 Overall simulation diagram of drive system

CHAPTER 4 RESULT ANALYSIS, AND DISCUSSION

The MATLAB/Simulink model of AA-LRT traction drive system that is based on the dynamic model equations developed in the previous chapter, is used to observe the change in motor variables while passenger overloading is happening in AA-LRT trams. As said before, three motor variables are chosen to be analyzed while the load torque imposed on the traction motor is changing. These variables are;

- Motor current (stator)
- The torque of the motor and,
- Speed of the motor (Rotor Speed)

From alteration of those motor variables due to passenger overloading, the impact on the motor is assessed by evaluation of:

- RMS of stator current to observe the load change while passenger overloading is happening while the train is traveling between two passenger stations.
- Performance of the traction motor in terms of its torque and speed characteristics variation with passenger overloading.
- Power consumption of traction motor on its journey by showing both active and reactive power consumption.
- Copper loss on the traction motor (both stator and rotor copper losses).

For separately observing the condition of the traction motor at various loading scenarios in different track geometries, five interstation trips of the train in the North to South line are chosen to be tested on the software. The selection criteria are based on the magnitude of gradient and radius of curvature, and length of slopes as well as the length of curves. Those selected cases are between;

1. NS22 (Abnet) to NS23 (Sebategna), (with 5% grad)
2. NS21 (Darmar) to NS22 (Abnet) (with 4.6% grad)

Those interstation areas listed above are selected of having a relatively higher gradient.

1. NS15 (Meshwalekia) to EW16 (Stadium) (with 52.5meter radius of curvature, and gradient of 4.7%)
2. NS23 (Sebategna) to NS24 (Autobus Tera) (with 52.5 meter radius of curvature)

And the above two interstation track areas are selected of having a relatively shorter radius of curvature with high impact on train movement.

The other selected interstation track area is **NS11 (Nefas Silk 2) to NS12 (Lancha)**, used to observe the train movement conditions while moving in level track areas.

For the simulation, the train speed restriction by AA-LRT operation manual is used to set the maximum possible rpm of the motor as reference speed input of the v/f controller [46]. But the practical train operation speed limit is a bit lower than the designed speed restriction at various track areas.

Acceleration is;

- $\geq 1 m/s^2$ when the train is traveling from 0 to 40km/hr
- $\geq 0.5 m/s^2$ when the train is traveling from 0 to 70km/hr

The running time of the train between two stations is recorded for different hours of the day, for about 3 times and travel time used for simulation is extracted from that data.

In this simulation, the input total mass of the train in Kg is considered;

- 59240 kg at a rated number of passengers (254 people plus mass of car body), called rated passenger load
- 63020 kg at allowed overloaded passenger volume (317 people plus the mass of car body), called permissible passenger overload.
- 66620 kg at improperly overloaded passenger volume (377 people plus the mass of car body), called improper passenger overload.

This simulation calculates the load torque dynamically with change in speed of the motor/train. The train movement resistive forces get speed from rotor actual speed, and the load torque is directly fed to the motor.

In the coming sections, all the results found from the simulation of traction drive system will be provided for all the five interstation cases i.e when the train is travelling from;

1. NS22 (Abnet) to NS23 (Sebategna),
2. NS21 (Darmar) to NS22 (Abnet)
3. NS15 (Meshwalekia) to EW16 (Stadium)
4. NS23 (Sebategna) to NS24 (Autobus Tera)
5. NS11 (Nefas Silk 2) to NS12 (Lancha)

On this section, the figures show various behavior of the traction motor marked with the following line color:

- Red, stands for the behavior when train has ‘Improper passenger load’.
- Black, stands for the behavior when train is carrying ‘Permissible passenger overload’, and
- Green, stands for the behavior when train has ‘Rated passenger load’.

4.1 Train travel from NS22 (Abnet) to NS23 (Sebategna)

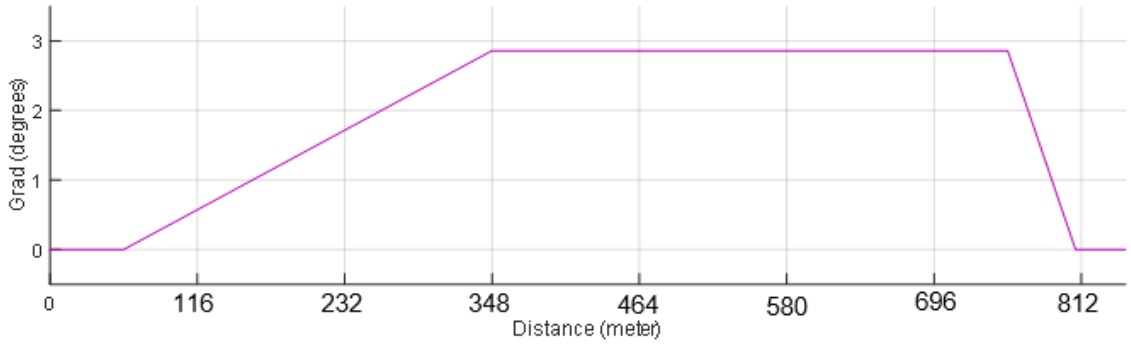

Figure 4-1 Gradient in between Abnet and Sebategna

Figure 4.1 represents signal input of the gradient for the line from Abnet to Sebategna track with the maximum gradient of 5%. The corresponding variation of load torque input (in Nm) to the motor is illustrated in Figure 4.2.

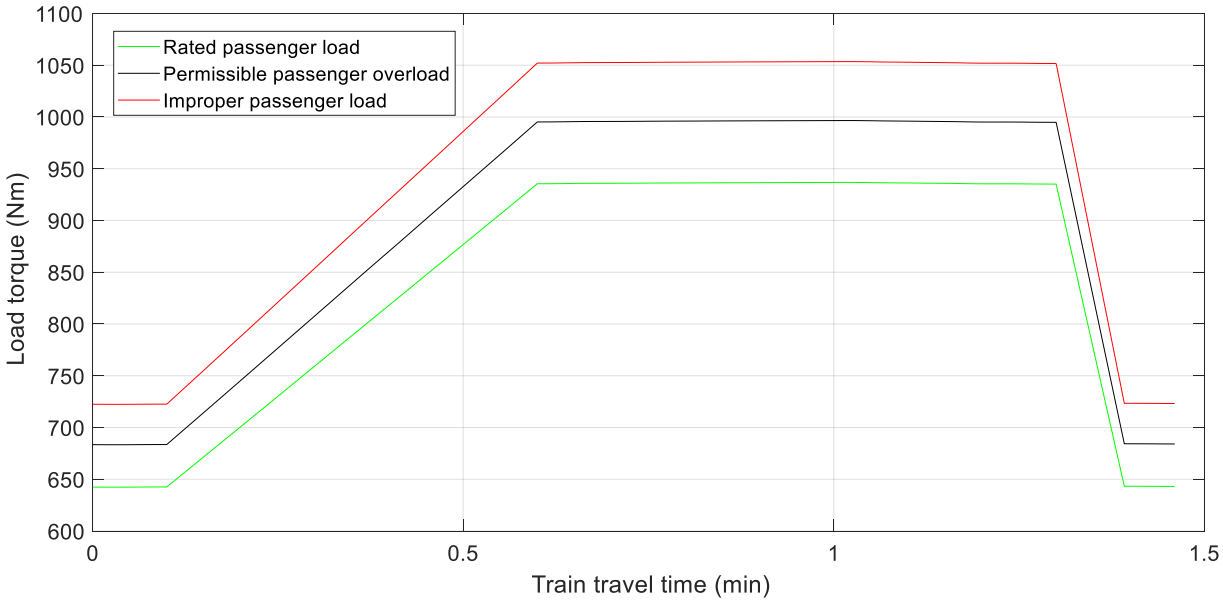

Figure 4-2 Load torque input of traction motor when travelling from Abnet to Sebategna

The following, figure 4.3 shows the sinusoidal current waveform drawn by traction motor when the train is travelling from Abnet to Sebategna. In the figure below three current waveforms (in red, black and green), are showing motor current flow in different passenger loading cases.

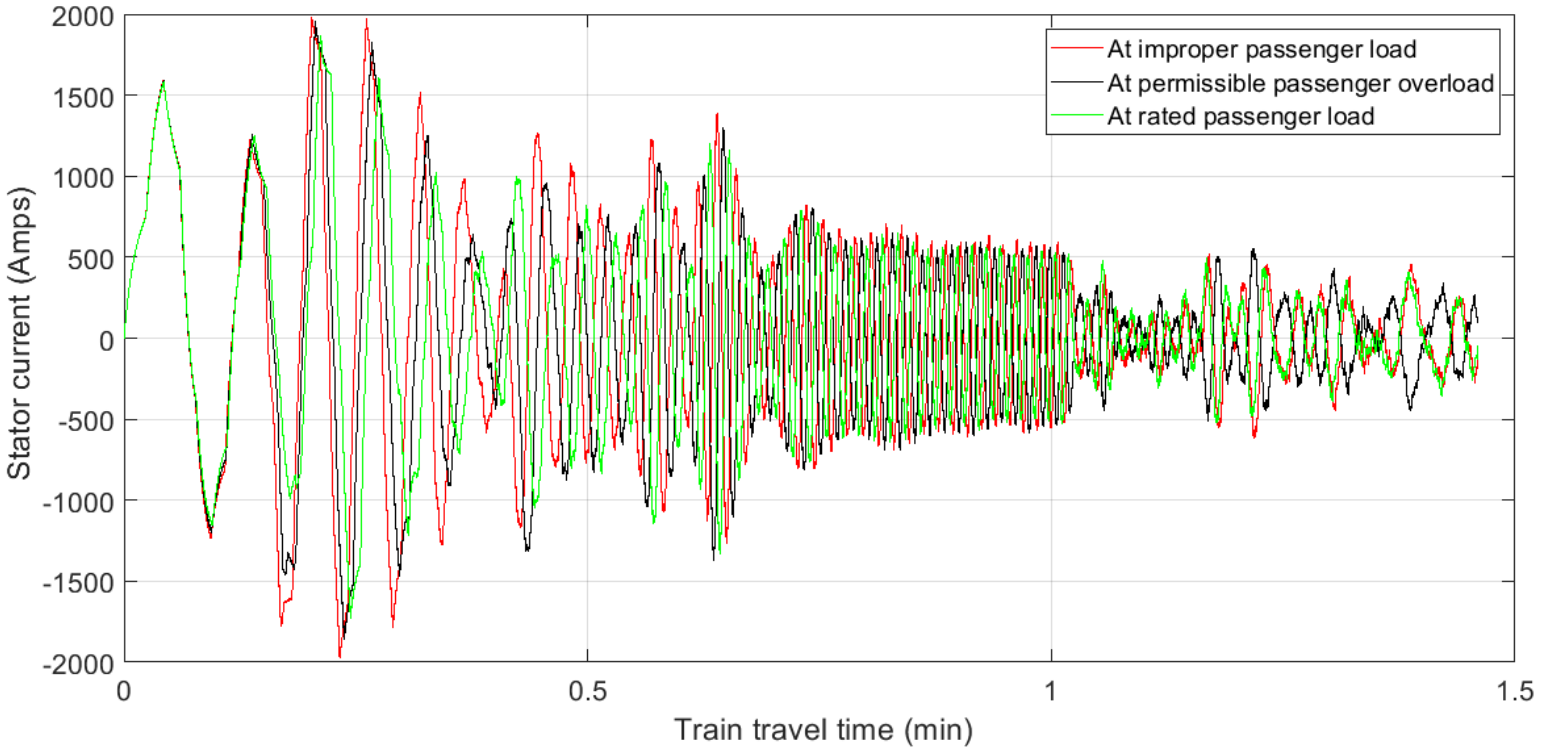

Figure 4-3 Stator current waveform when traveling from Abnet to Sebategna

From the above current waveform it is observed that when the train is loaded by improper number of passengers and accelerating, the peak value of the current in the traction motor exceeds by about 1000A to 500A as compared to the rated passenger load, and the permissible passenger overload respectively.

For comparing the RMS value of motor current in various passenger loading, The RMS of the motor current when the train is travelling from Abnet to Sebategna is shown for the cases in figure 4-4.

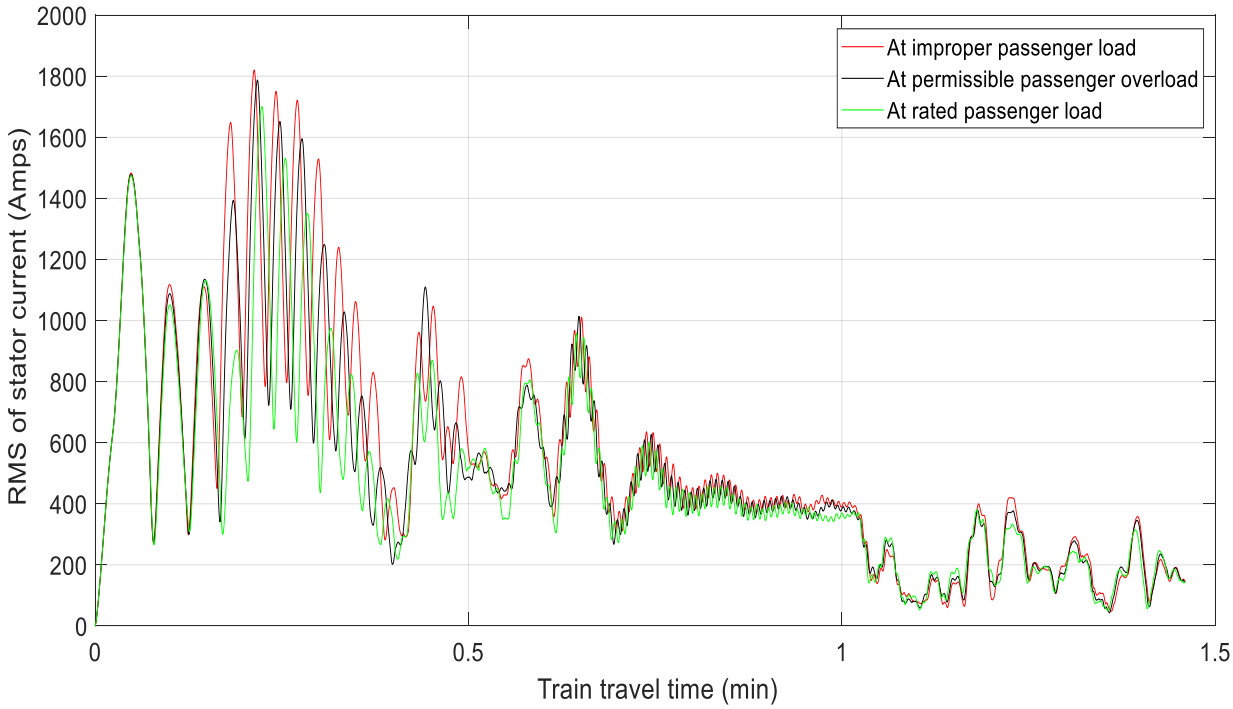

Figure 4-4 RMS of stator current when travelling from Abnet to Sebategna

As seen from the above Figure 4.4, when the train is in acceleration period, it is clearly seen that the RMS of motor current at improper passenger load is about 83.33% greater than the RMS of the motor current for rated passenger load, and about 17.86% greater than in the permissible passenger overload conditions. At the free running, and decelerating region of the train, the RMS of the traction motor is generally higher with less magnitude for improper passenger load case than other passenger load cases.

At this point, it is worth to mention here that the temperature of the windings is directly proportional to load on induction motor, and coil temperature rises in induction motors and is inversely proportional to efficiency of the motor [47]. Thermal stress is one of the major causes for stator winding faults/failures. As a thumb of rule, for every 10^{o} C increase in temperature, the insulation life gets halved due to thermal aging [48].

All the graphs below (in this page) showing relationship of temperature with various motor parameters [47].

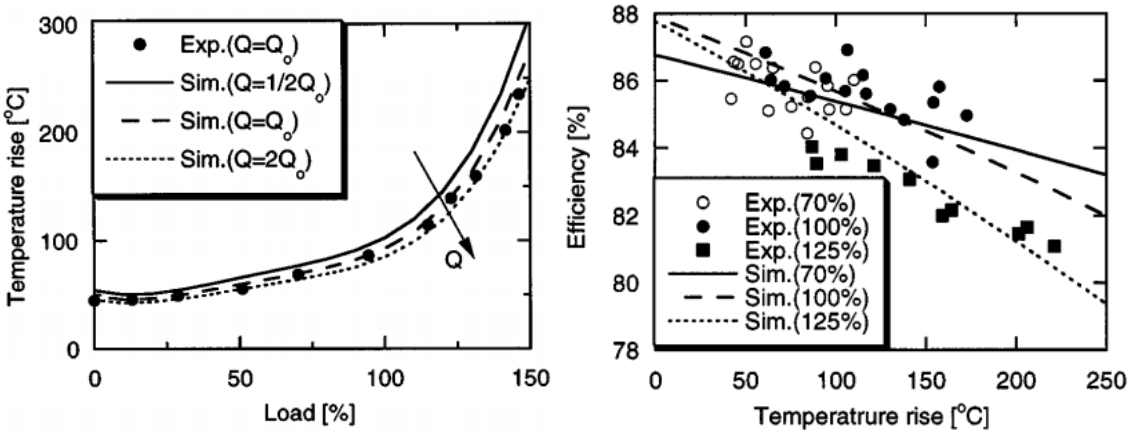

(a) (b)

Figure 4-5 (a). Efficiency variation with cooling airflow rate, (b). Stator coil loss with coil temperature [47]

Where Q stands for flow rate of the outer cooling air, Exp. stands for experiment, and Sim. stands for simulation.

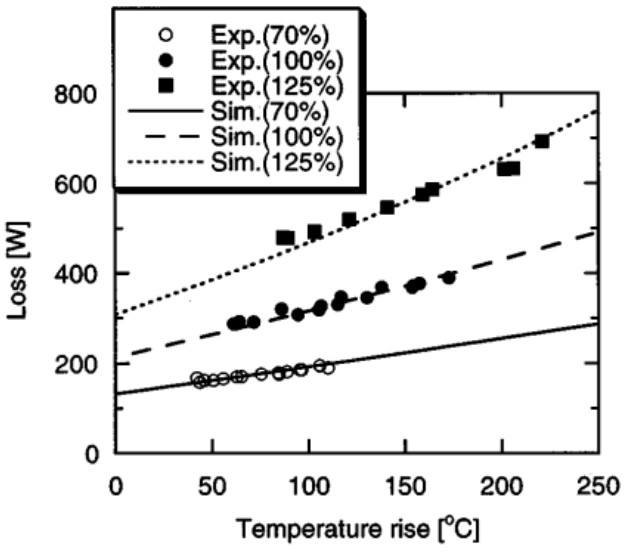

Figure 4-6 Rotor bar loss with coil temperature [47].

The following, Figure 4.7 shows the corresponding electromagnetic torque produced by traction motor when the motor is running from Abnet to Sebategna.

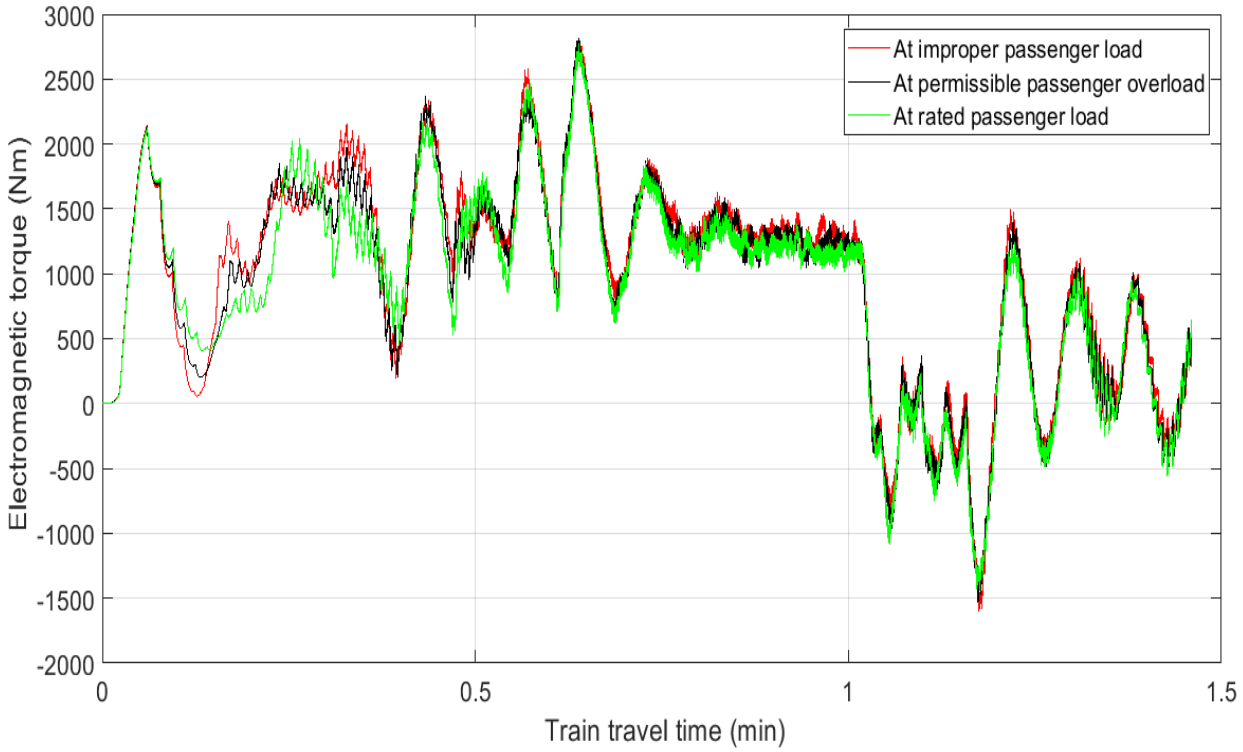

Figure 4-7 Electromagnetic torque, when travelling from Abnet to Sebategna

As can be seen from the graph above, when the train starts accelerating while there is improper passenger load, the electromagnetic torque produced by the traction motor is about 80% less than the torque produced in rated passenger load, and about 60% less than in permissible passenger load. In other periods of train movement, the torque has same behavior for all passenger load conditions other than a small magnitude increment with load.

As illustrated in Figures 4.8 and 4.9, when the train is accelerating, while it has improper passenger load, speed of the traction motor and speed of the train, are decreased as compared to the speed in rated passenger load, and permissible passenger overload. Other than in acceleration period, there observes no difference in speed for the various passenger loading cases.

Figures 4.8 and 4.9 shows speed variation of motor and train when travelling from NS22 to NS23.

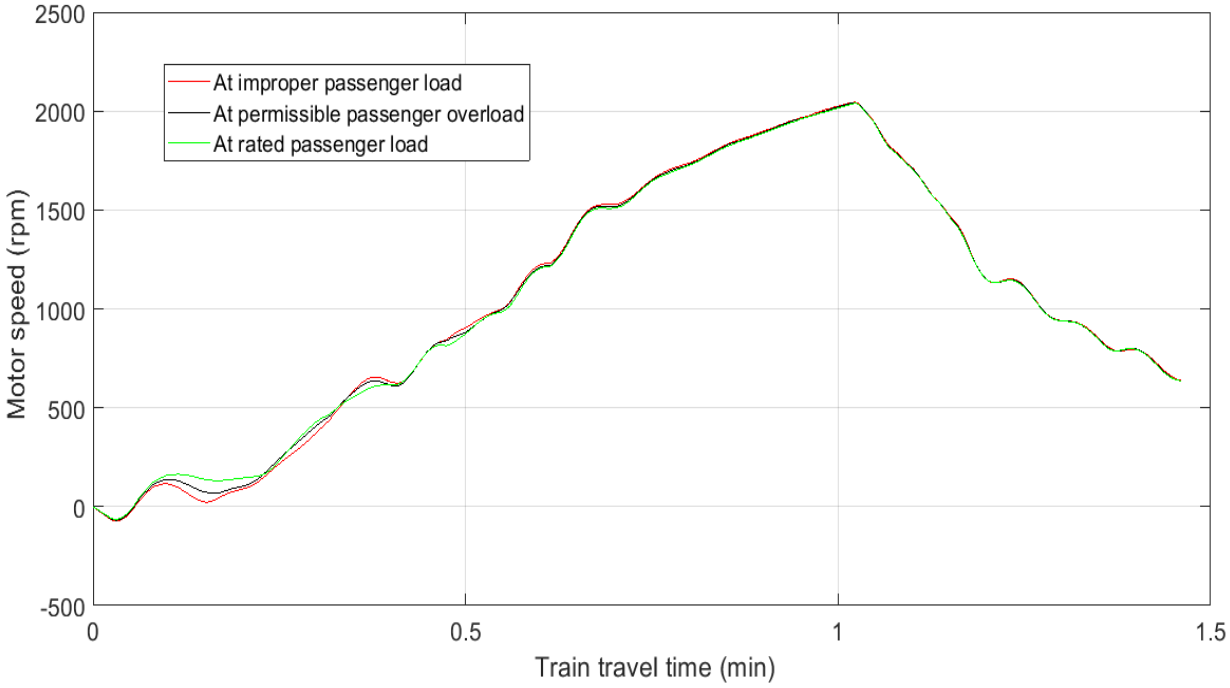

Figure 4-8 Speed of traction motor when train is travelling from Abnet to Sebategna

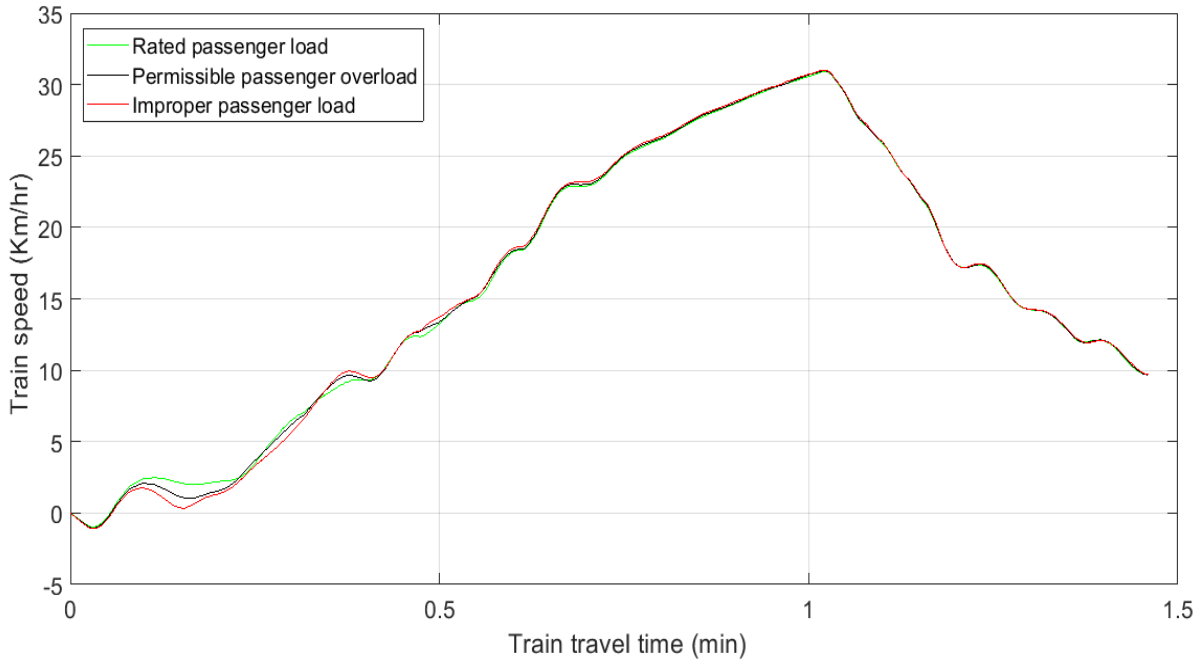

Figure 4-9 Speed of the train when travelling from Abnet to Sebategna

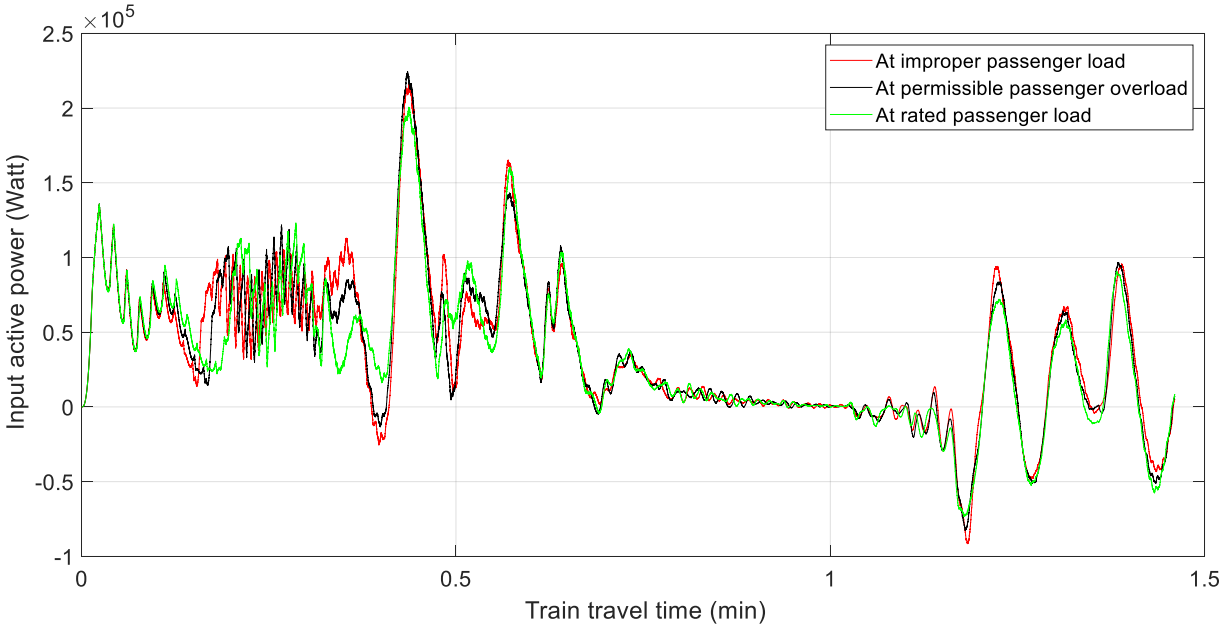

Figure 4-10 Active power input to traction motor when train goes from Abnet to Sebategna

As shown in Figure 4.10 above, during the acceleration period of the train, for few seconds the active power consumption for improper passenger load is about 75% greater than that of rated passenger load, and 25% greater than that of permissible passenger load, but it is almost the same during free running and deceleration period of the train.

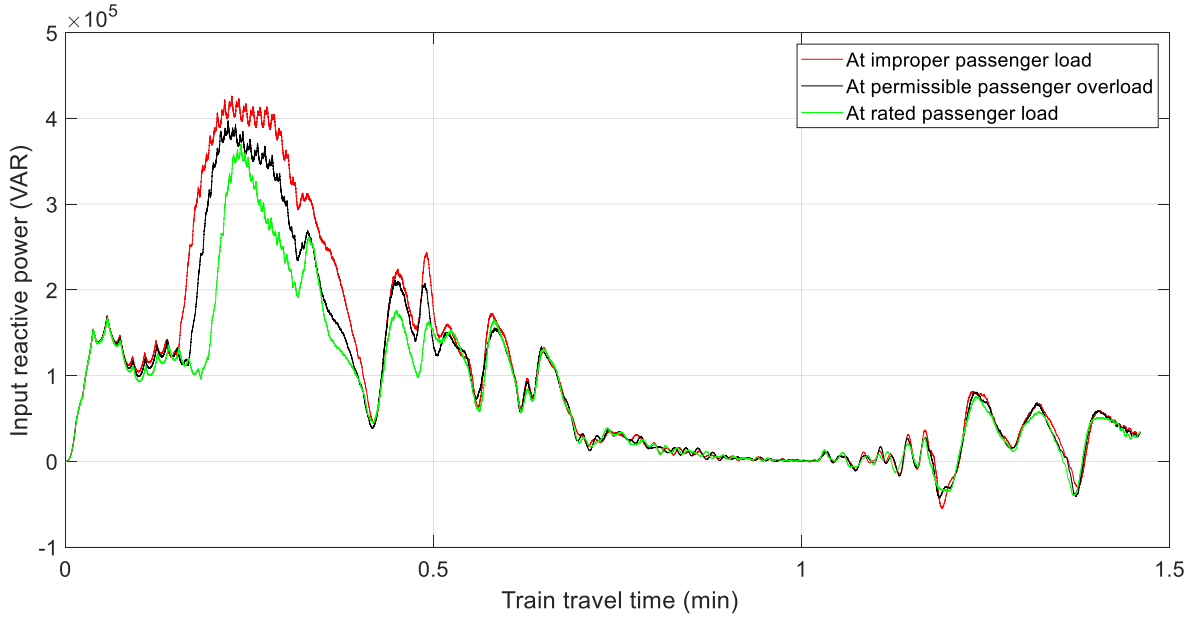

Figure 4-11 Reactive power of traction motor when train goes from NS22 to NS23

When the train is accelerating from Abnet to Sebategna with improper passenger load, the reactive power consumed by the traction motor is about 17.14% greater than that of the rated passenger load, and about 10.8% greater than that of the permissible passenger overload. In the free running and deceleration period of the train, the reactive power consumption due to passenger load has no significant difference.

The below figure shows copper loss in traction when train travelling from NS21 to NS22.

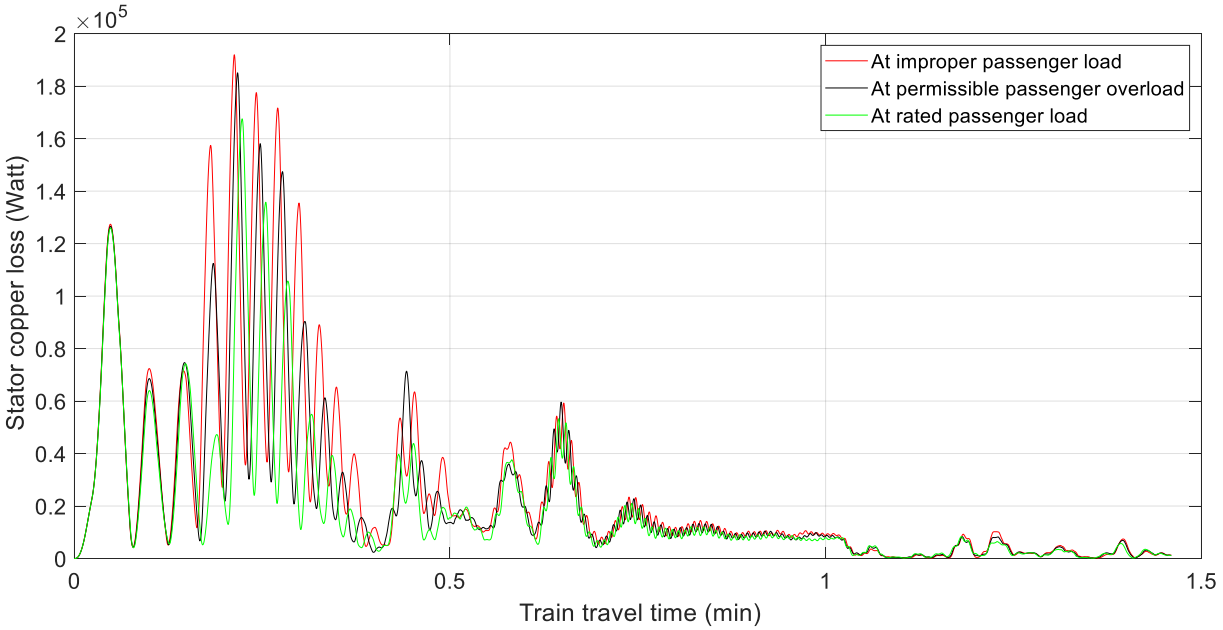

Figure 4-12 Stator copper loss of when train travelling from Abnet to Sebategna

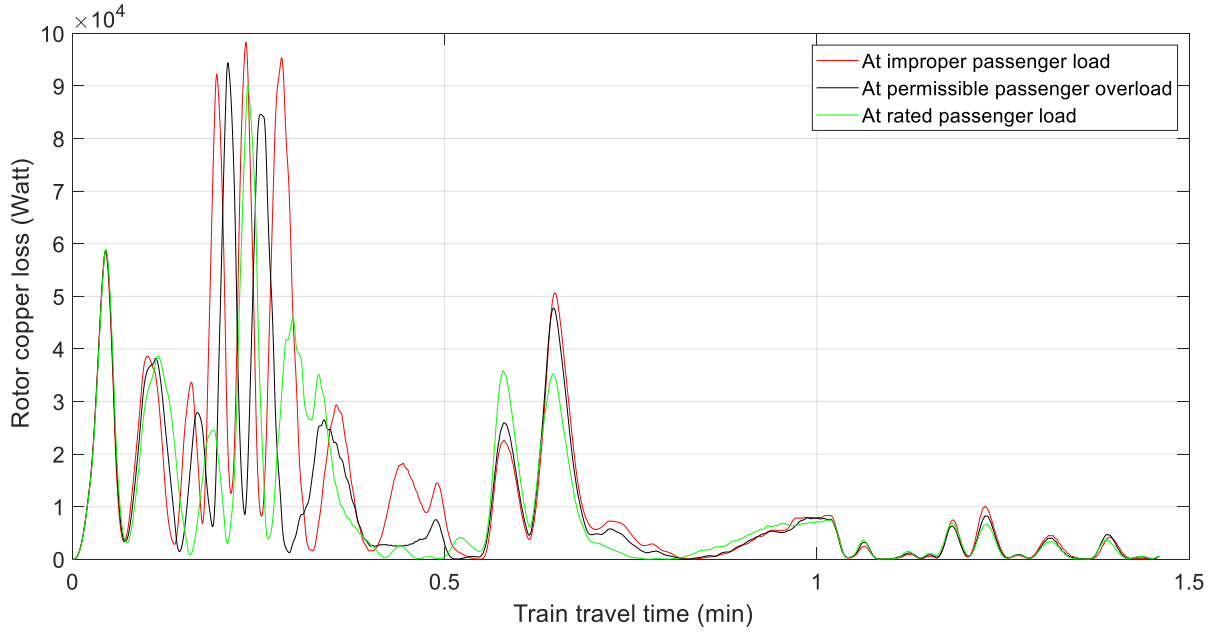

Figure 4-13 Rotor copper loss when train travelling from Abnet to Sebategna

Carrying improper passenger load, when the train is accelerating from Abnet to Sebategna, the traction motor has stator copper loss of 253% greater than the rated passenger load case, and 30.18% greater than that of the permissible passenger overload.

With improper passenger load, when the train is about to finish acceleration period and reach maximum speed, the rotor copper loss is about 50% greater than that of the rated passenger load for the permissible passenger overload conditions.

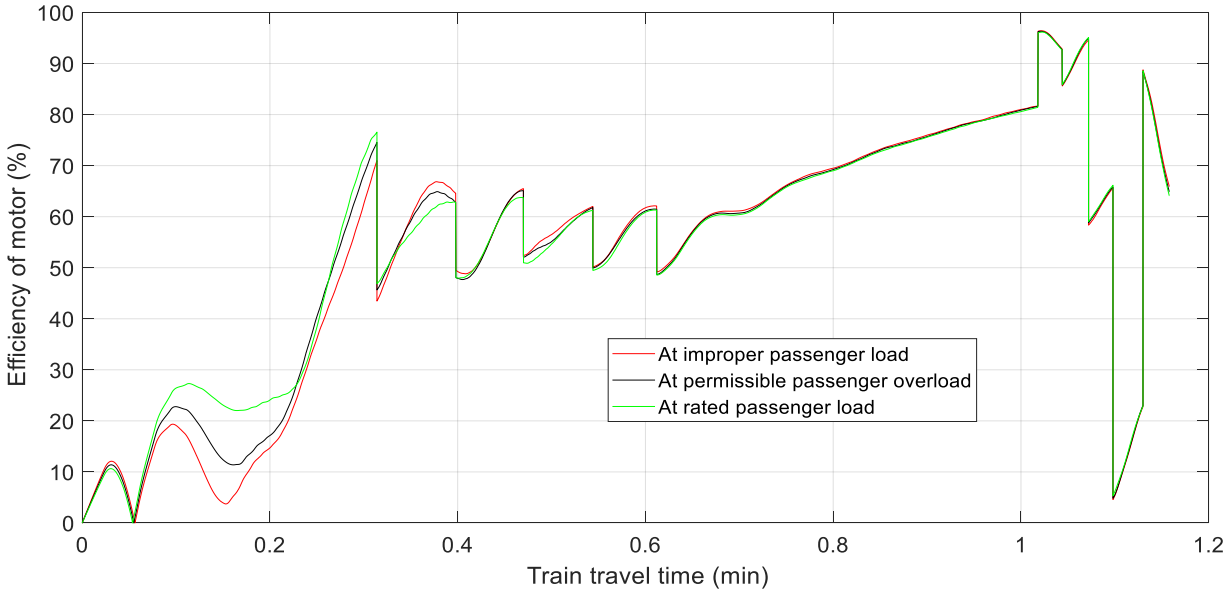

Figure 4-14 Efficiency of traction motor when the train travelling from Abnet to Sebategna

As seen from Figure 4.14, when the train is about starting acceleration having improper passenger load, the efficiency of the traction motor is about 81.8% less than in the rated passenger load, and about 66.7% less than that of permissible passenger overload conditions. In the free running and deceleration periods, the traction motor efficiency is almost the same in all passenger loading conditions.

4.2 Train travel from NS23 (Sebategna) to NS24 (Auto bus tera)

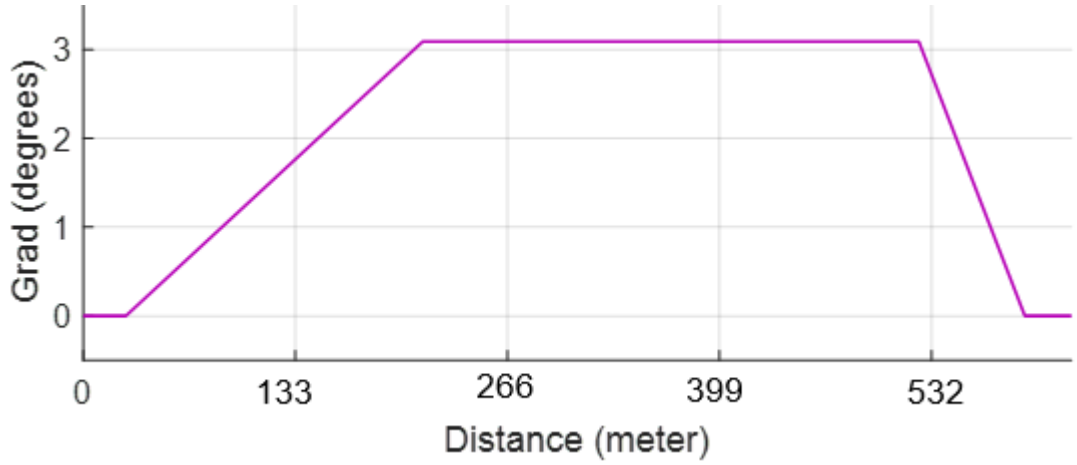

Figure 4-15 Gradient input signal of the track area from Sebategna to Autobus tera

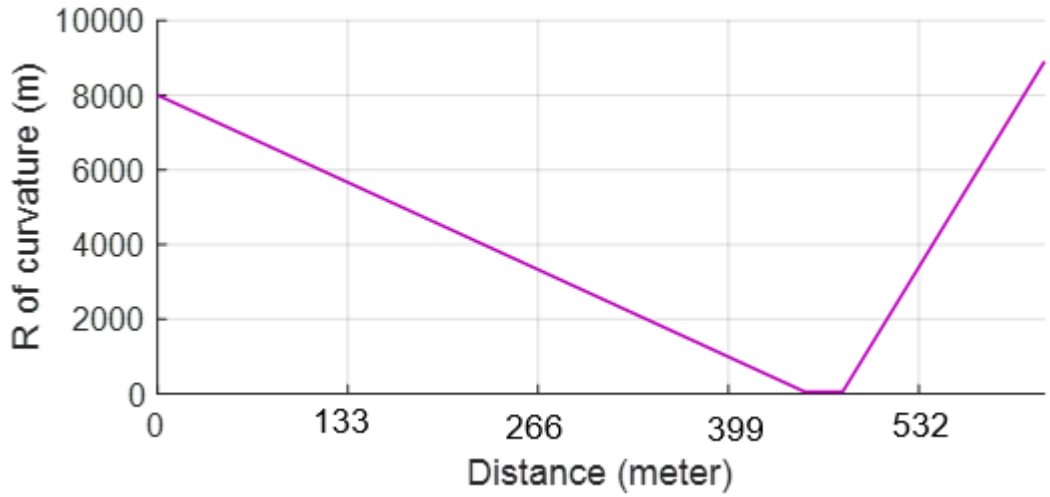

Figure 4-16 Radius of curvature input signal of the track area from Sebategna to Autobus tera

The above Figures 4.15 and 4.16 respectively are used to feed gradient input and radius of curvature input, for the traction motor load torque calculation, when the train is travelling from Sebategna to Autobus tera. Maximum gradient is about 5.4%, and minimum radius of curvature is about 52 m.

The following, Figure 4.17 shows the real time variation of load torque input of the motor when the train is travelling from Sebategna to Autobus tera.

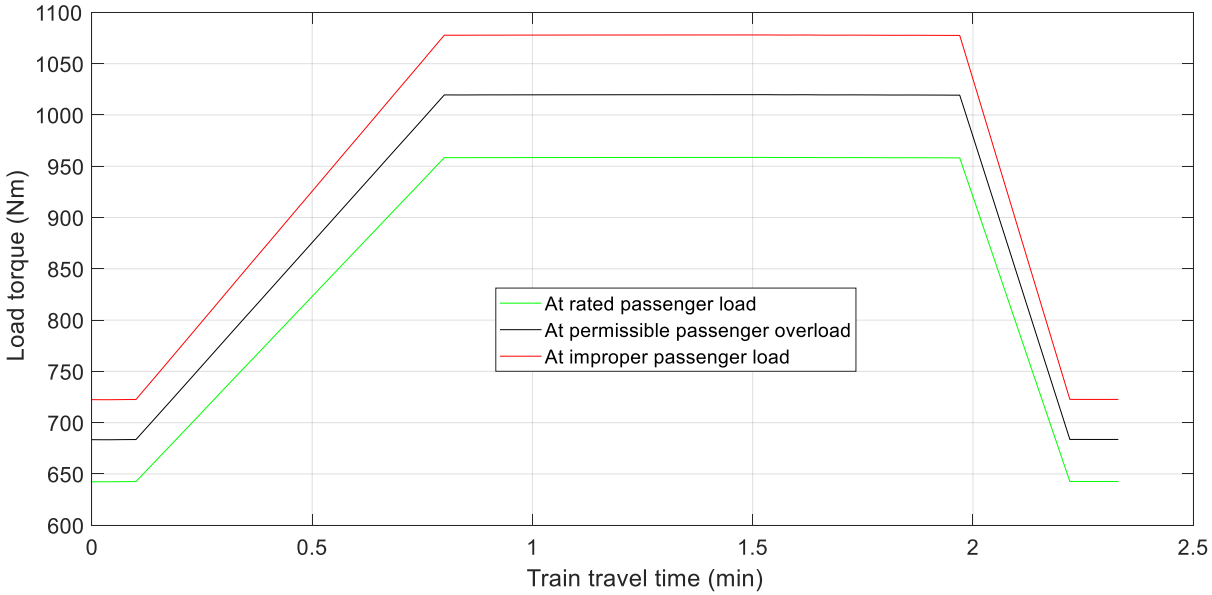

Figure 4-17 Variation of load torque for train travelling from Sebategna to Auto bus tera

As seen above, when the train is travelling from Sebategna to Autobus tera the load torque imposed on the motor is increasing with gradient. The load torque when the train has improper passenger load is about 23.9% greater than in rated passenger load, and about 9% greater than that of the permissible passenger overload.

The following figure shows the sinusoidal current waveform drawn by traction motor when the train is travelling from Sebategna to Autobus tera. In the figure below three current waveforms (in red, black and green), are showing motor current flow in different passenger loading cases.

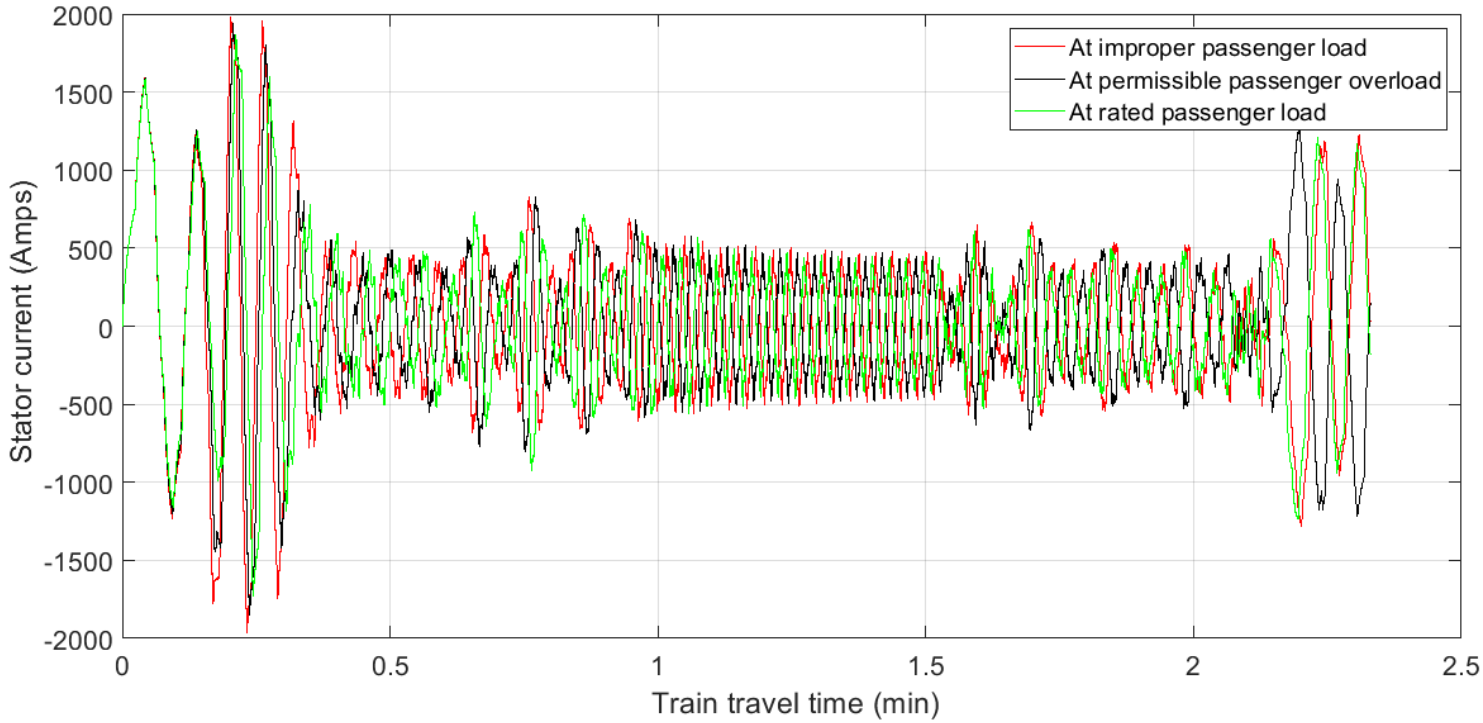

Figure 4-18 Stator current waveform when train travelling from Sebategna to Autobus tera

From the above current waveform it is been observed that when the train is loaded by improper number of passengers and accelerating, the peak value of the current in the traction motor exceeds by 500A to 250A as compared to the rated passenger loading as well as the permissible passenger overload respectively.

For comparing the RMS value of motor current in various passenger loading, the RMS of the motor current when the train is travelling from Sebategna to Autobus tera is shown in the following figure;

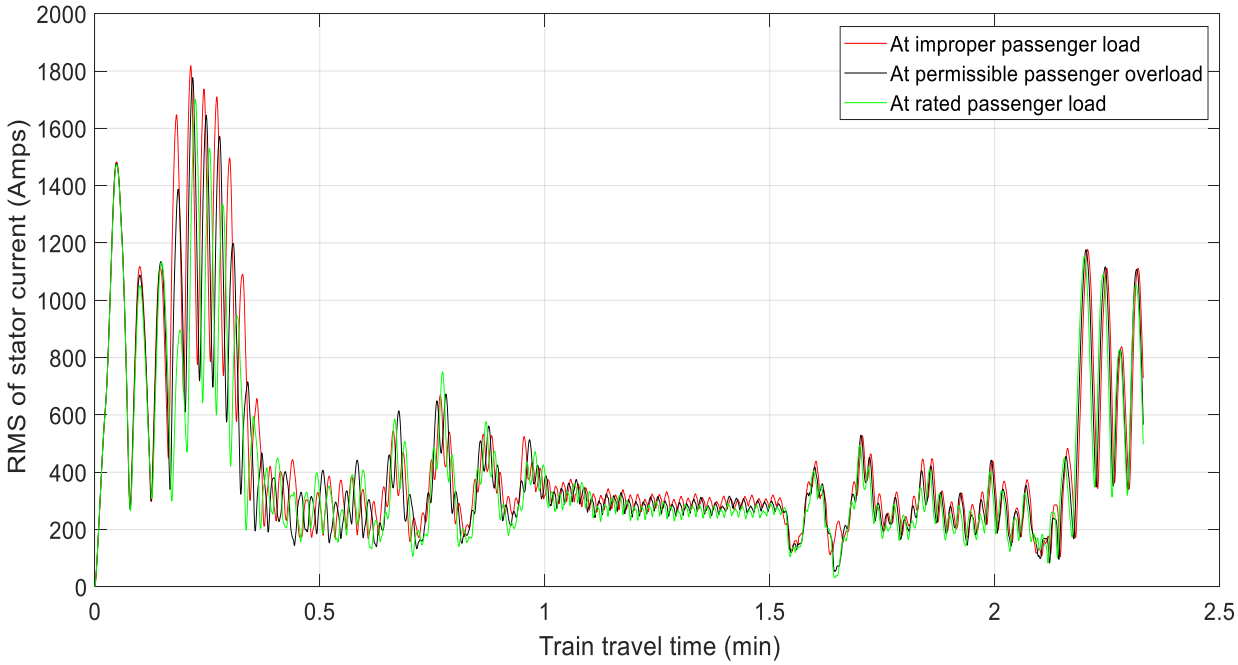

Figure 4-19 RMS of stator current when travelling from Sebategna to Autobus tera

As seen from the above figure, when the train is in acceleration period it is clearly seen that the RMS of motor current at improper passenger load is about 78.9% greater than the RMS of the motor current for rated passenger load, and about 15% than permissible passenger overload conditions. At the free running, and decelerating region of the train, the RMS of the traction motor is generally higher with small magnitude in improper passenger load case than other passenger load cases.

The following figure shows the corresponding electromagnetic torque produced by traction motor when the motor is running from Sebategna to Autobus tera.

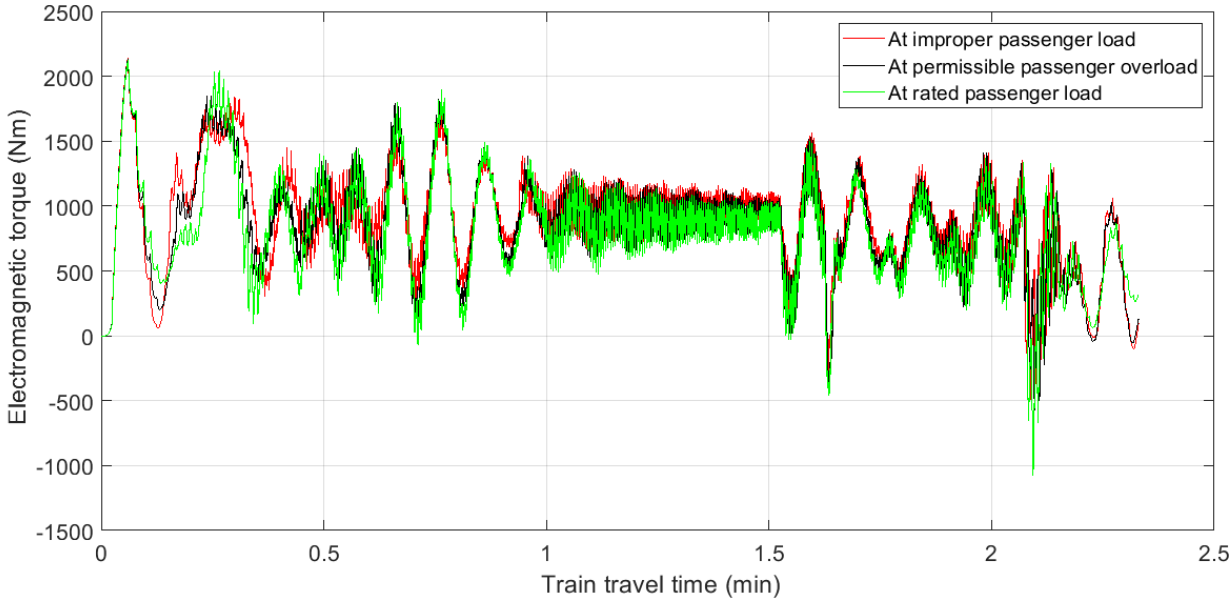

Figure 4-20 Electromagnetic torque, when travelling from Sebategna to Autobus tera

As can be seen from the graph above, when the train starts accelerating while having improper passenger load, the electromagnetic torque produced by the traction motor is about 80% less than the torque produced when there is rated passenger load, and about 60% less than in the permissible passenger load. In other periods of train movement, the torque has almost same behavior for all passenger load conditions other than small magnitude increment with load.

As illustrated in figures 4.21 and 4.22, when train is in acceleration while having improper passenger load, speed of the traction motor and speed of the train is smaller than in rated passenger load and in permissible passenger overload conditions. In other periods of train movement, there observes no significant difference in speed for the various passenger loading cases.

Figures 4.21 and 4.22 show speed variation of motor and train when travelling from NS23 to NS24.

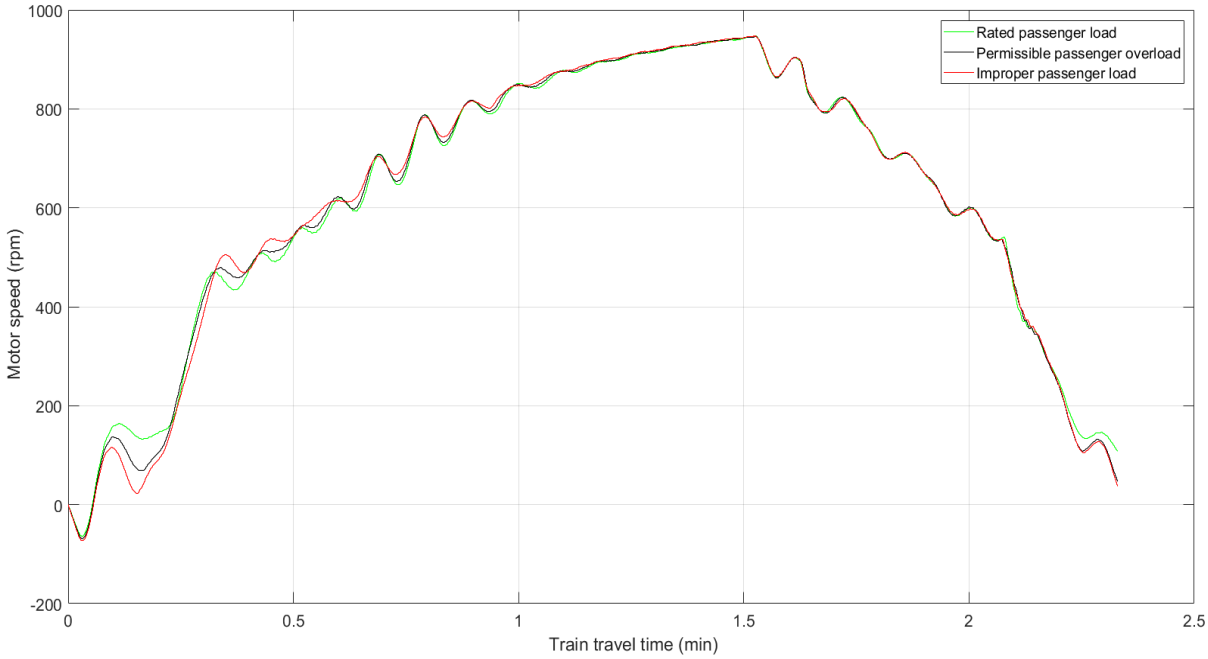

Figure 4-21 Traction motor speed variation when train travelling from NS23 to NS24

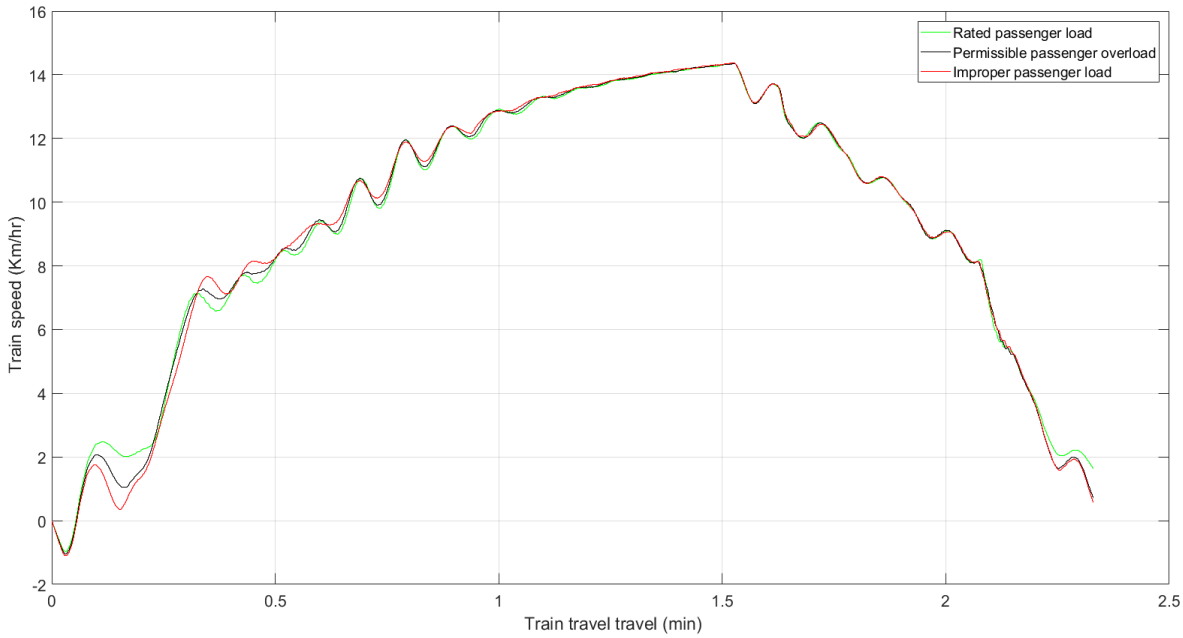

Figure 4-22 Train speed variation when travelling from Sebategna to Autobus tera

The following figures 4.23 and 4.24 show the active power, and reactive power consumption of the traction motor when train is travelling from Sebategna to Autobus tera.

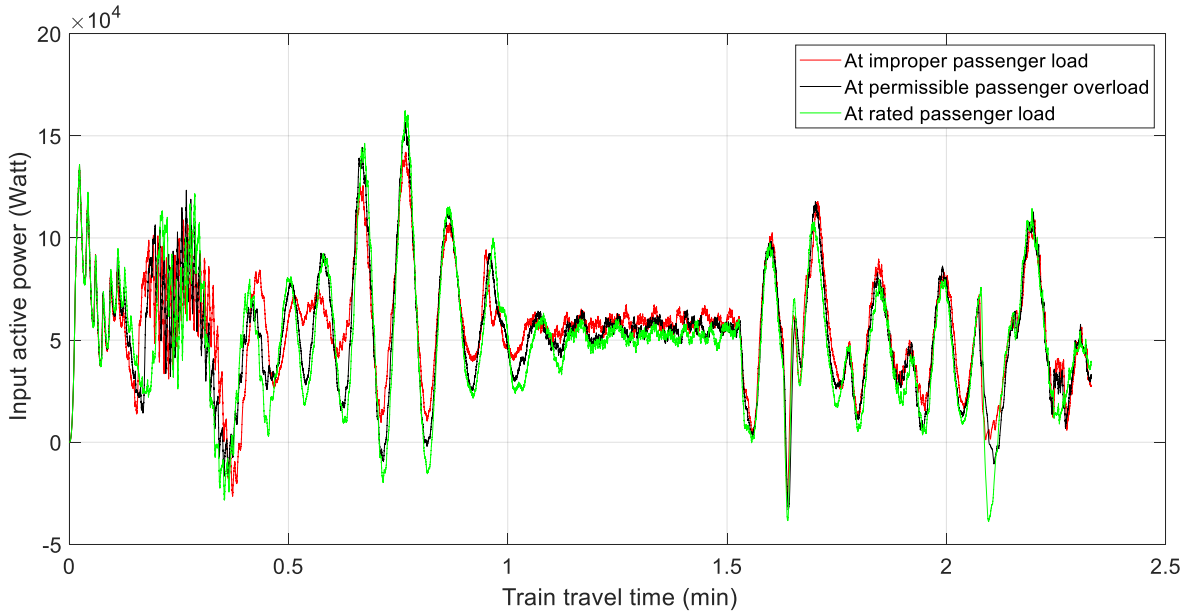

Figure 4-23 Active power consumption of motor when travelling from NS23 to NS24

As shown above when the train is about to finish acceleration period for achieving maximum speed, for few seconds active power consumption for improper passenger load is about 6% greater than in rated passenger load, and 33.33% greater than in permissible passenger load, but it is almost the same in free running and deceleration period of the train other than relatively small increment as with load.

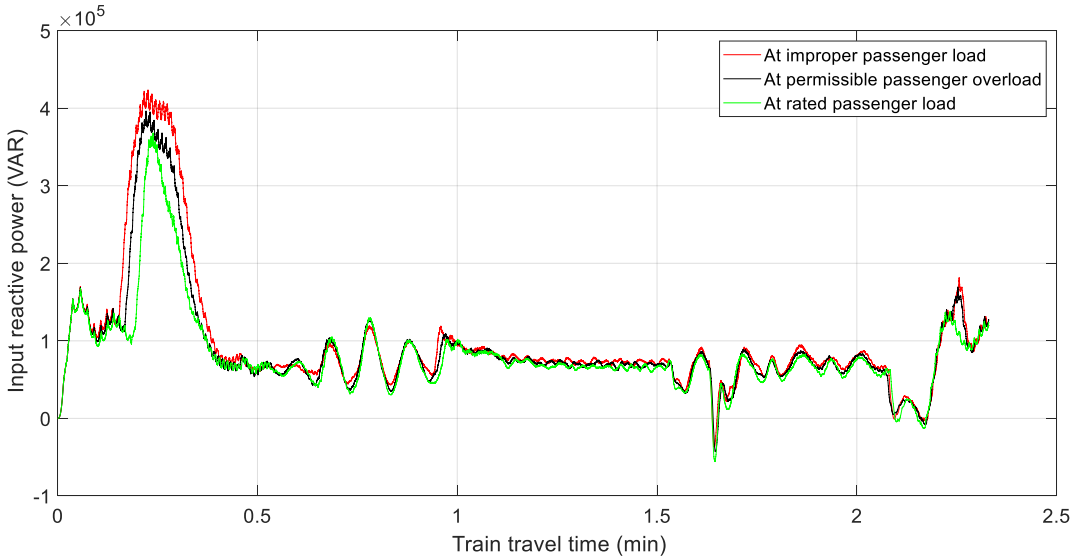

Figure 4-24 Reactive power consumption, when travelling from NS23 to NS24

When the train is accelerating from Sebategna to Autobus tera with improper passenger load, the reactive power consumed by the traction motor is about 10.8% greater than in the rated passenger load, and about 5.13% greater than in the permissible passenger overload. In the free running and deceleration period of the train, the reactive power consumption due to passenger load has no significant difference than relatively high, small amount reactive power with load.

The next figures show the copper loss in in the traction motor when the train is travelling from Abnet to Autobus tera.

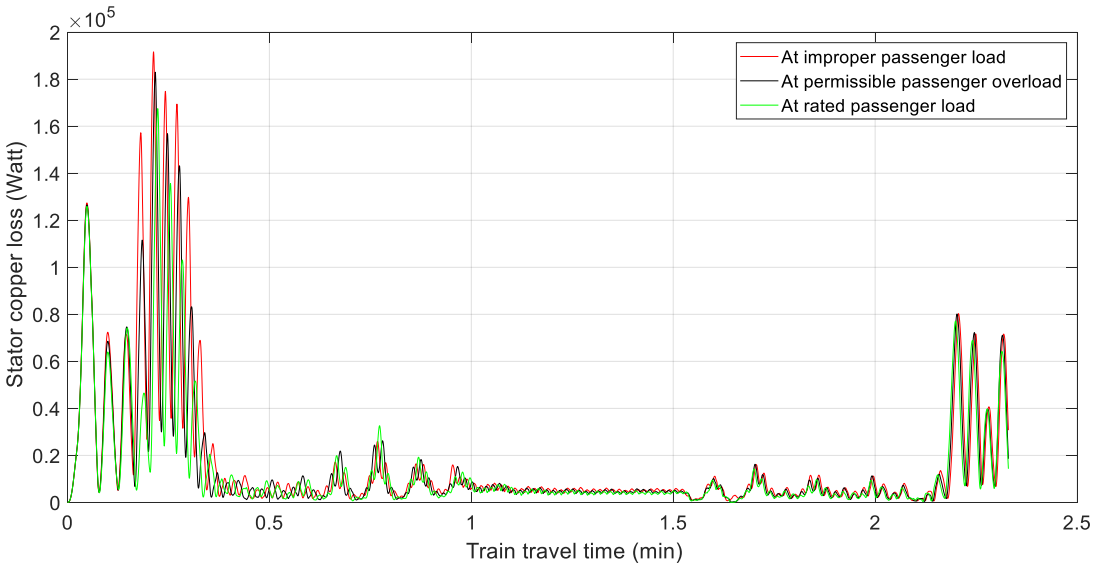

Figure 4-25 Stator copper loss in traction motor when train travelling from NS23 to NS24

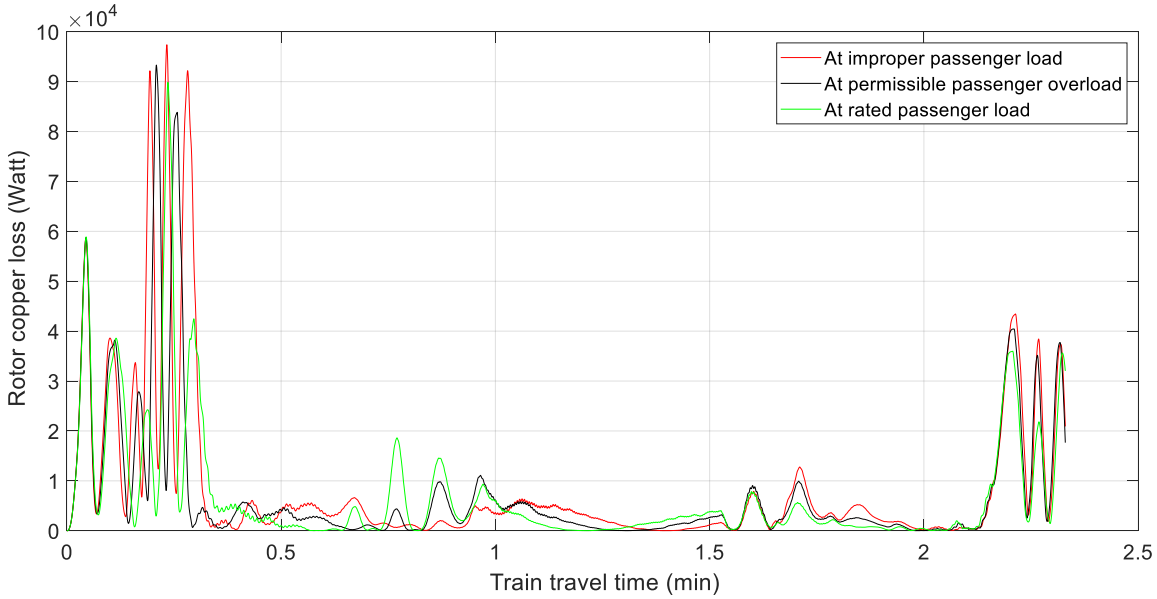

Figure 4-26 Rotor copper loss, when the train is travelling from NS23 to NS24

Carrying improper passenger load, when the train accelerating from Sebategna to Autobus tera, the traction motor has stator copper loss of 297% greater than that of rated passenger load, and 44.5% greater than that of the permissible passenger overload.

With improper passenger load, when the train is accelerating and free running, the rotor copper loss is about 150% greater than in the rated passenger load, and about 25% greater than in the permissible passenger overload conditions.

The following, Figure 4.27 shows the efficiency curve of the traction motor when the train is running from Sebategna to Autobus tera.

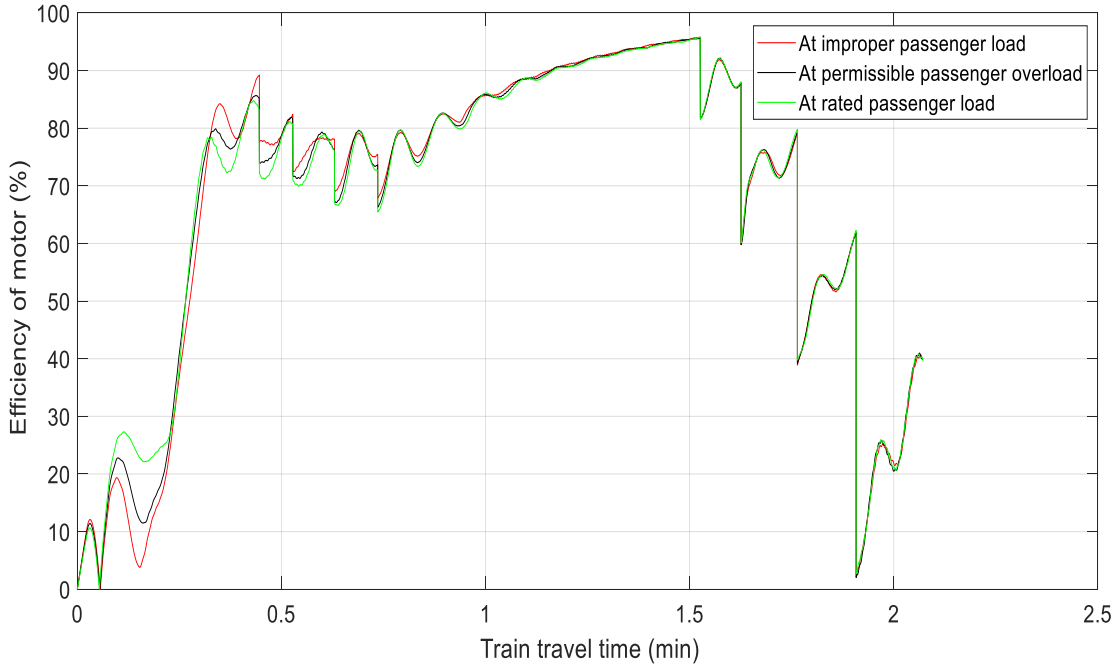

Figure 4-27 Efficiency of traction motor when train travelling from NS23 to NS24

As seen from the above figure when the train is in acceleration period (for few seconds) having improper passenger load, the efficiency of the traction motor is about 475% less than in the rated passenger load, and about 91.7% less than in the permissible passenger overload conditions. In the free running and deceleration periods, the traction motor efficiency is almost the same in all passenger loading conditions.

4.3 Train travelling from NS21 (Darmar) to NS22 (Abnet)

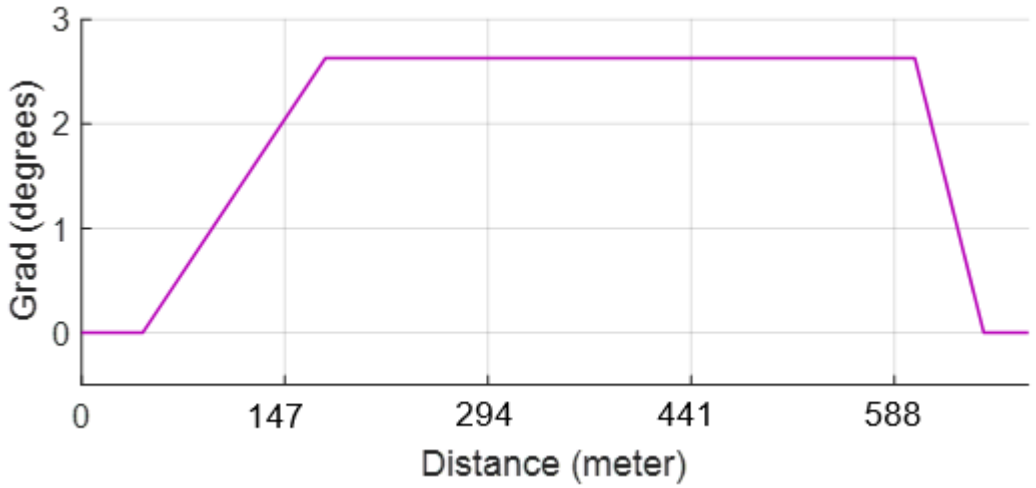

Figure 4-28 Track gradient from Darmar to Abnet

As seen from figure 4.28 above, the track geometry of AALRT line from Darmar to Abnet has a maximum gradient of 4.6%. This gradient is built as a signal input changing with distance to be imposed on the motor as shown above.

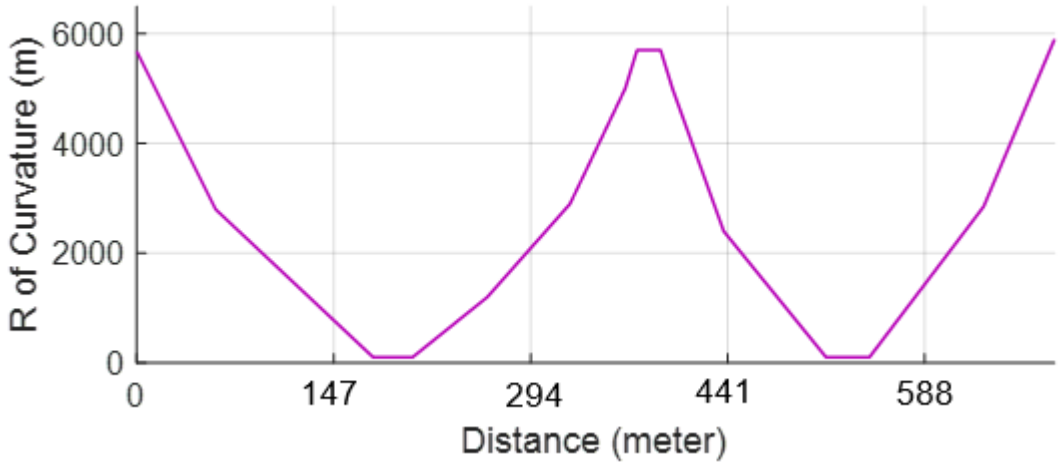

Figure 4-29 Track curvature from Darmar to Abnet

Figure 4.29 above shows the curve found in between Darmar and Abnet. The figure is a signal of input representing the radius of curvature to be used on the simulation while the train is running from Darmar to Abnet. There are two curves with 102.5m radius.

The following figure shows the real time variation of load torque input of the motor when the train is travelling from Darmar to Abnet.

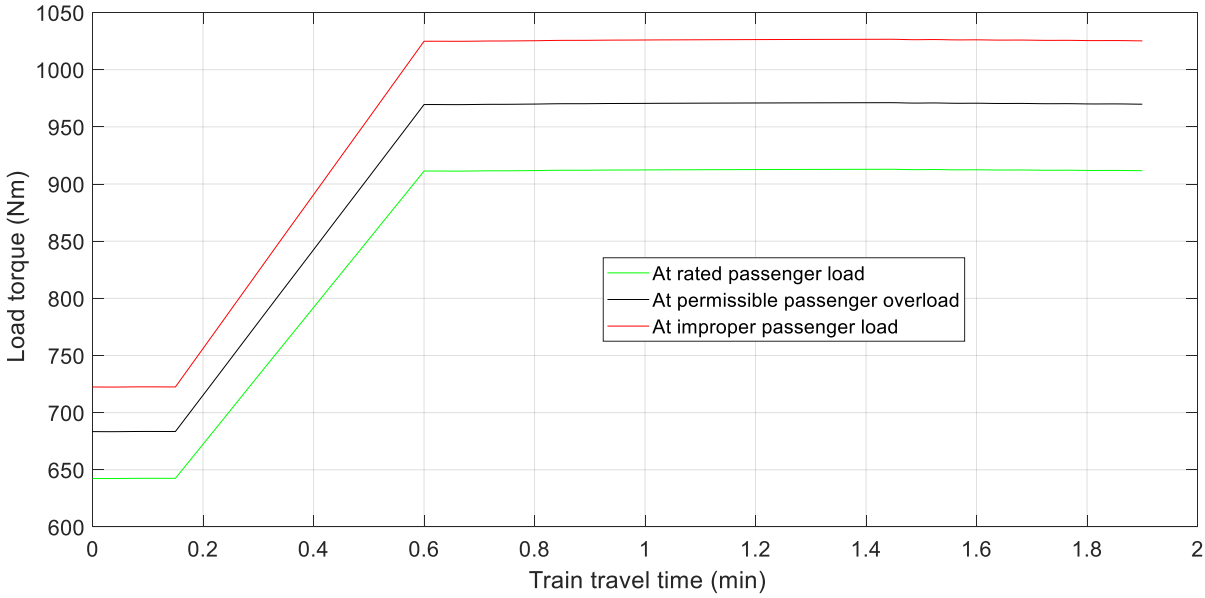

Figure 4-30 Variation of load torque when travelling from Darmar to Abnet

As seen above, when the train is travelling from Darmar to Abnet, the load torque imposed on the motor is increasing with gradient. The load torque when the train has improper passenger load, is about 11.9% greater than that of the rated passenger load, and about 9% greater than that of the permissible passenger overload throughout the journey.

The following figure shows the sinusoidal current waveform drawn by traction motor when the train is travelling from Darmar to Abnet. In the figure below three current waveforms (in red, black and green), are showing motor current flow in different passenger loading cases.

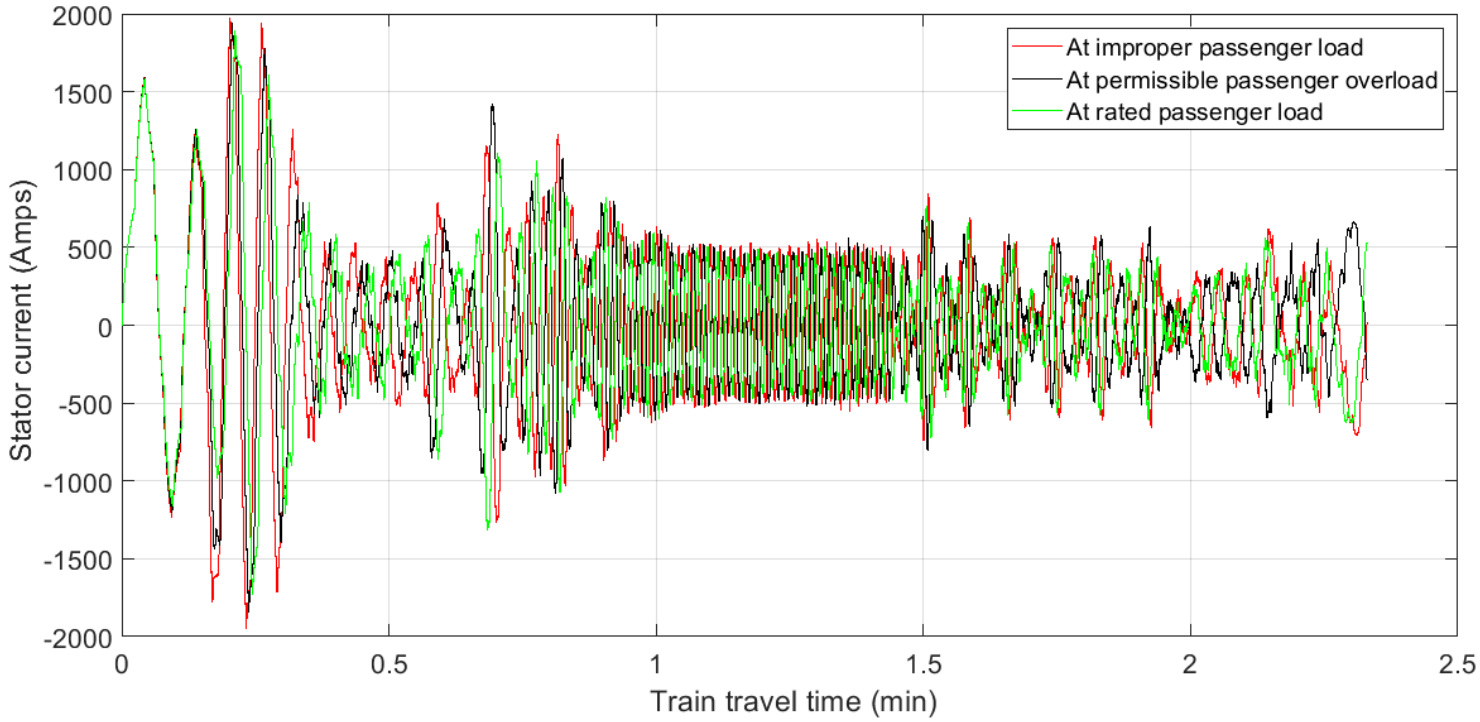

Figure 4-31 Stator current waveform of traction motor when train travelling from Darmar to Abnet

From the above current waveform, it is observed that when the train is accelerating having improper number of passengers, the peak value of the current in the traction motor exceeds by about 750A to 500A as compared to the current in the rated passenger load as well as in the permissible passenger overload respectively.

The figure below shows the RMS of stator current of traction motor when the train is travelling from Darmar to Abnet.

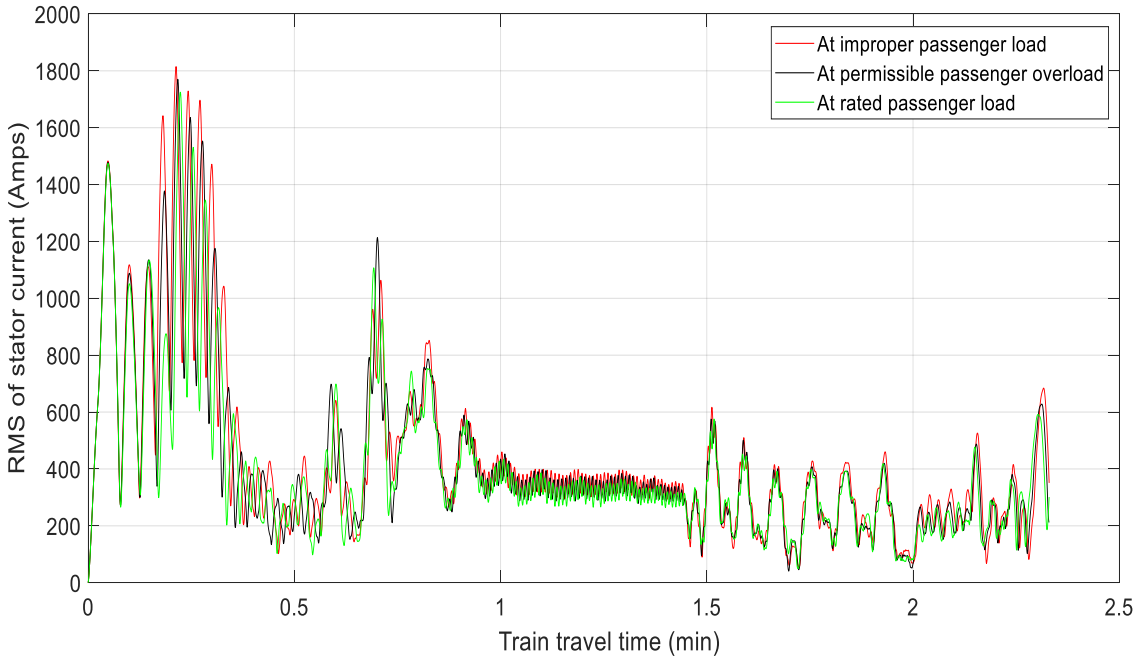

Figure 4-32 RMS of stator current when travelling from Darmar to Abnet

As seen from the above figure, when the train is in acceleration period it is clearly seen that the RMS of motor current at improper passenger load is about 50.5% greater than the RMS of the motor current for rated passenger load, and about 25.2% greater than RMS current in permissible passenger overload conditions. At the free running, and decelerating region of the train, the RMS of the traction motor is generally higher with small magnitude as with load increment.

When the train is travelling from Darmar to Abnet, the traction motor generates the following kind of electromagnetic torque;

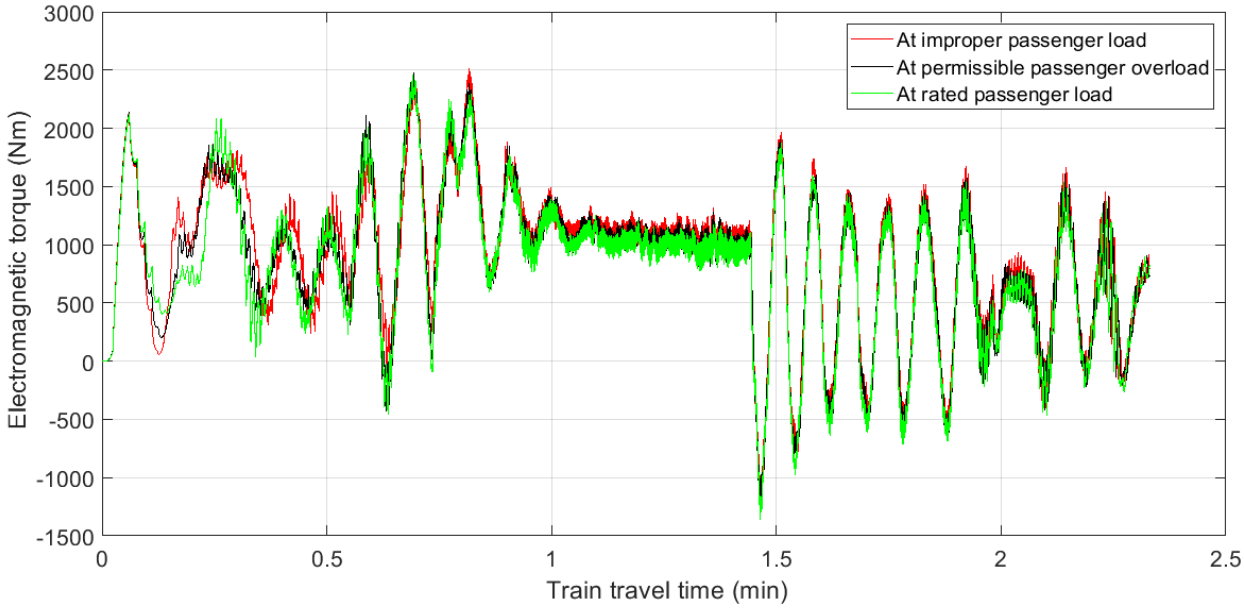

Figure 4-33 Electromagnetic torque of motor when travelling from Darmar to Abnet

As can be seen from the graph above, when the train starts accelerating while there is improper passenger load, the electromagnetic torque produced by the traction motor is about 77% less than the torque value in rated passenger load, and about 60% less than that of the torque value in permissible passenger load. In other periods of train movement, the torque has almost same behavior for all loading conditions other than its small magnitude increment with load.

As illustrated in figures 4.34 and 4.35, when the train is accelerating while it has improper passenger load, speed of the traction motor and speed of the train is lower than the speed when there is rated passenger load and permissible passenger overload. In other periods of the train movement, there observed no significant difference in speed with the various passenger loading cases.

Figures 4.34 and 4.35 show speed variation of traction motor and train when travelling from NS21 to NS22.

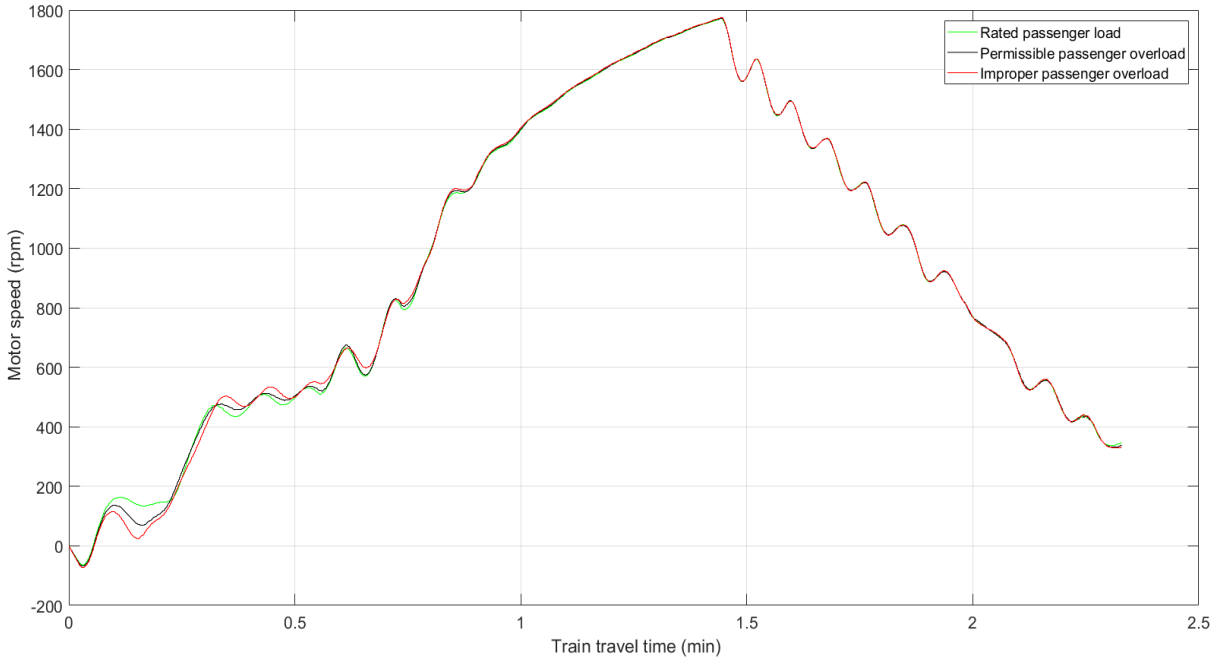

Figure 4-34 Speed of traction motor in rpm when travelling from Darmar to Abnet

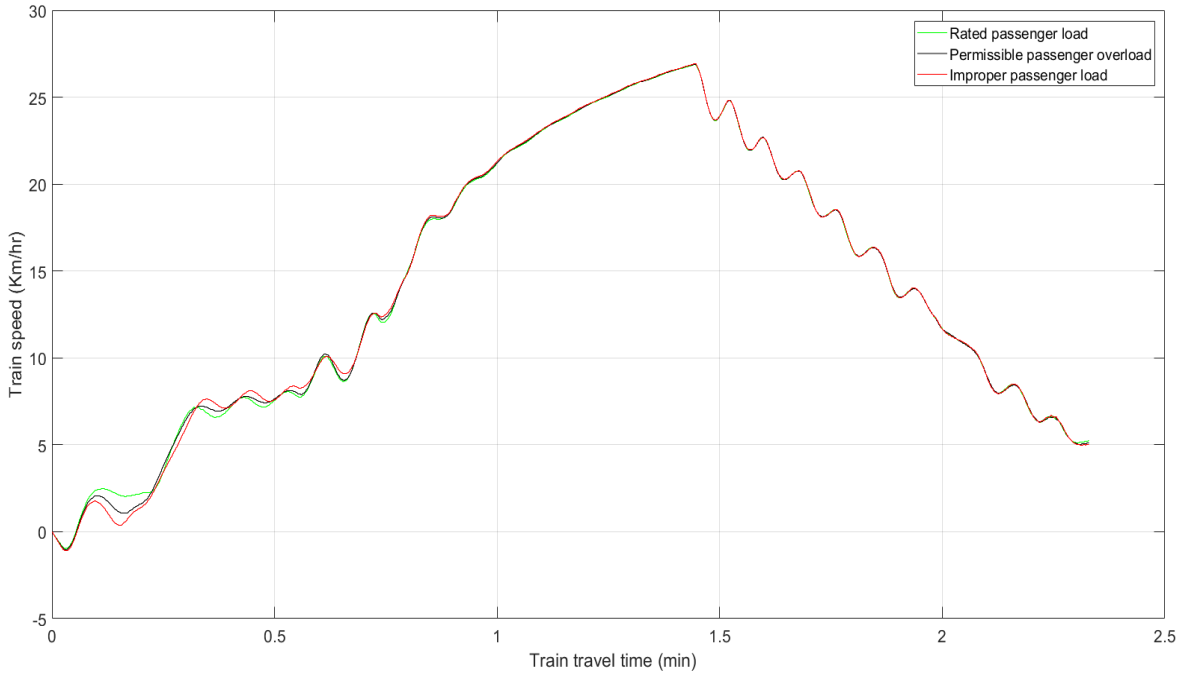

Figure 4-35 Speed of train in Km/hr when travelling from Darmar to Abnet

The following figures 4.36 and 4.37 show the active power, and reactive power consumption of the traction motor when train is travelling from Darmar to Abnet.

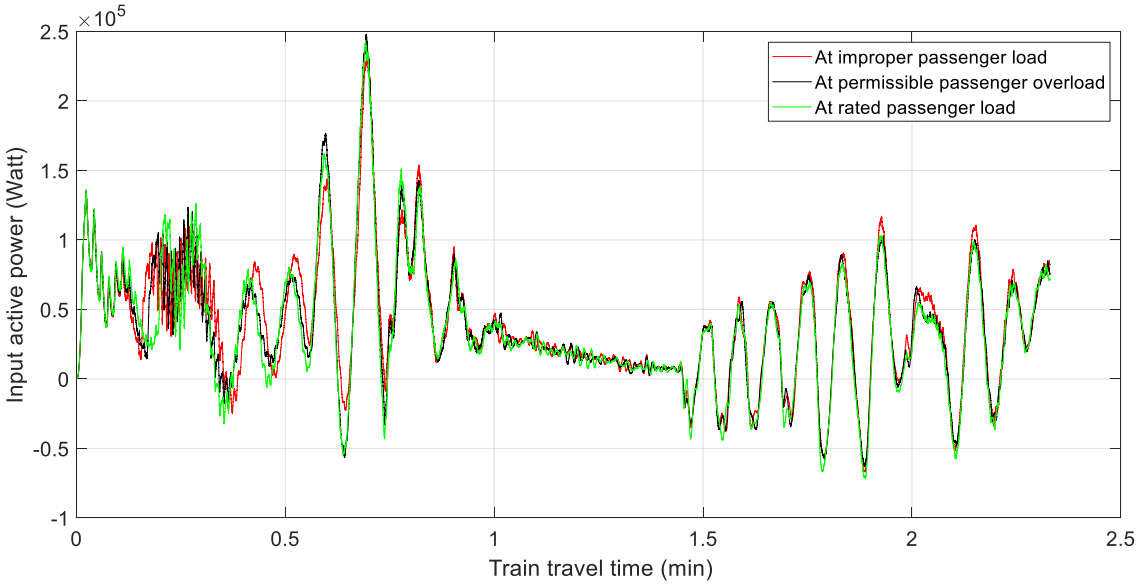

Figure 4-36 Active power consumption of motor when travelling from NS21 to NS22

As shown above when the train is accelerating the active power consumption for improper passenger load is about 30% greater than that of the rated passenger load, and 116% greater than that of the permissible passenger load, but it is almost the same in free running and deceleration period of the train.

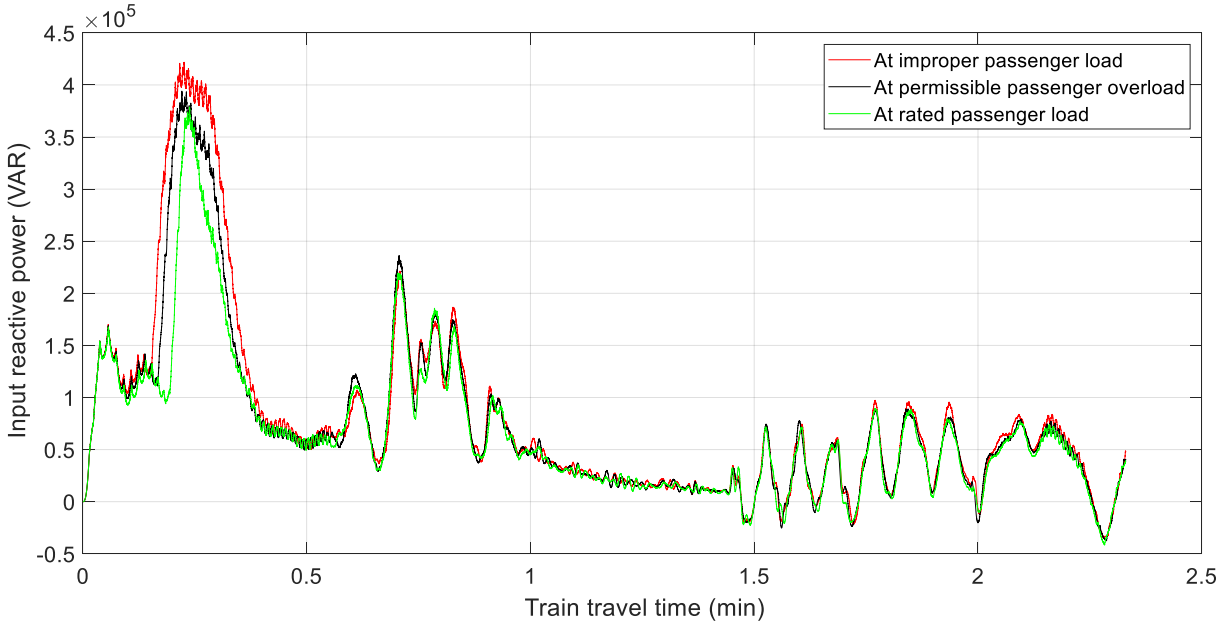

Figure 4-37 Reactive power, when train travelling from NS21 to NS22

When the train is accelerating from Darmar to Abnet with improper passenger load, the reactive power consumed by the traction motor is about 13.3% greater than that of the rated passenger load, and about 9% greater than that of the permissible passenger overload. In the free running and deceleration period of the train, the reactive power consumption due to passenger load has no significant difference with the passenger loading.

The figures below shows copper losses in the traction motor when train is travelling from Darmar to Abnet.

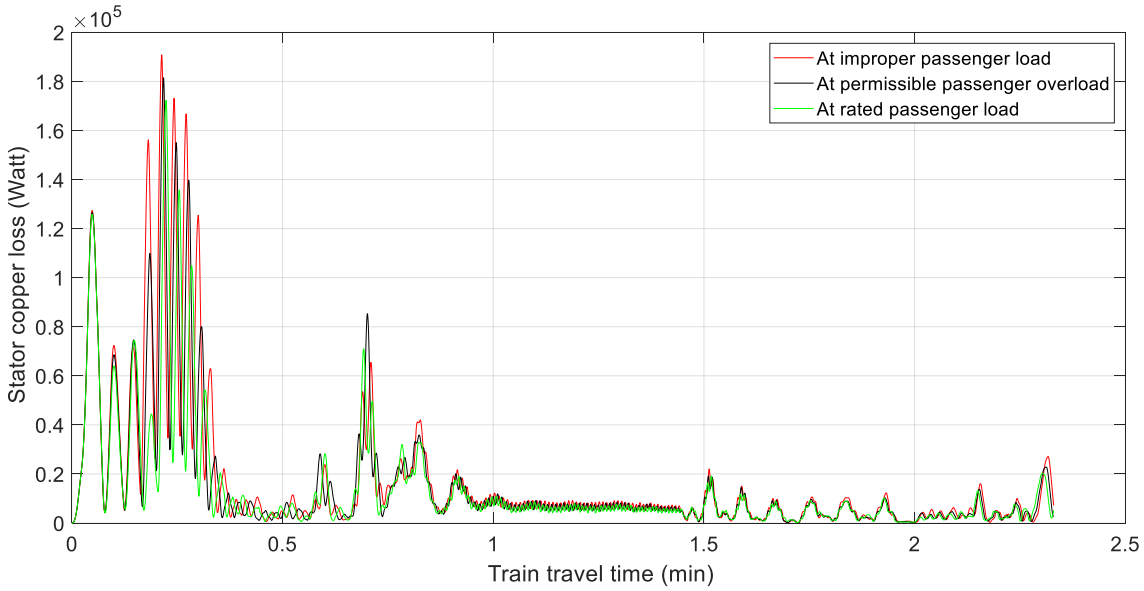

Figure 4-38 Stator copper loss in traction motor when travelling from NS21 to NS22

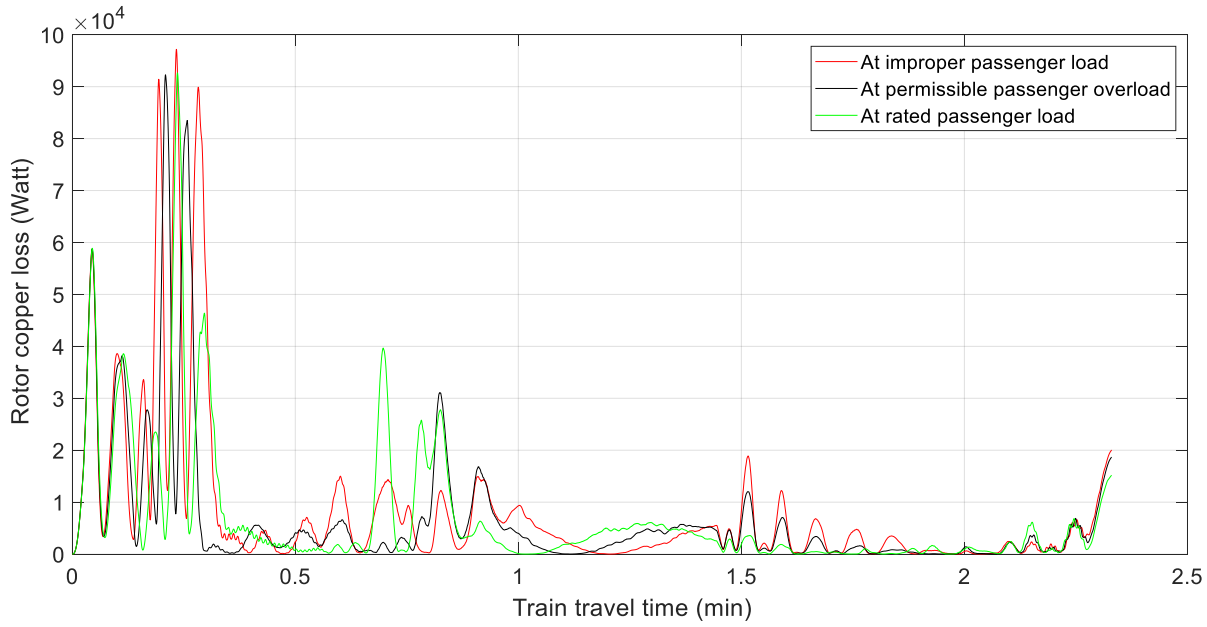

Figure 4-39 Rotor copper loss in traction motor when travelling from NS21 to NS22

Carrying improper passenger load, when the train accelerating from Darmar to Abnet, the traction motor has stator copper loss of 55.5% greater than in the rated passenger load, and 20% greater than in the permissible passenger overload.

With improper passenger load, when the train is decelerating and free running, the rotor copper loss is about 500% greater than in the rated passenger load, and about 50% greater than in the permissible passenger overload conditions.

The following, figure 4.40 shows the efficiency curve of the traction motor when the train is running from Darmar to Abnet.

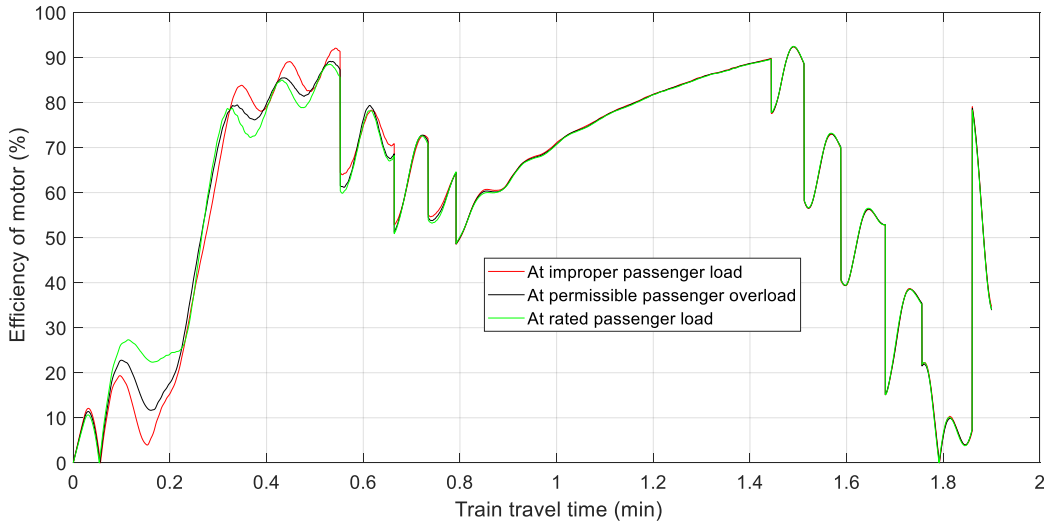

Figure 4-40 Efficiency curve of traction motor when travelling from Darmar to Abnet

As seen from the above Figure 4.40, when the train is starting accelerating, having improper passenger load, the efficiency of the traction motor is about 78.3% less than in the rated passenger load, and about 58.33% less than in the permissible passenger overload conditions. In the free running and deceleration periods, the traction motor efficiency is almost the same in all passenger loading conditions.

4.4 Train travel from NS15 (Meshwalekia) to EW16 (Stadium)

The following two figures 4.41 and 4.42 are showing the signal inputs representing the gradient and curved paths when the train is travelling from Meshwalekia to Stadium.

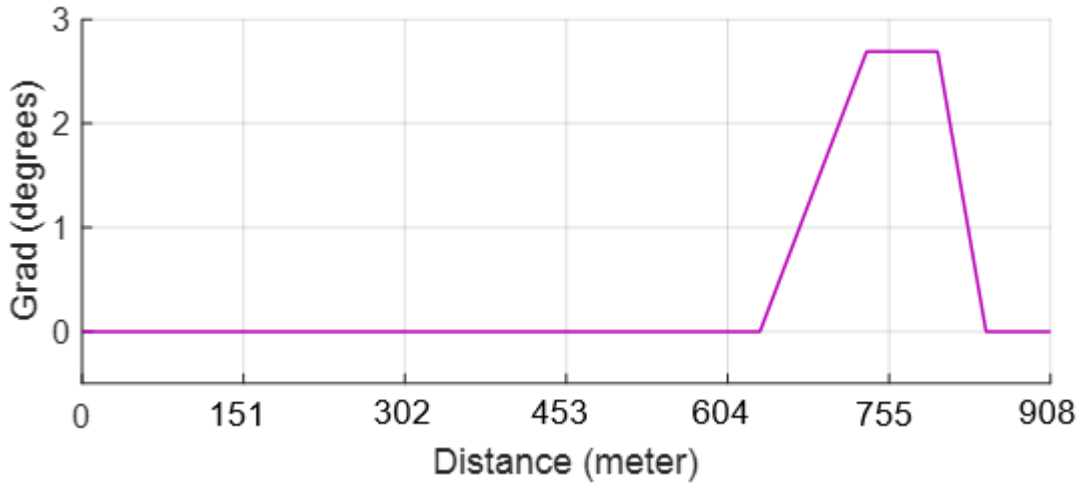

Figure 4-41 Track gradient from Meshwalekia to Stadium

As seen in figure 4.41 above, at around Stadium passenger station there is a short distance slope having a maximum of 4.7% gradient, and a curved path with a minimum of 52.5m radius of curvature as shown in figure 4.42 below.

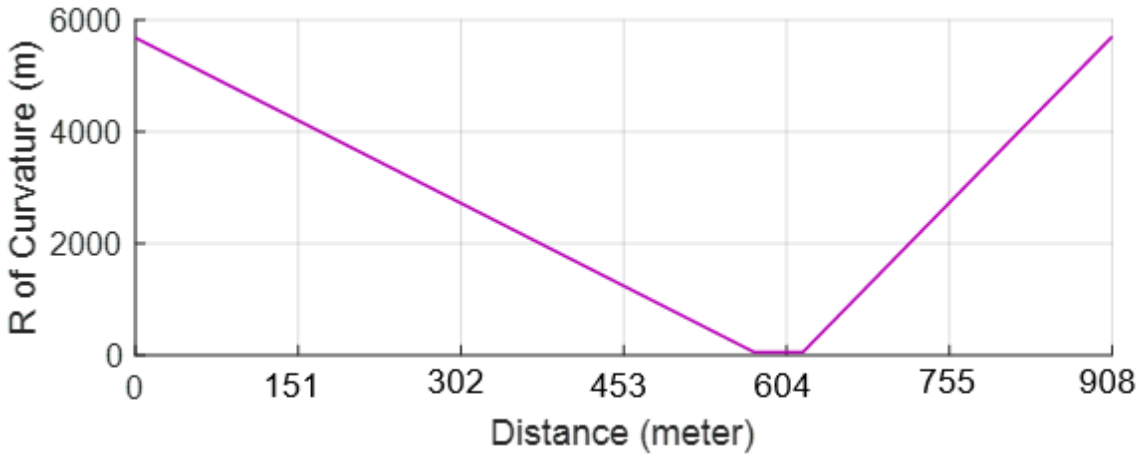

Figure 4-42 Track curve from Meshwalekia to Stadium

The following figure shows the real time variation of load torque input of the motor when the train is travelling from Meshwalekia to Stadium.

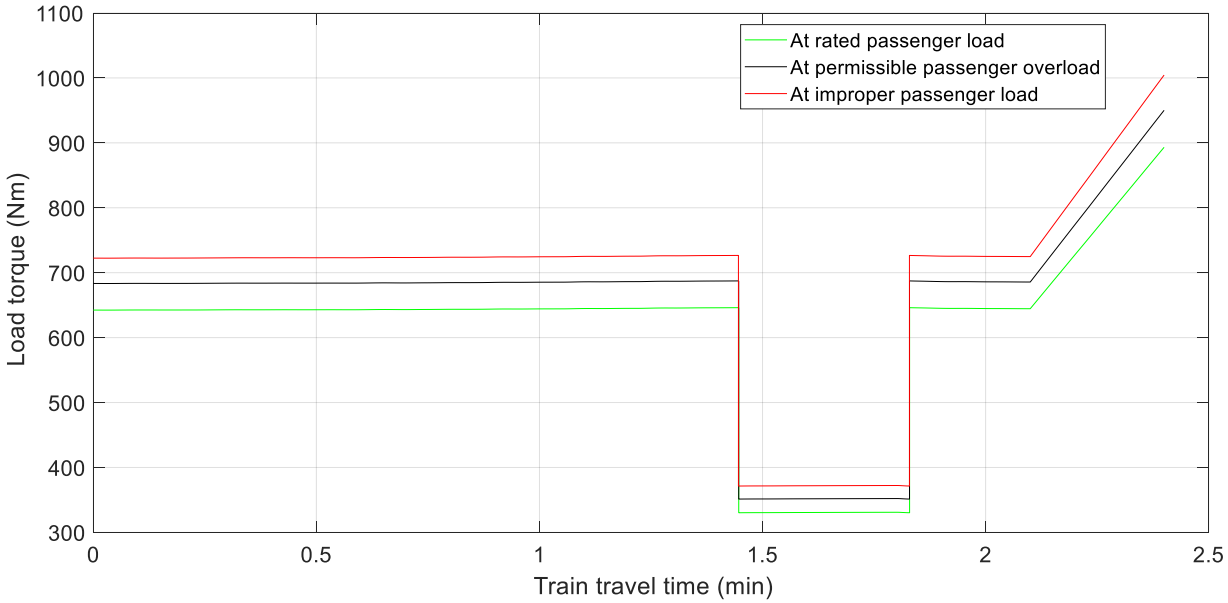

Figure 4-43 Load torque variation from Meshwalekia to Stadium

As seen above, when the train is travelling from Meshwalekia to Stadium, the load torque imposed on the motor was constant, then when the train speed is increasing beyond 40Km/hr, the acceleration is supposed to decrease from $1m/s^2$ to $0.5m/s^2$ then the load torque also be halved. When the train is approaching to Stadium, it meets the curve and its speed decreased back, and load torque also increased. When the train is passing through the curve, no significant variation is observed on the load torque. Whereas the load torque has increased when the train reaches the gradient area at Stadium. The load torque when the train has improper passenger load, is about 3.07% greater than in rated passenger load, and about 1.9% greater than in permissible passenger overload throughout the journey.

The following figure shows the sinusoidal current waveform drawn by traction motor when the train is travelling from Meshwalekia to Stadium. In the figure below three current waveforms (in red, black and green), are showing motor current flow in different passenger loading cases.

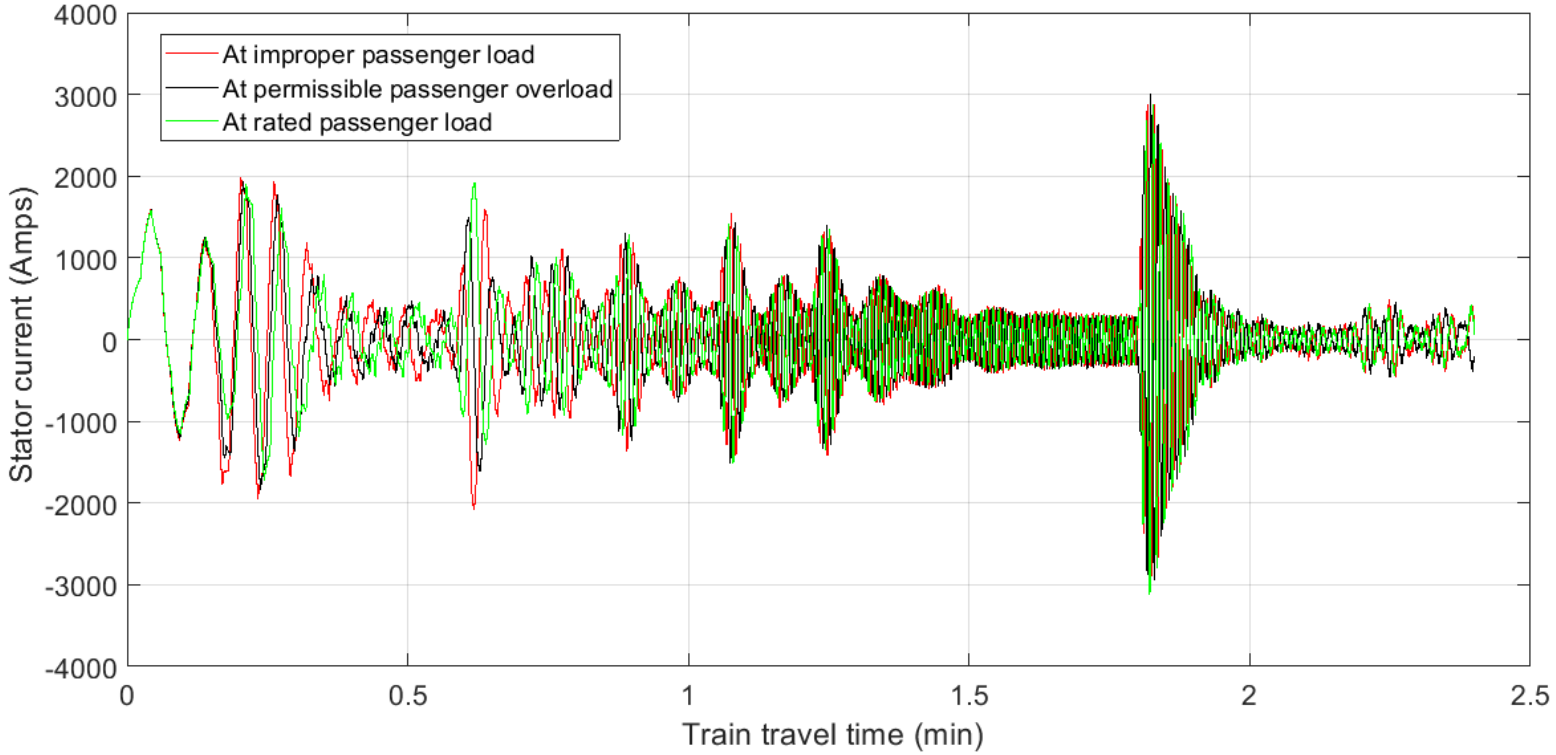

Figure 4-44 Stator current waveform of traction motor when train travelling from Meshwalekia to Stadium

From the above current waveform it is observed that when the train is accelerating while having improper number of passengers, the peak value of the current in the traction motor exceeds by about 500A to 300A as compared to the rated passenger loading as well as the permissible passenger overload respectively.

The figure below shows the RMS of stator current of traction motor when the train is travelling from Meshwalekia to Stadium.

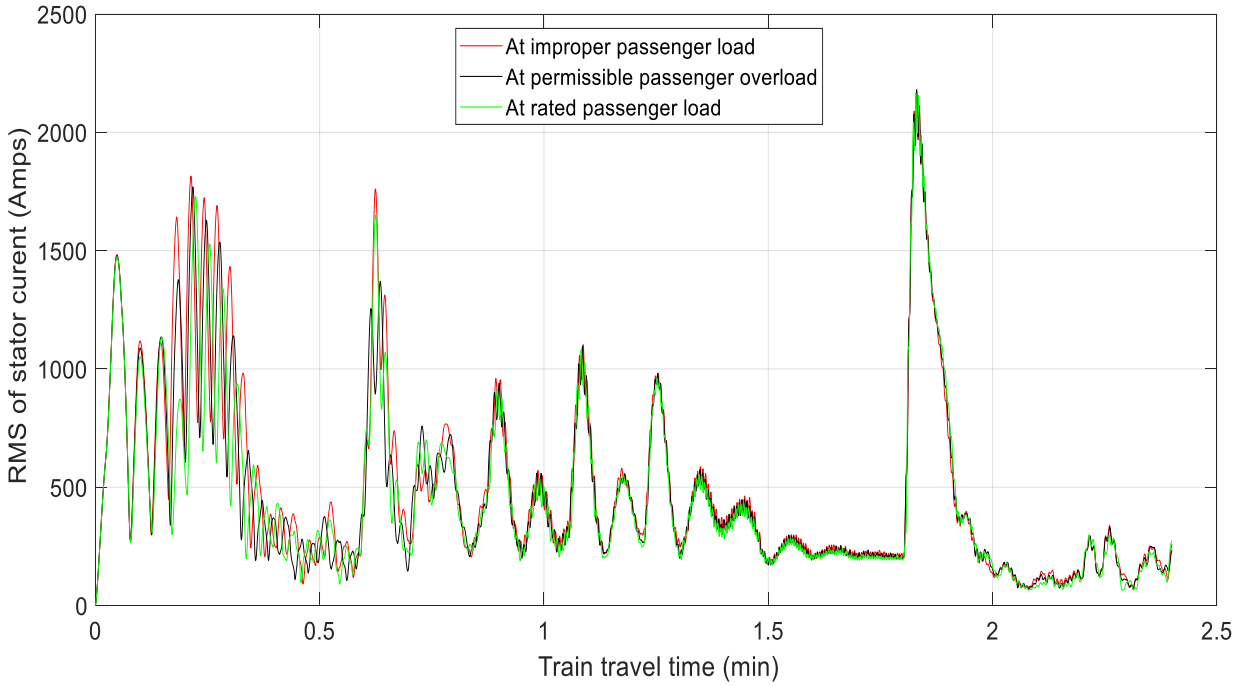

Figure 4-45 RMS of stator current when travelling from Meshwalekia to Stadium

As seen from Figure 4.45, when the train is in acceleration period, the RMS of motor current at improper passenger load is about 123% greater than the RMS of the motor current for rated passenger load, and about 58.3% than that of the permissible passenger overload conditions. At the free running, and decelerating region of the train, the RMS of the traction motor is generally higher with small magnitude in improper passenger load case than other passenger load cases.

When the train is travelling from Meshwalekia to Stadium, the traction motor generates the following kind of electromagnetic torque;

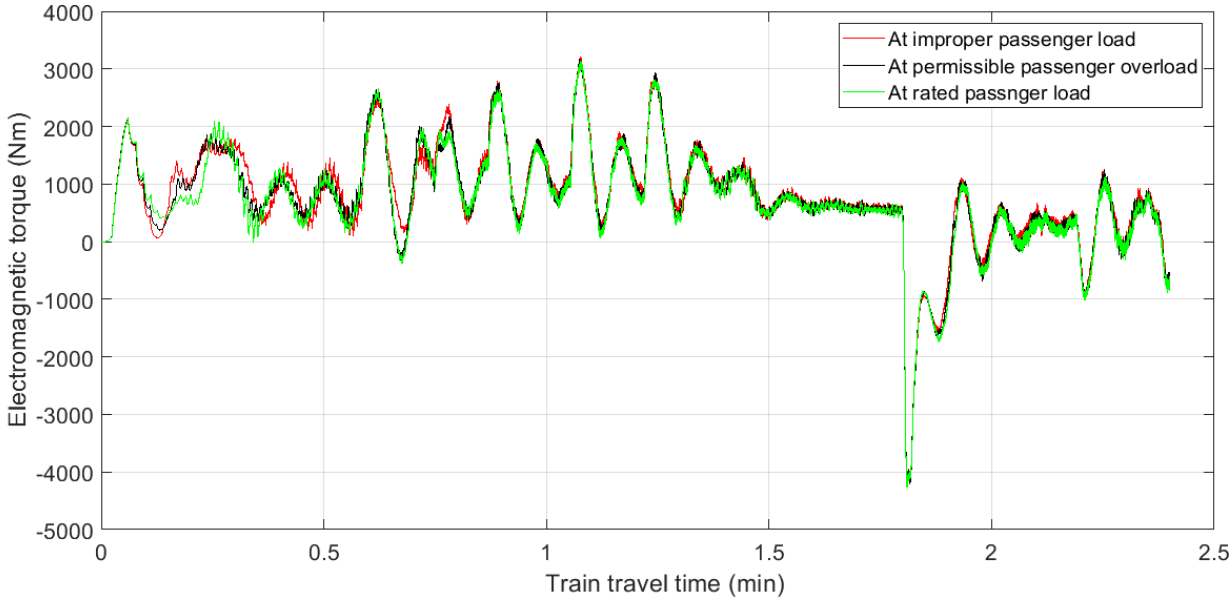

Figure 4-46 Electromagnetic torque, when travelling from Meshwalekia to Stadium

As can be seen from the graph above, when the train starts accelerating having improper passenger load, the electromagnetic torque produced by the traction motor is about 58.3% less than the torque produced when there is rated passenger load, and about 33.3% less than in the permissible passenger load. In the other periods of train movement, the torque has almost same behavior for all passenger load conditions other than its small magnitude increment with load.

As illustrated by Figures 4.47 and 4.48, when the train starts acceleration having improper passenger load, speed of the traction motor and speed of the train is less than the torque in rated passenger load as well as permissible passenger overload. In other periods of train movement, there observed no significant difference in speed for the various passenger loading cases.

Figures 4.47 and 4.48 show speed variation of traction motor and train when travelling from NS15 to EW16.

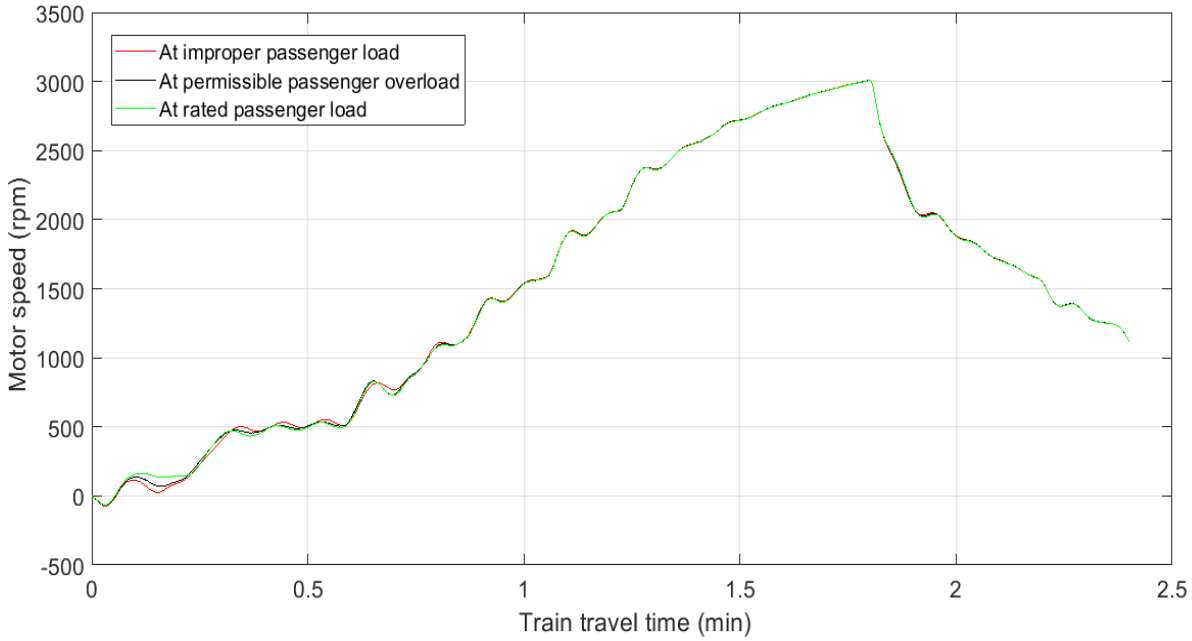

Figure 4-47 Speed of traction motor in rpm when travelling from Meshwalekia to Stadium

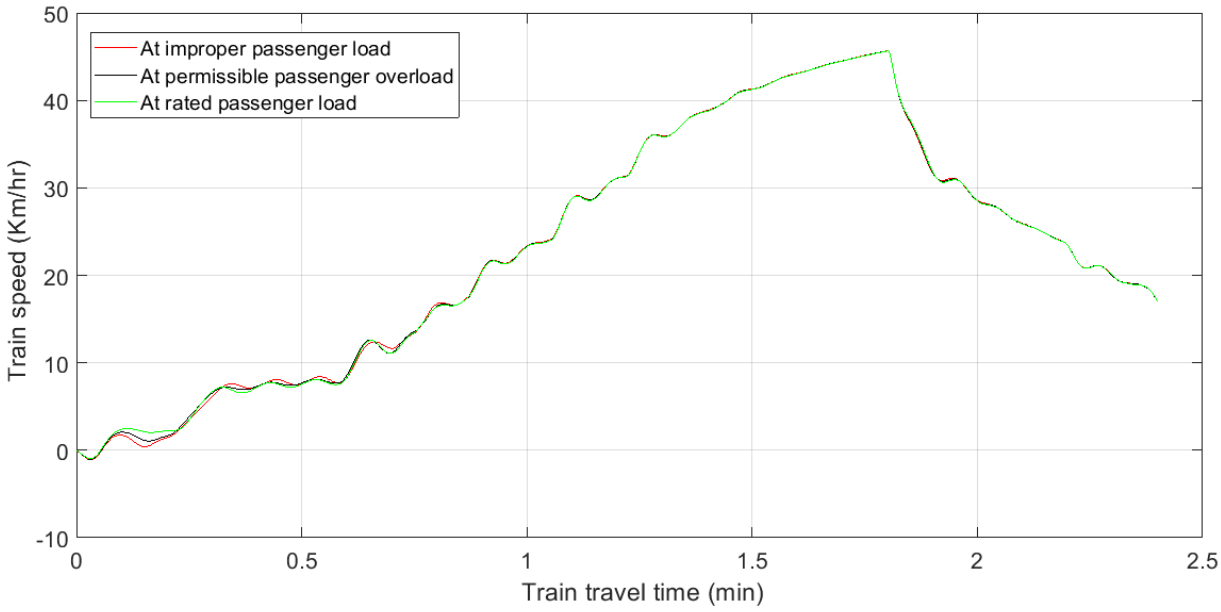

Figure 4-48 Train speed in Km/hr while train is travelling from Meshwalekia to Stadium

The following Figures 4.49 and 4.50 show the active power, and reactive power consumption of the traction motor when train is travelling from Meshwalekia to Stadium.

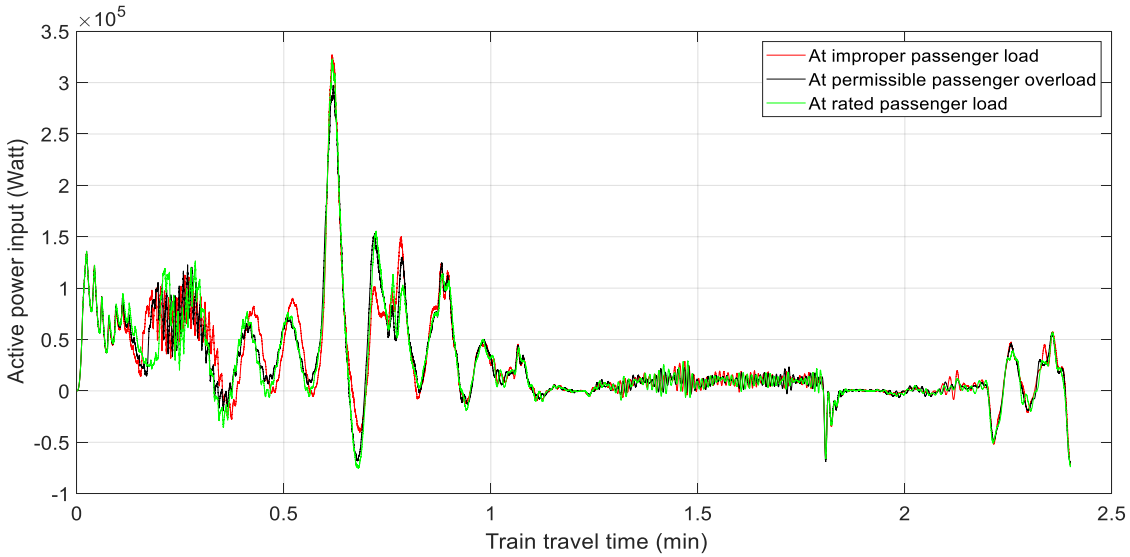

Figure 4-49 Active power consumption of motor when travelling from NS21 to NS22

As shown above when the train is accelerating the active power consumption for improper passenger load is about 6.7% greater than in rated passenger load, and about 33.3% greater than in permissible passenger load, but it is almost the same in free running and deceleration period of the train.

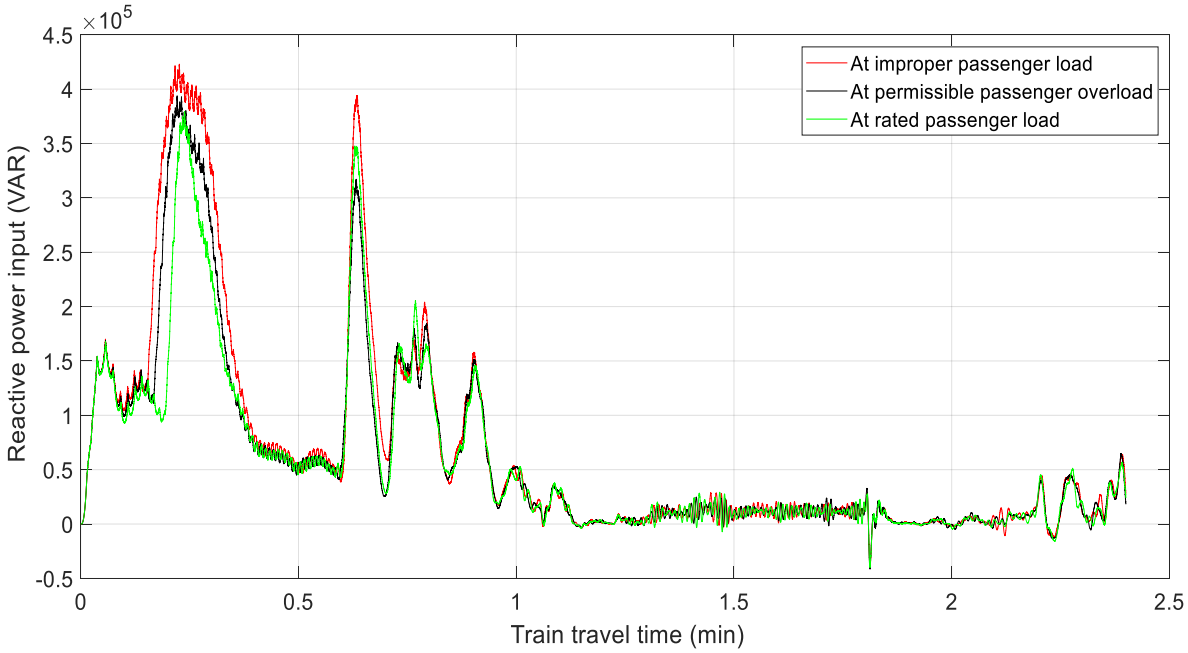

Figure 4-50 Reactive power in traction motor when travelling from NS15 to EW16

When the train is accelerating from Meshwalekia to Stadium with improper passenger load, the reactive power consumed by the traction motor is about 12% greater than in the rated passenger load, and about 6.33% greater than in the permissible passenger overload. In the free running and deceleration period of the train, the reactive power consumption due to passenger load has no significant difference with the passenger loading.

The Figures 4.51 and 4.52 below shows copper losses in the traction motor when train is travelling from Meshwalekia to Stadium.

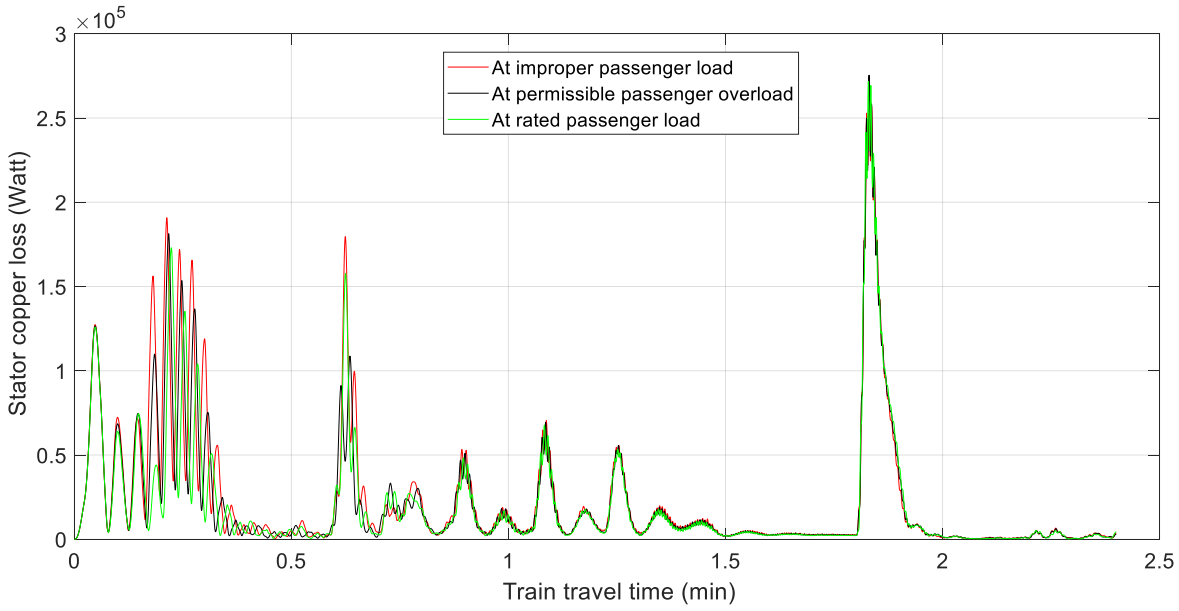

Figure 4-51 Stator copper loss in traction motor when travelling from NS15 to EW16

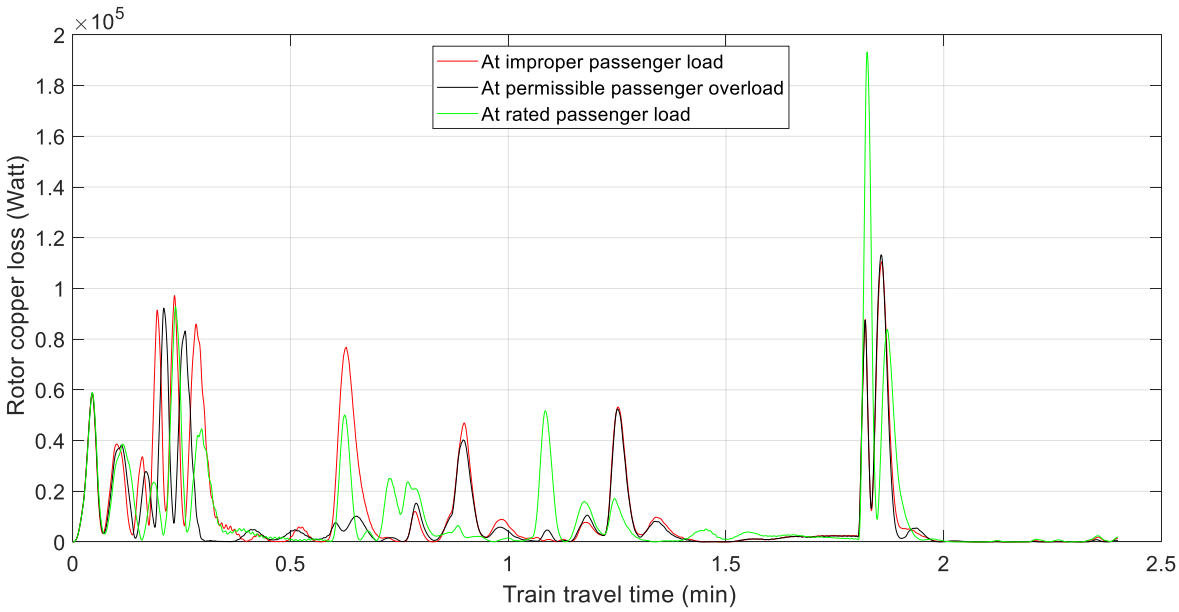

Figure 4-52 Rotor copper loss in traction motor when travelling from NS15 to EW16

Carrying improper passenger load, when the train accelerating from Meshwalekia to Stadium, the traction motor has stator copper loss of about 277.5% greater than in the rated passenger load, and about 31.3% greater than in the permissible passenger overload.

With improper passenger load, when the train is decelerating and free running, the rotor copper loss is about 191% greater than in the rated passenger load, and about 34.6% greater than in the permissible passenger overload conditions.

The following figure shows the efficiency curve of the traction motor when the train is running from Meshwalekia to Stadium.

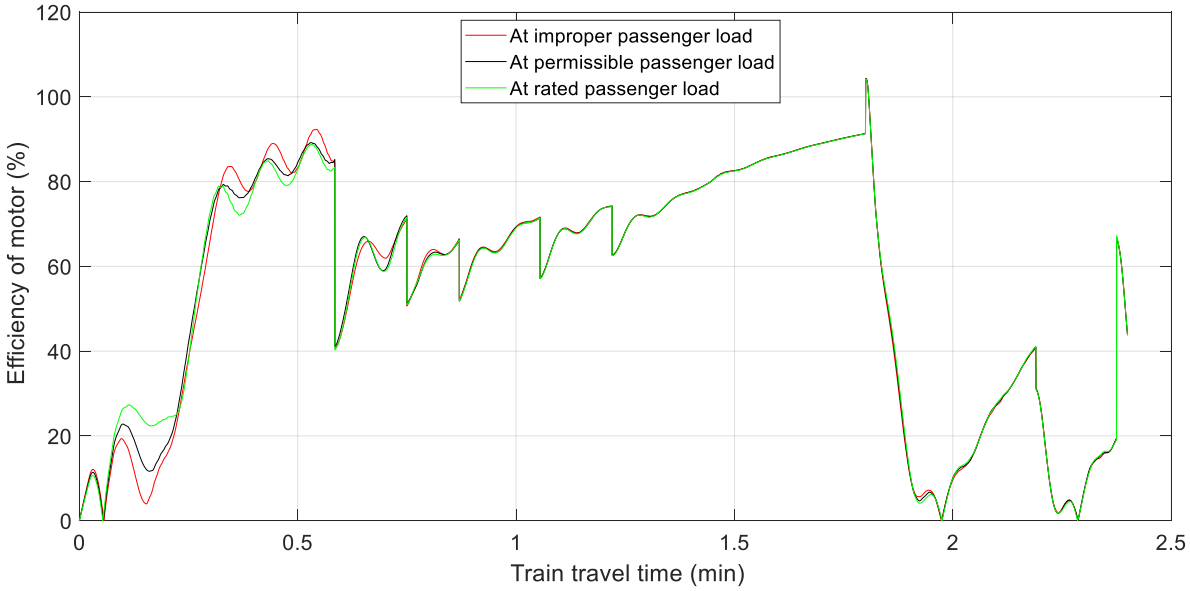

Figure 4-53 Efficiency curve of traction motor when travelling from Meshwalekia to Stadium

As seen from Figure 4.53 when the train is accelerating, having improper passenger load, the efficiency of the traction motor is about 82.6% less than in the rated passenger load, and about 63.6% less than in the permissible passenger overload conditions. In the free running and deceleration periods, the traction motor efficiency is almost the same in all passenger loading conditions.

4.5 Train travel from NS11 (Nefas Silk 2) to NS12 (Lancha)

The following two figures are showing the signal inputs representing the gradient and curved paths when the train is travelling from Nefas silk 2 to Lancha.

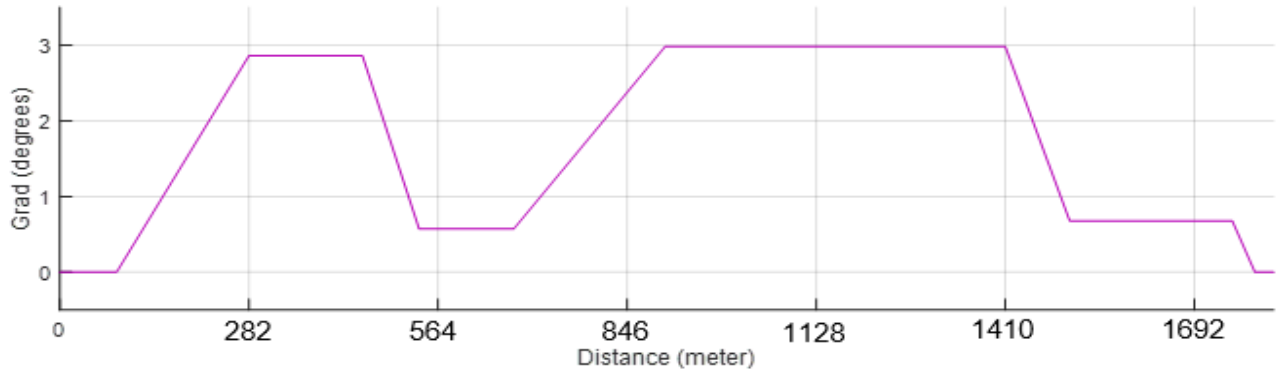

Figure 4-54 Track gradient from Nefas silk 2 to Lancha

As seen in figure 4.54 above, although the track area from Nefas silk 2 to Lancha has long distance with almost level geometry, there are gradients near the departure of Nefas silk 2 and, around the arrival of Lancha station. There is a maximum gradient of 5% at around the departure of Nefas silk 2, with shorter distance.

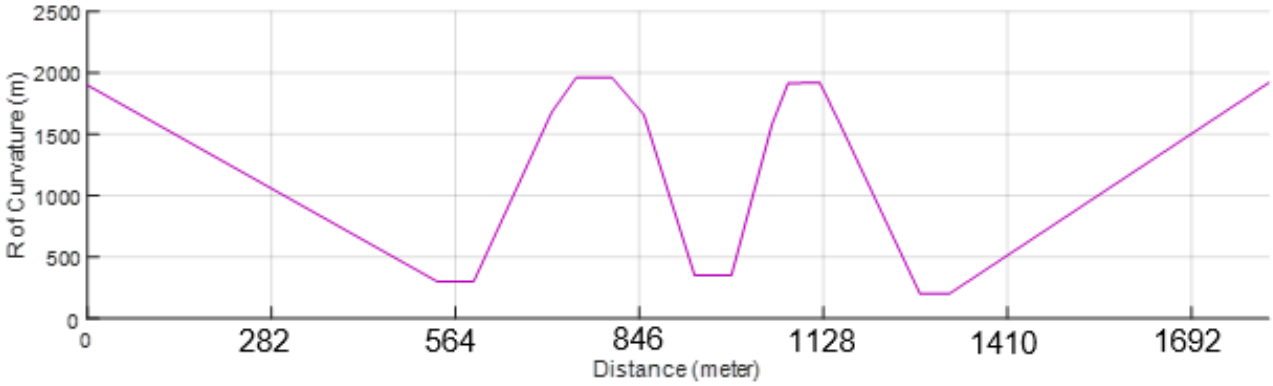

Figure 4-55 Curved path from Nefas silk 2 to Lancha

Figure 4.55 shows the signal input representing the magnitude and pattern of curves found from Nefas silk 2 station to Lancha station. When travelling from Nefas silk 2 to Lancha, there found three curves with radius of curvature 302m, 352m, and 202m respectively.

The following figure shows the real time variation of load torque input of the motor when the train is travelling from Nefas silk 2 to Lancha.

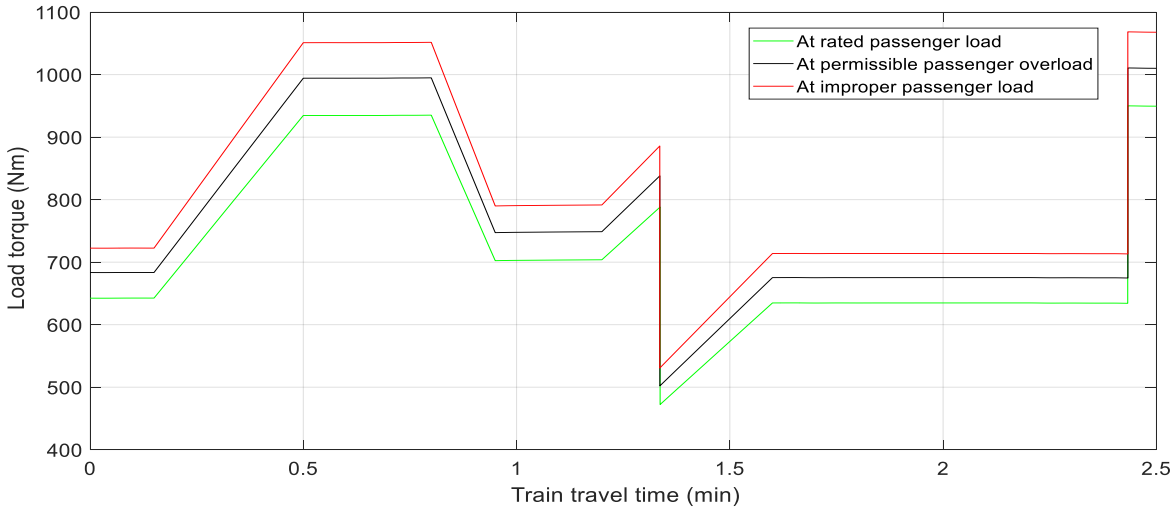

Figure 4-56 Load torque variation from Nefas silk 2 to Lancha

As seen in Figure 4.56 above, when the train is travelling from Nefas silk 2 to Lancha, the load torque imposed on the motor varies directly with gradient, then when the train speed is increasing beyond 40Km/hr, the acceleration is supposed to decrease from $1m/s^2$ to $0.5m/s^2$ then the load torque also be halved but still follows the change pattern of gradient. When the train is approaching to Lancha, it meets a gradient and its speed decreased back, and load torque also increased. When the train is passing through the curve, no significant variation is observed on the load torque. The load torque when the train has improper passenger load, is about 11.5% greater than in rated passenger load, and about 5.07% greater than in permissible passenger overload throughout the journey.

The following, figure 4.57 shows the sinusoidal current waveform drawn by traction motor when the train is travelling from Nefas silk 2 to Lancha. In the figure below three current waveforms (in red, black and green), are showing motor current flow in different passenger loading cases.

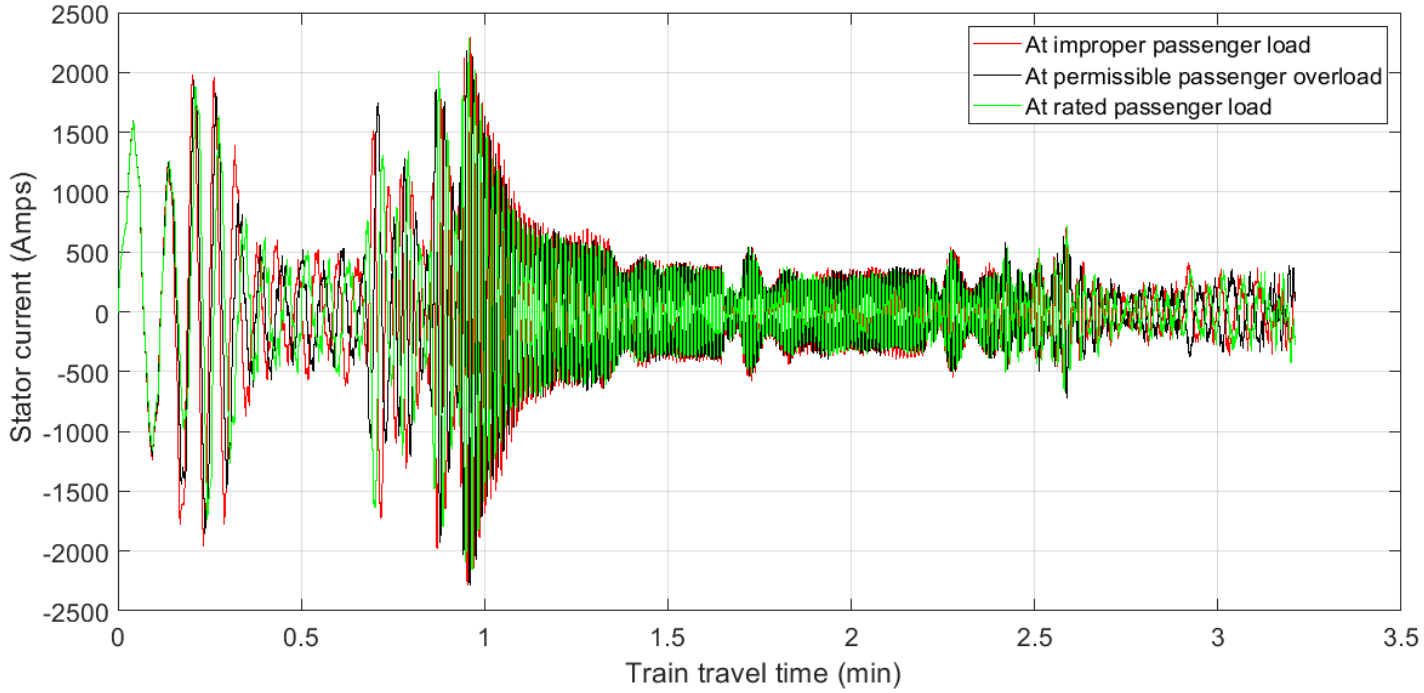

Figure 4-57 Stator current waveform of traction motor when train travelling from Nefas silk2 to Lancha

From the above current waveform it observed that when the train is accelerating having improper number of passengers, the peak value of the current in the traction motor exceeds by about 700A to 400A as compared to the rated passenger loading as well as the permissible passenger overload respectively.

Figure 4.58 below shows the RMS of stator current of traction motor when the train is travelling from Nefas silk 2 to Lancha.

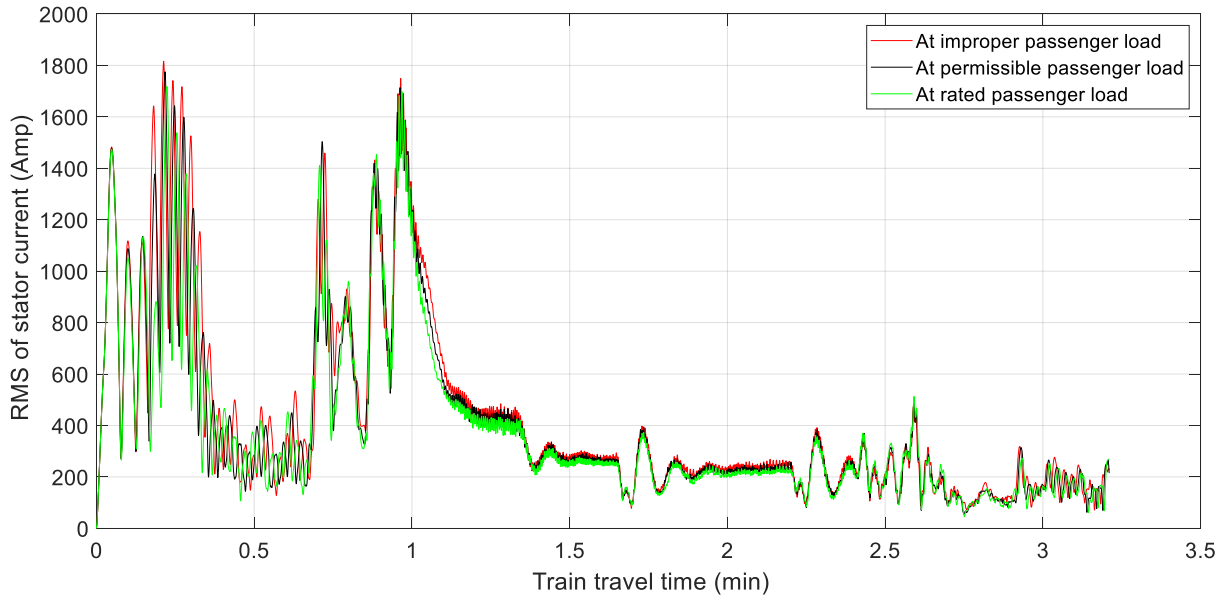

Figure 4-58 RMS of stator current when travelling from Nefas silk 2 to Lancha

As seen from Figure 4.58 above, when the train is in acceleration period, the RMS of motor current at improper passenger load is about 83% greater than the RMS of the motor current in rated passenger load, and about 16.5% greater than in permissible passenger overload conditions. At the free running, and decelerating region of the train, the RMS of the traction motor is generally higher with small magnitude as with increment of the load.

When the train is travelling from Nefas silk 2 to Lancha, the traction motor generates the following kind of electromagnetic torque;

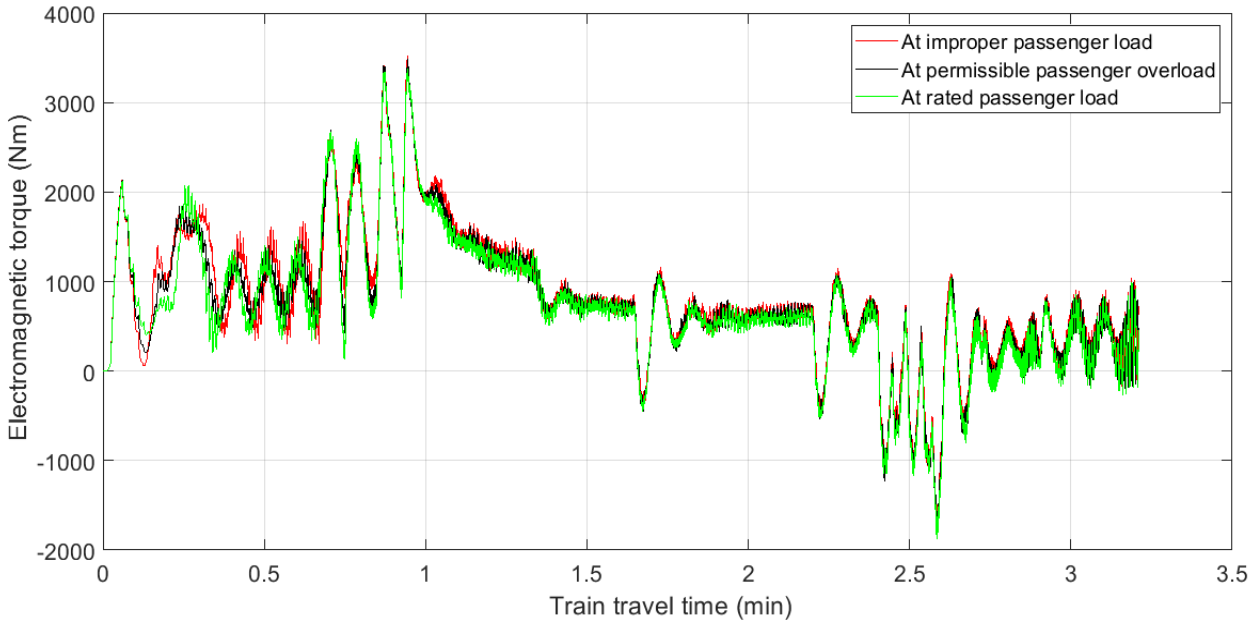

Figure 4-59 Electromagnetic torque of motor when travelling from Nefas silk 2 to Lancha

As can be seen from the graph above, when the train starts accelerating having improper passenger load, the electromagnetic torque produced by the traction motor is about 350% less than the torque produced in rated passenger load, and about 80% less than in the permissible passenger load. In other periods of train movement, the torque has almost same behavior for all passenger load conditions other than its small magnitude increment with load.

As illustrated in Figures 4.60 and 4.61, when the train starts accelerating having improper passenger load, speed of the traction motor and speed of the train is less than the speed in rated passenger load and in permissible passenger overload. In other periods of train movement, there observed no significant difference in speed for the various passenger loading cases.

Figures 4.60 and 4.61 show speed variation of motor and train when travelling from NS11 to NS12.

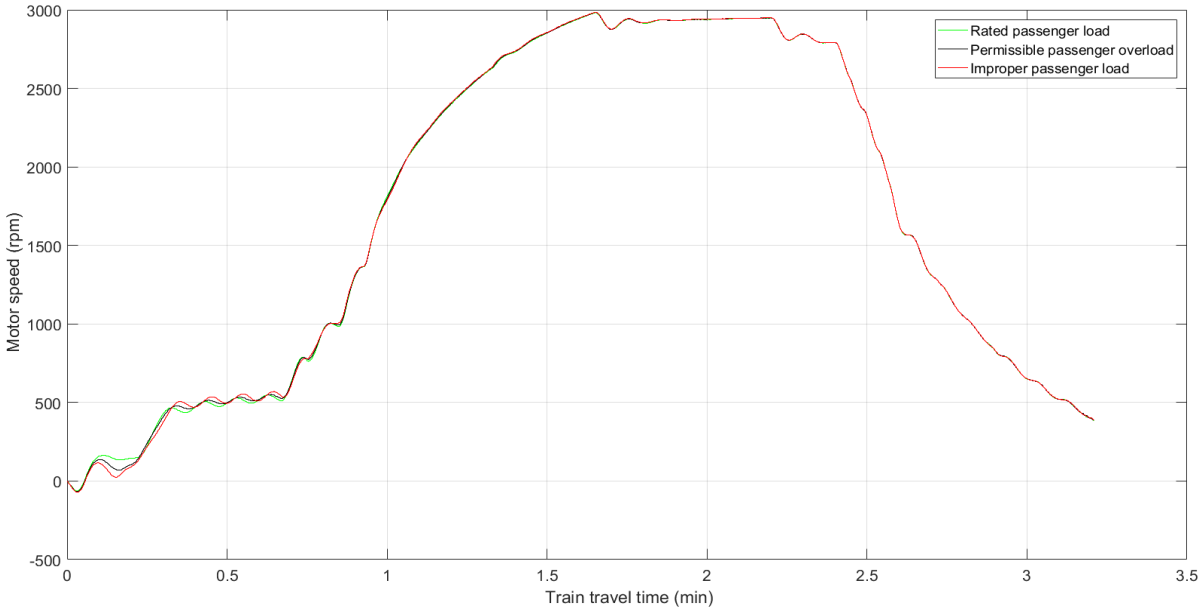

Figure 4-60 Speed of traction motor in rpm when travelling from NS11 to NS12

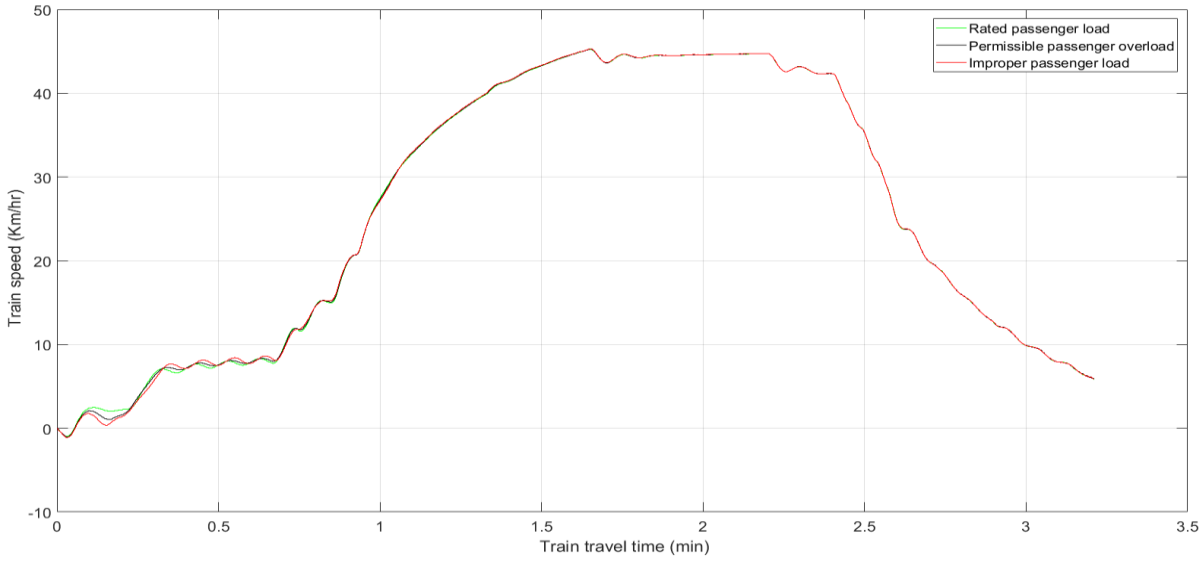

Figure 4-61 Speed of train in Km/hr when travelling from NS11 to NS12

The following figures 4.62 and 4.63 show the active power, and reactive power consumption of the traction motor when train is travelling from Nefas silk 2 to Lancha.

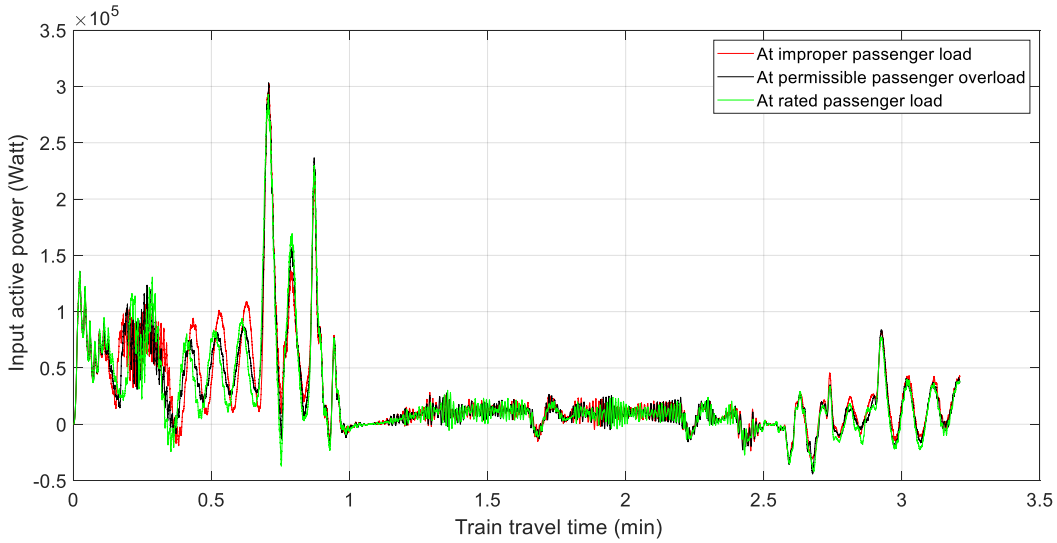

Figure 4-62 Active power consumption of motor when travelling from NS11 to NS12

As shown above when the train is accelerating the active power consumption for improper passenger load is about 57.2% greater than in rated passenger load, and about 22.2% greater than in permissible passenger load, but it is almost the same in free running and deceleration period of the train.

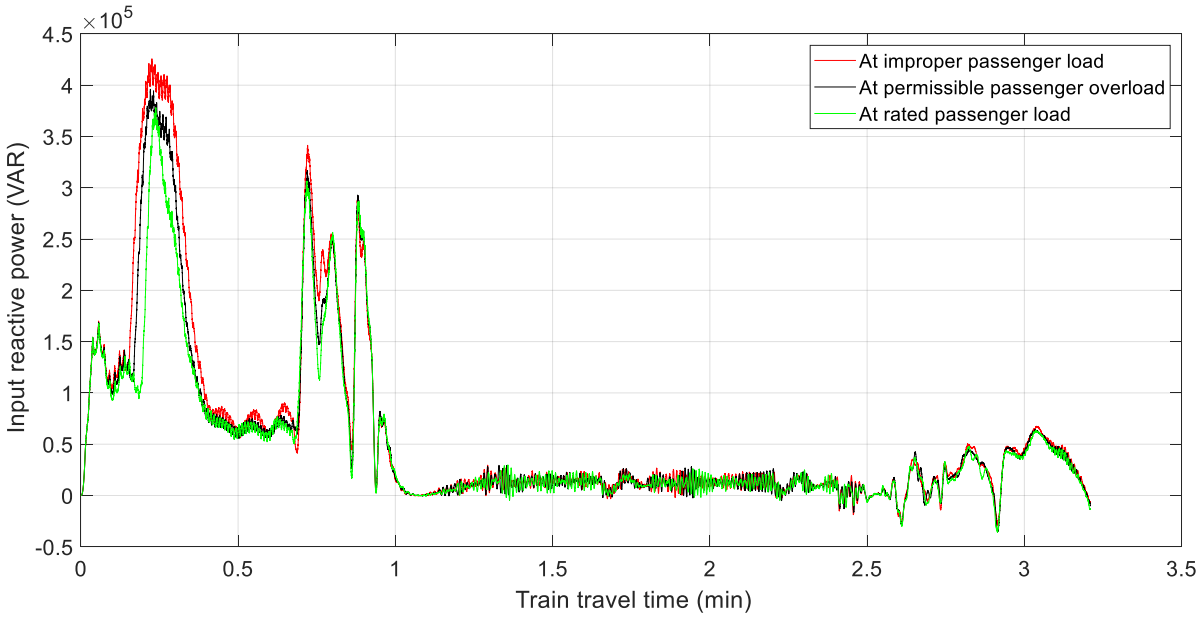

Figure 4-63 Reactive power in traction motor when travelling from NS11 to NS12

When the train is accelerating from Nefas silk 2 to Lancha with improper passenger load, the reactive power consumed by the traction motor is about 13.06% greater than in the rated passenger load, and about 7.34% greater than in the permissible passenger overload. In the free running and deceleration period of the train, the reactive power consumption due to passenger load has no significant difference with the passenger loading.

The figures below shows copper losses in the traction motor when train is travelling from Nefas silk 2 to Lancha.

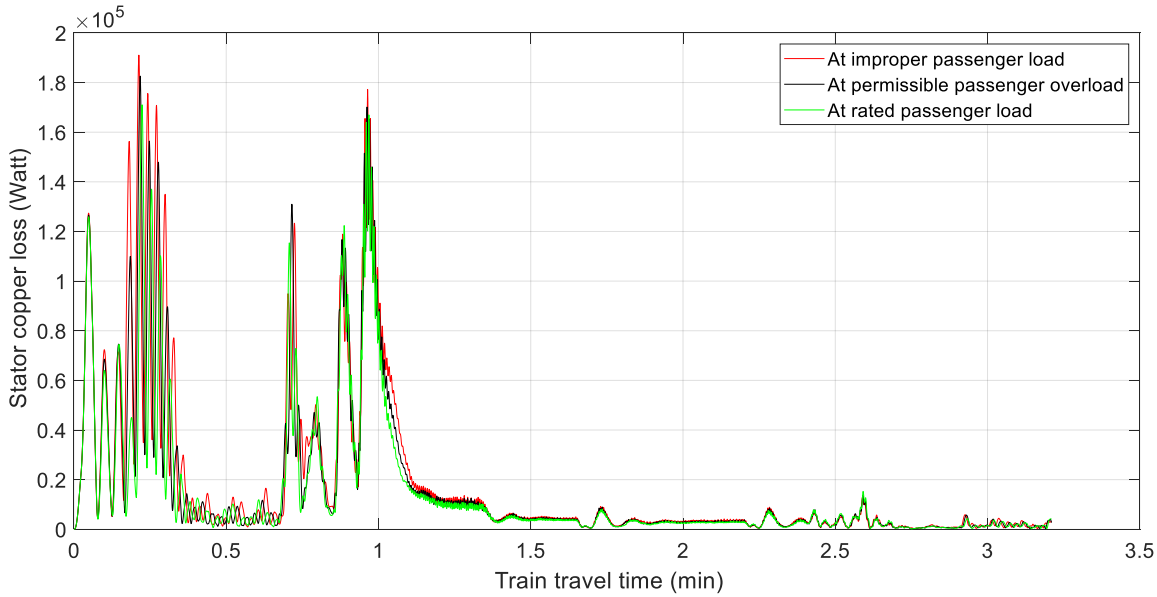

Figure 4-64 Stator copper loss in traction motor when travelling from NS11 to NS12

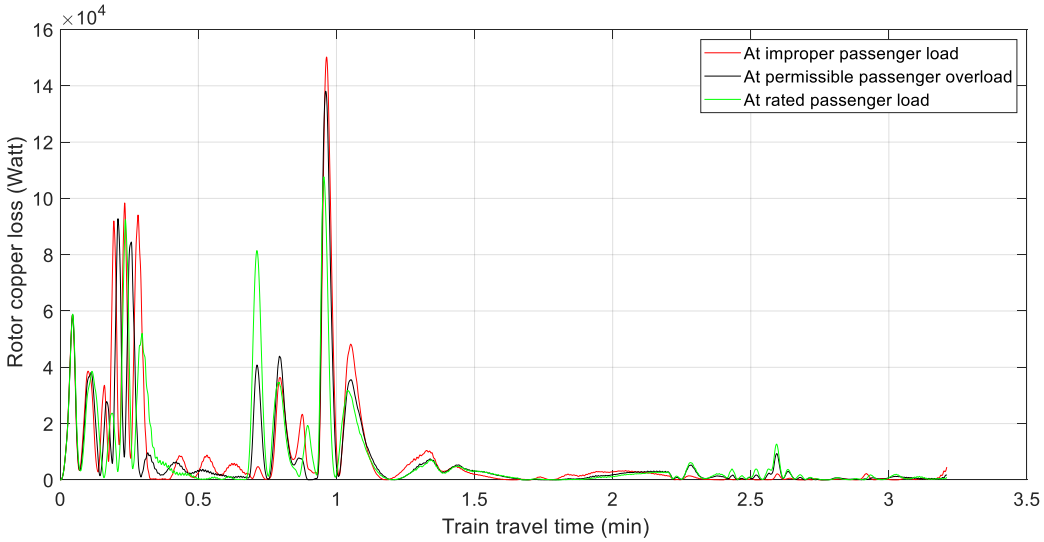

Figure 4-65 Rotor copper loss in traction motor when travelling from NS11 to NS12

Carrying improper passenger load, when the train accelerating from Nefas silk 2 to Lancha, the traction motor has stator copper loss of about 276.2% greater than in the rated passenger load, and about 43.6% greater than in the permissible passenger overload.

With improper passenger load, when the train is decelerating and free running, the rotor copper loss is about 133% greater than in the rated passenger load, and about 40% greater than in the permissible passenger overload conditions.

Figure 4.66 below shows the efficiency curve of the traction motor when the train is running from Nefas silk 2 to Lancha.

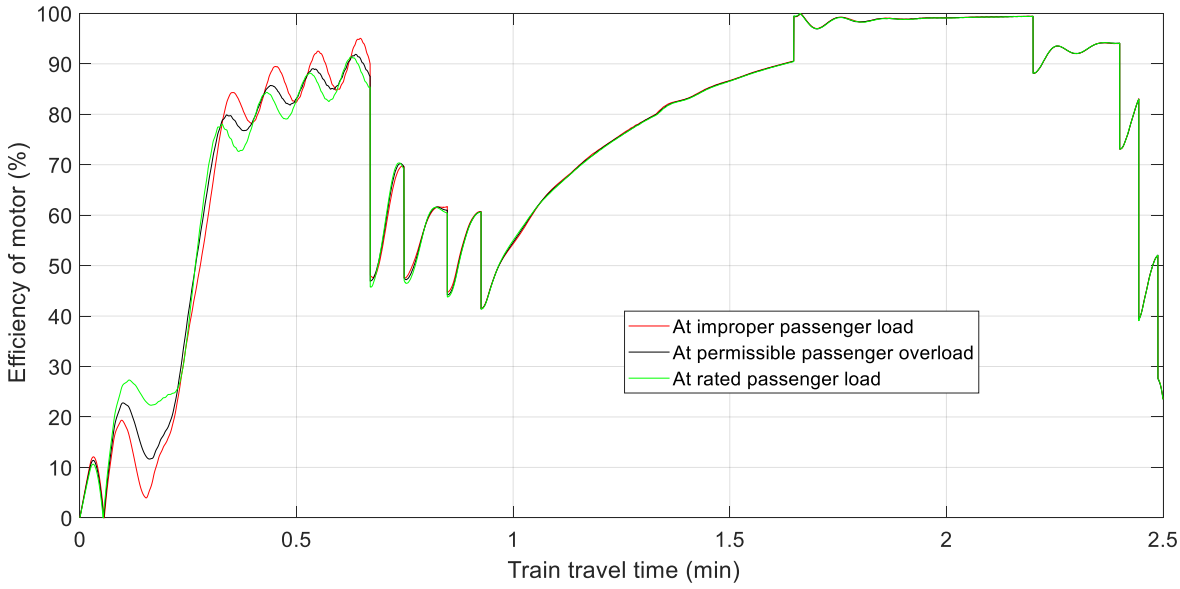

Figure 4-66 Efficiency curve of traction motor when travelling from Nefas silk 2 to Lancha

As seen from Figure 4.66 when the train is accelerating having improper passenger load, the efficiency of the traction motor is about 78.3% less than in the rated passenger load, and about 58.3% less than in the permissible passenger overload conditions. In other periods of train movement, the traction motor efficiency is almost the same in all passenger loading conditions.

Table 5 Comparison of traction motor condition in improper passenger load with the rated passenger load

Track geometry	Sampled inter-stations	Percentage deviation of motor parameters due to improper passenger load						
		I RMS	Speed	Active power	Reactive power	Stator copper loss	Rotor copper loss	Efficiency
Gradient	Abnet to Sebategna	83.33%	-80%	75%	17.14%	253%	50%	-81.80%
	Darmar to Abnet	50.50%	-77%	30%	13.30%	55.50%	500%	-78.30%
Curves	Meshwalekia to Stadium	123%	-58.30%	6.70%	12%	277.50%	191%	-82.60%
	Sebategna to Autobus tera	78.90%	-80%	6%	10.80%	297%	150%	-475%
Level	Nefas silk 2 to Lancha	83%	-350%	57.20%	13.06%	276.20%	133%	-78.30%
Period of train movement		Acceleration	Start Accelerate	Acceleration	Acceleration	Acceleration	Acceleration	Accelerati

Table 6 Comparison of traction motor condition in improper passenger load with the permissible passenger overload

Track geometry	Sampled inter-stations	Percentage deviation of motor parameters due to improper passenger load						
		I RMS	Speed	Active power	Reactive power	Stator copper loss	Rotor copper loss	Efficiency
Gradient	Abnet to Sebategna	17.86%	-60%	25%	10.80%	30%	50%	-66.70%
	Darmar to Abnet	25.20%	-60%	116%	9%	20%	50%	-58.33%
Curves	Meshwalekiato Stadium	58%	-33.30%	33.30%	6.33%	31.30%	34.60%	-63.60%
	Sebategna to Autobus tera	15%	-60%	33.33%	5.13%	44.50%	25%	-91.70%
Level	Nefas silk 2 to Lancha	16.50%	-80%	22.20%	7.34%	43.60%	40%	-58.30%
Period of train movement		Acceleration	Start Accelerate	Acceleration	Acceleration	Acceleration	Acceleration	Accelerati

4.6 Impacts on the motor caused by improper passenger load

From the results found, the impact of the improper passenger on the traction motor can be stated based on RMS current variation, reduction in speed, power consumption, reactive power consumption, copper losses, and variation of efficiency of the motor. The effect of improper passenger load on the traction motor has considerable impact especially in the acceleration period of the train.

As the load on the motor is increased, the current also increases and the winding temperature will get higher. Thermal stress can cause a fault in the stator. The following charts show the comparison of the various interstation area with their RMS current variation at improper passenger load on the traction motor.

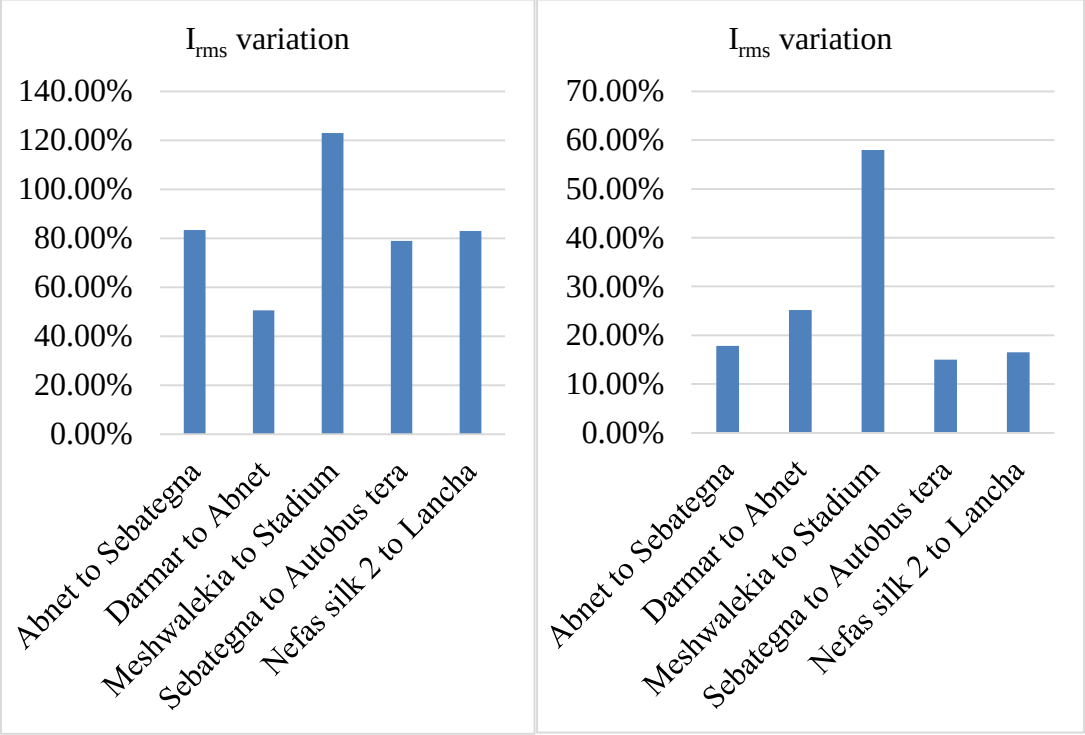

(a) *(b)*

Figure 4-67 Comparison of Irms in improper passenger load variation for various track areas (a) with rated passenger load, (b) with permissible passenger load

Although there exist overloading protection relays with motors, but they only act with time based on the designed properties of the motor.

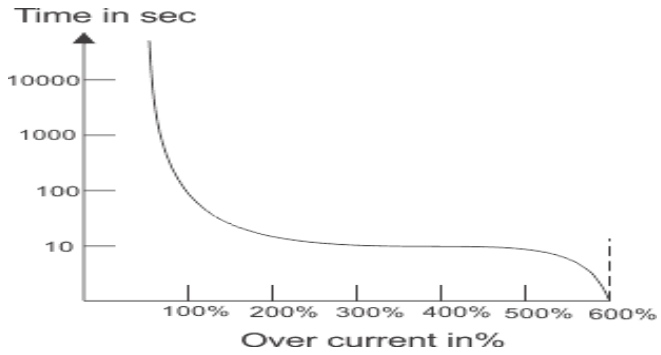

Figure 4-68 Thermal overload relay operating curve

But in traction applications due to surge current in starting time, and variation of loads, the overcurrent relay should tolerate that.

Improper passenger load in trains also makes the traction power consumption to be greater as compared to rated passenger load, and permissible passenger overload conditions. High reactive power can lead to a reduction in power factor then followed by penalty with the monthly energy price of the company. The following graphs show the percentage increase of active and reactive powers due to improper passenger load in comparison with rated passenger load, and permissible passenger overload.

(a)

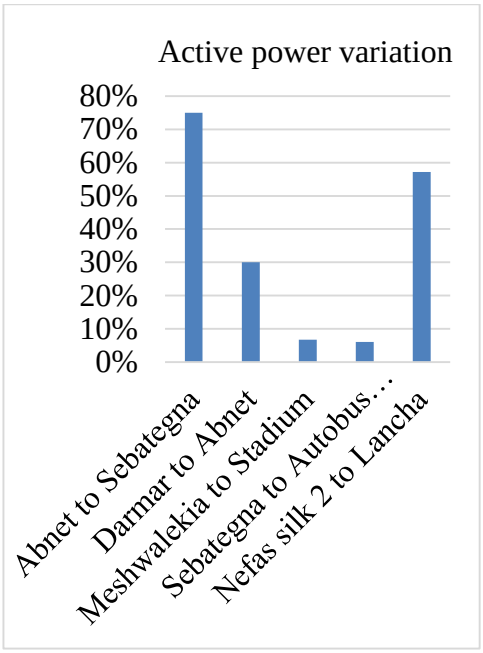

(b)

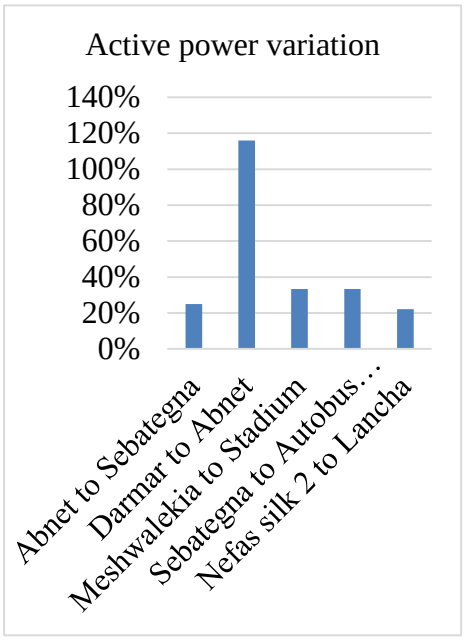

Figure 4-69 Comparison of active power in improper passenger load for various track areas (a) with rated passenger load, (b) with permissible passenger load

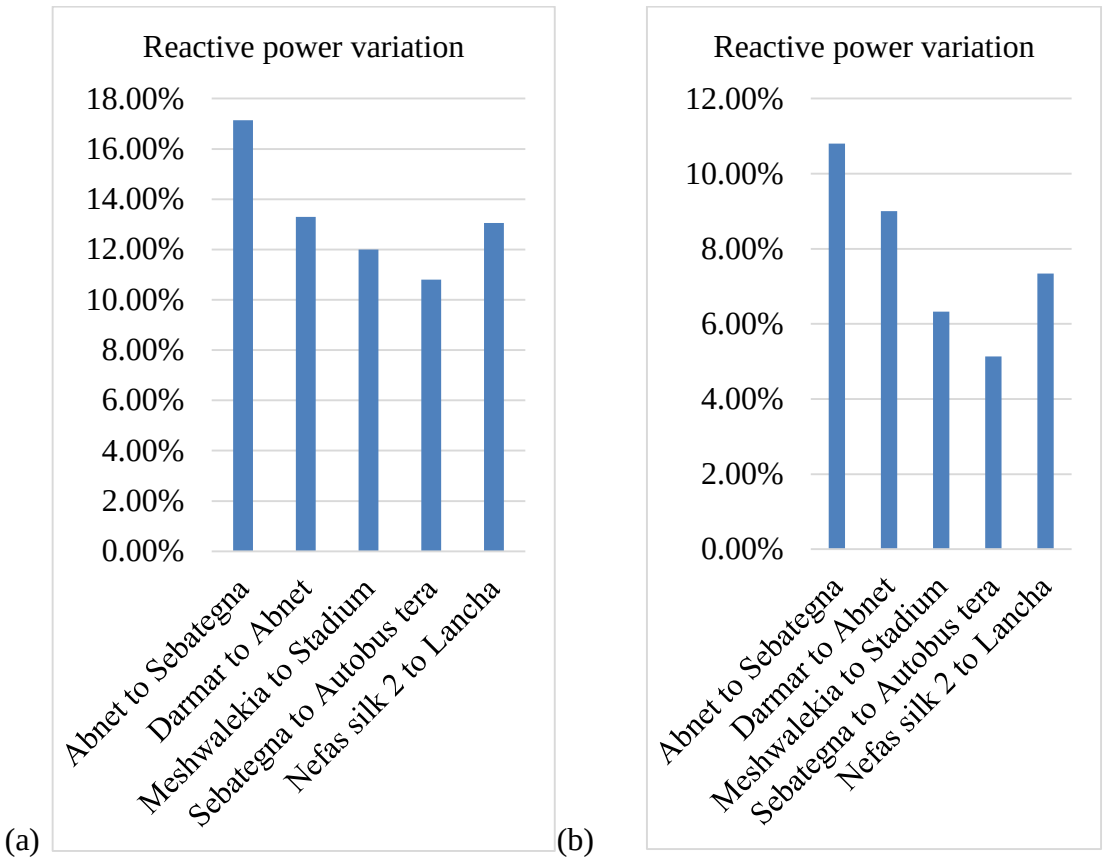

Figure 4-70 Comparison of reactive power in improper passenger load for various track areas (a) with rated passenger load, (b) with permissible passenger load

The copper loss in traction motors of the train is higher when there is improper passenger load, than in rated passenger load as well as permissible passenger overload. This can cause heating on the motor, and motor will not be able to deliver sufficient power to the load. The following figures are showing the percentage increment of copper loss due to improper passenger load while train is travelling across various interstation areas.

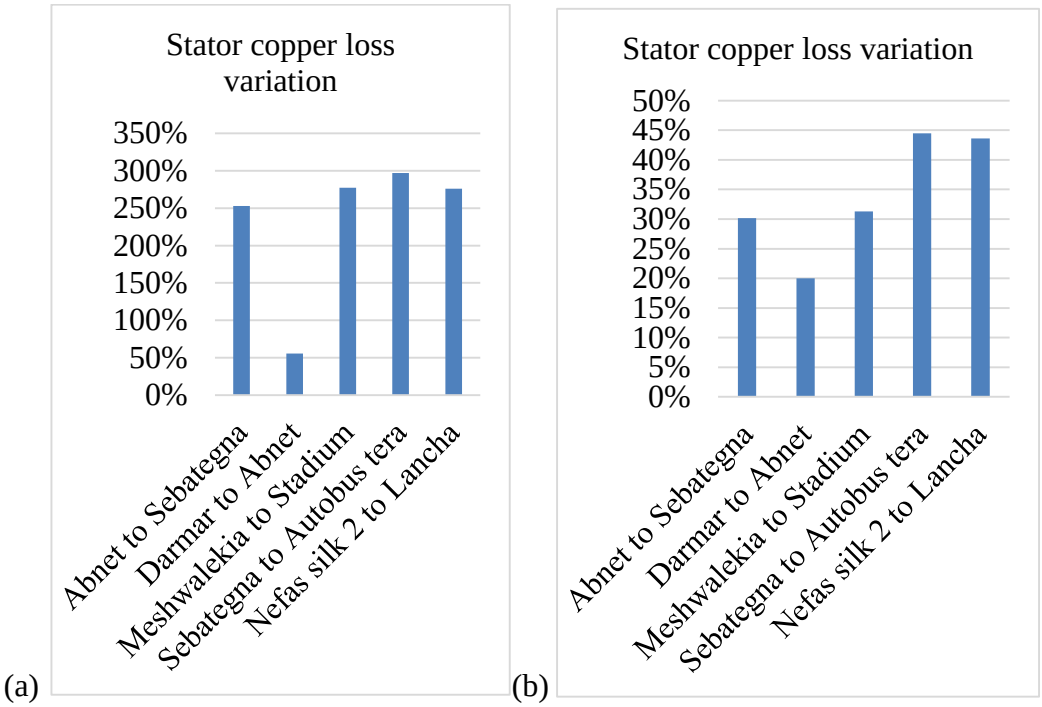

Figure 4-71 Comparison of stator copper loss in improper passenger load for various track areas (a) with rated passenger load, (b) with permissible passenger load

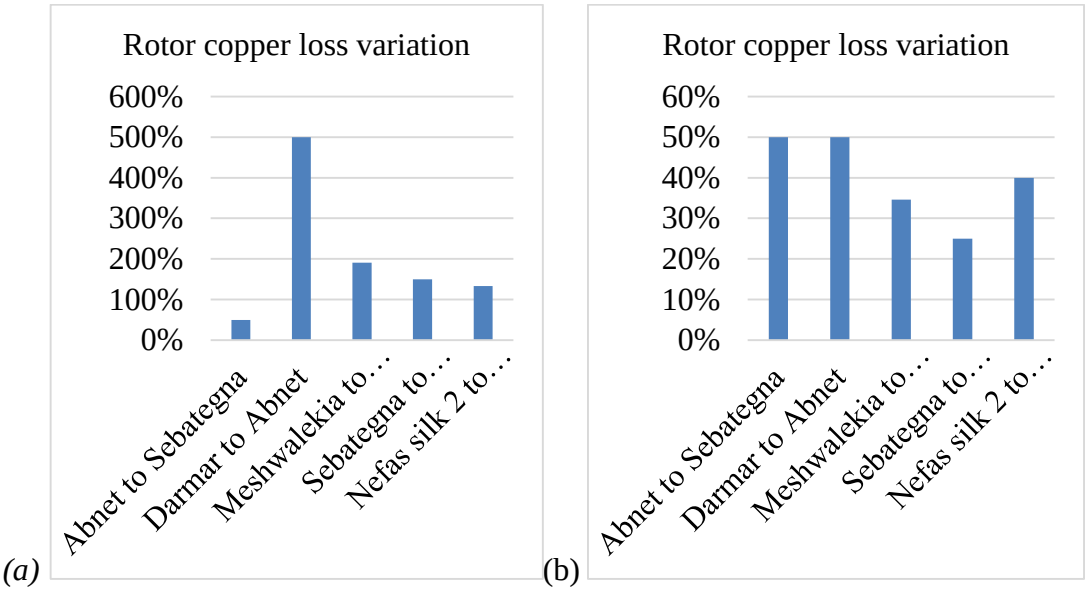

Figure 4-72 Comparison of rotor copper loss in improper passenger load for various track areas (a) with rated passenger load, (b) with permissible passenger load.

Finally, when the train has improper passenger load and accelerating, the traction motor has less efficiency. The reduction in efficiency of the traction motor while the train has improper passenger load is put in the following graph by comparison with the rated passenger load, and permissible passenger overloading conditions for various track areas.

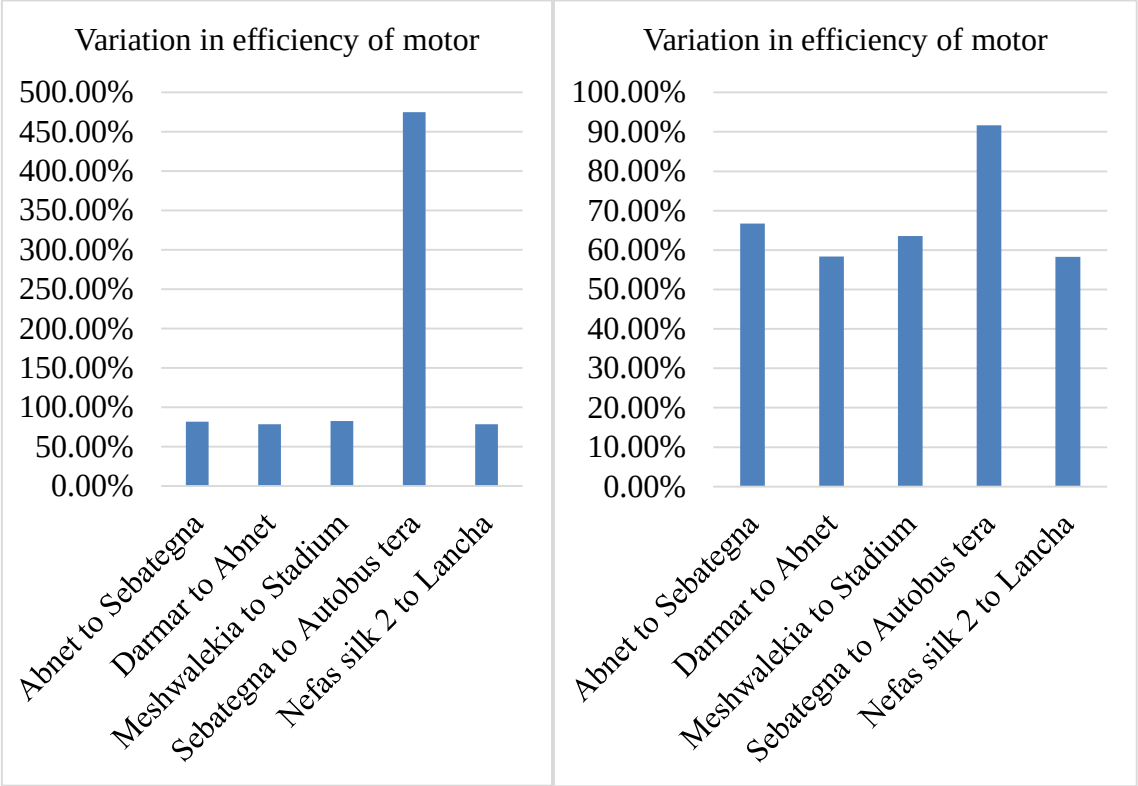

(a) **(b)**

Figure 4-73 Comparison of efficiency of traction motor in improper passenger load for various track areas (a) with rated passenger load, (b) with permissible passenger load

Note that one train has four traction motors driving it, and the improper passenger loading condition for one motor is done in this paper. Although the study is performed for one motor, all the four motors have same type and operation so this study is valid for all the four motors inside the train.

4.7 Possible remedies for reducing the problem

- Inspecting the condition of the traction motor.
- Increasing number of trains working on the line.
- Increasing capacity of the traction motors.
- Optimizing the speed profile of the trains traveling along North to South line.
- Managing number of passengers inside a train.
- Optimizing the train timetable so that the best possible minimum dwell time can be achieved.

Addis Ababa Light Rail Transit (AA-LRT) has to consider the passenger overloading condition of the train to ensure safe and effective operation of the trains.

CHAPTER 5 CONCLUSIONS AND RECOMMENDATION

5.1 Conclusion

In the south to the north line of Addis Ababa Light Rail Transit, the number of passengers occupying one train is found to be overcrowded than the specified overloaded number of passengers especially during peak hours of the day. Although designers recommended the overload capacity of one train as 317 passengers, practically a passenger load scenario of about 377 Persons inside one train is found in the high traffic times. The impact of these on the electric motor driving the train was studied in this paper. For five worst-case interstation track areas considering various track geometry in North to South line of A-ALRT, a fully dynamic simulation of the traction drive has done.

It is observed that improper passenger load has a significant impact on the traction motor in the acceleration period of the train. The following are those impacts found from simulation result, when improper passenger load has prevailed in the train;

- The traction motor draws about 86.75% of RMS current greater than in rated passenger load, and about 36.5% of RMS current greater than in permissible passenger overload, which can cause thermal stress in the windings in turn followed by stator faults.
- The speed of traction motor is reduced by about 204.15% when compared to rated passenger load case, and by about 56.65% when compared to permissible passenger overload, which can cause dynamic instability and incapability on the train.
- Active power consumption of about 40.5% greater than in rated passenger load, and about 69.1% greater than in permissible passenger overload. Which is costing much money for the company.
- The reactive power consumed by the traction motor while there is improper passenger load is about 13.97% greater than in rated passenger load, and about 9.9% greater than in permissible passenger load. High reactive power can be followed by a penalty by the power provider company on AA-LRT.
- Stator copper loss of about 176.25% greater than in rated passenger load, and about 32.25% greater than in permissible passenger overload.

- Rotor copper loss of about 275% greater than in rated passenger load, and about 37.5% greater than in permissible passenger overload is observed. Copper loss can cause thermal rise, as well as performance reduction on the motor.

Finally, due to improper passenger load, the efficiency of the traction motor is reduced by about 276.65% than in rated passenger load, and by about 75% than in permissible passenger overload for some minutes in the acceleration of the train.

Tracks with gradient have found to be challenging for the traction motor, while curves have no significant impact.

Impacts on the traction motor due to passenger overloading are getting severe as with increasing speed of the train. Even, it will be disastrous on traction motor, if the speed of the train keeps increasing after some critical speed limit.

This study has done for one of the traction motors out of the four motors used in one train. Since each of the four motors has same nature and same burden, the impacts studied are affecting all of the motors in exactly similar phenomena.

5.2 Recommendation for future work

As a recommendation for future work on this problem area, a real-time data of AA-LRT train's traction motor variables can be taken directly using measurement devices, or from traction motors operational history. From the magnitudes and waveform of traction motor variables, the real phenomena happening on it can be assessed to figure out the condition of the motor at various passenger loading situations. By doing so, this research can be extended based on a real-time data, to accurately evaluate the impacts of improper passenger load on the traction motors of AA-LRT trams.

REFERENCES

[1] S. Hillmansen and R. Ellis, "Electric railway traction systems and techniques for energy saving," in *IET 13th Professional Development Course on Electric Traction Systems*, 2014, pp. 3 (6 .)-3 (6 .).

[2] K. Wang, H. Hu, C. Chen, Z. He, and L. Chen, "A simulation platform to assess comprehensive power quality issues in electrified railways," *Int. J. Rail Transp.*, vol. 00, no. 00, pp. 1–22, 2018.

[3] M. Ehsani, Y. Gao, S. Longo, and K. Ebrahimi, *Modern electric, hybrid electric, and fuel cell vehicles*. CRC press, 2018.

[4] Q. Wu, M. Spiryagin, and C. Cole, "Longitudinal train dynamics: an overview," *Veh. Syst. Dyn.*, vol. 54, no. 12, pp. 1688–1714, 2016.

[5] China Railway Group Limited, "Technical Specifications of Vehicles," 2013.

[6] China Railway Group Limited, "Control Circuirt-ERC Train.pdf." .

[7] Ehetaferaw Berhanu, "Overload effect on the lifecycle of carbody under frame steel structure for AALRT trains," AddisAbaba University, 2017.

[8] D. M. Muturi, "A study of crowding on light rail transit; A case study of Addis Ababa Light Rail Transit," AddisAbaba University.

[9] D. Ronanki, S. A. Singh, and S. S. Williamson, "Comprehensive topological overview of rolling stock architectures and recent trends in electric railway traction systems," *IEEE Trans. Transp. Electrif.*, vol. 3, no. 3, pp. 724–738, 2017.

[10] H. Abu-Rub, S. Bayhan, S. Moinoddin, M. Malinowski, and J. Guzinski, "Medium-voltage drives: Challenges and existing technology," *IEEE Power Electron. Mag.*, vol. 3, no. 2, pp. 29–41, 2016.

[11] Y. Gritli, A. Bellini, C. Rossi, D. Casadei, F. Filippetti, and G. A. Capolino, "Condition monitoring of mechanical faults in induction machines from electrical signatures: Review of different techniques," in *2017 IEEE 11th International Symposium on Diagnostics for Electrical Machines, Power Electronics and Drives (SDEMPED)*, 2017, pp. 77–84.

[12] S. Nandi, H. A. Toliyat, and X. Li, "Condition monitoring and fault diagnosis of electrical motors—A review," *IEEE Trans. energy Convers.*, vol. 20, no. 4, pp. 719–729, 2005.

[13] S. Approaches, Z. Gao, S. Member, C. Cecati, and S. X. Ding, "A Survey of Fault Diagnosis and Fault-Tolerant Techniques — Part I : Fault Diagnosis With," *IEEE Trans. Transp. Electrif.*, vol. 62, no. 6, pp. 3757–3767, 2015.

[14] E. Sikanen, J. Nerg, J. E. Heikkinen, M. G. Tehrani, and J. Sopanen, "Fatigue life calculation procedure for the rotor of an embedded magnet traction motor taking

into account thermomechanical loads," *Mech. Syst. Signal Process.*, vol. 111, pp. 36–46, 2018.

[15] C. Uyulan, M. Gokasan, and S. Bogosyan, "Modeling , simulation and slip control of a railway vehicle integrated with traction power supply," *Cogent Eng.*, vol. 17, no. 1, pp. 1–17, 2017.

[16] H. Douglas, C. Roberts, S. Hillmansen, and F. Schmid, "An assessment of available measures to reduce traction energy use in railway networks," *Energy Convers. Manag.*, vol. 106, pp. 1149–1165, 2015.

[17] S. K. Sharma and A. Kumar, "Impact of electric locomotive traction of the passenger vehicle Ride quality in longitudinal train dynamics in the context of Indian railways," *Mech. Ind.*, vol. 18, no. 2, p. 222, 2017.

[18] D. Y. Ohm, "Dynamic model of induction motors for vector control," *Drivetech, Inc., Blacksburg, Virginia*, pp. 1–10, 2001.

[19] C. Cole, M. Spiryagin, Q. Wu, and Y. Q. Sun, "Modelling , simulation and applications of longitudinal train dynamics," *Veh. Syst. Dyn.*, vol. 0, no. 0, pp. 1–74, 2017.

[20] "NoTitle."[Online].Available: https://www.google.com/search?q=rolling+resistance+formula+for+train&oq=rolling+resistance+formula+for+train&aqs=chrome..69i57j0.4875j0j4&sourceid=chrome&ie=UTF-8.

[21] "Electric traction," in *Principles of power system*, pp. 1700–1750.

[22] "Metro Train Simulation." [Online]. Available: http://www.metrotrainsimulation.com/definition.html#ques4. [Accessed: 26-Aug-2019].

[23] C. W. Ayers, *Traction Drive and Gearing Design Comparisons for Multiple Manufacturers and Models Prepared by*, no. October. 2013.

[24] Y. K. Abadi, "Development of Adaptive Control for Railway Vehicles Braking System: Case study for AA-LRT," Addis Ababa University, 2017.

[25] CRRC, "Datasheet of 70% low floor vehicle.pdf."

[26] A. Hughes and B. Drury, *Electric motors and drives : fundamentals, types and applications*. Newnes, 2013.

[27] P. Wach, *Dynamics and Control of Electrical Drives*. Springer Science & Business Media, 2011.

[28] R. Araújo, *Induction motors: Modelling and Control*. BoD–Books on Demand, 2012.

[29] D. Y. Ohm, "Dynamic Model of Induction Motors for Vector Control," *Drivetech,*

pp. 1–10, 2001.

[30] G. Abad, *Power Electronics and Electric Drives for Traction Applications*. wiley, 2016.

[31] P. Krause, O. Wasynczuk, S. Sudhoff, and S. Pekarek, *Analysis of electric machinery and drive systems*. New York: IEEE press, 2002.

[32] J. Peña, E. D.-2016 I. ANDESCON, and undefined 2016, "Implementation of V/f scalar control for speed regulation of a three-phase induction motor," *ieeexplore.ieee.org*.

[33] P. Krause, C. T.-I. transactions on power, and undefined 1965, "Simulation of symmetrical induction machinery," *ieeexplore.ieee.org*.

[34] O. Wasynczuk, S. S.-I. T. on Power, and undefined 1996, "Automated state model generation algorithm for power circuits and systems," *ieeexplore.ieee.org*.

[35] A. Trzynadlowski, *Control of induction motors*. 2000.

[36] N. Mohan and T. Undeland, "Power electronics: converters, applications, and design," 2007.

[37] N. Hashemnia, B. A.-2008 18th I. C. on, and undefined 2008, "Comparative study of using different electric motors in the electric vehicles," *ieeexplore.ieee.org*.

[38] M. Ehsani, Y. Gao, S. Longo, and K. Ebrahimi, *Modern electric, hybrid electric, and fuel cell vehicles*. 2018.

[39] A. Visioli, *Practical PID control*. 2006.

[40] K. J. Åström and T. Hägglund, "The future of PID control," *Control Eng. Pract.*, vol. 9, no. 11, pp. 1163–1175, Nov. 2001.

[41] M. T. GUNESER, E. ERDIL, M. CERNAT, and T. OZTURK, "Improving the Energy Management of a Solar Electric Vehicle," *Adv. Electr. Comput. Eng.*, vol. 15, no. 4, pp. 53–62, 2015.

[42] S. A. Bhatti, S. A. Malik, and A. Daraz, "Comparison of P-I and I-P controller by using Ziegler-Nichols tuning method for speed control of DC motor," in *2016 International Conference on Intelligent Systems Engineering (ICISE)*, 2016, pp. 330–334.

[43] A. O'Dwyer, *Handbook of PI and PID Controller Tuning Rules*. IMPERIAL COLLEGE PRESS, 2006.

[44] A. Steimel, *Electric traction-motive power and energy supply: basics and practical experience*. 2008.

[45] M. H. Rashid, *Power Electronics Devices, Circuits & Applications*. 2014.

[46] China Railway Group Limited, "Ns up line track speed limit form NS."

[47] M. Yoon, C. Jeon, S. K.-I. T. on Energy, and undefined 2002, "Efficiency increase of an induction motor by improving cooling performance," *ieeexplore.ieee.org*.

[48] A. Siddique, G. Yadava, B. S.-I. transactions on energy, and undefined 2005, "A review of stator fault monitoring techniques of induction motors," *ieeexplore.ieee.org*.

APPENDIX A

Date(in GC)	No of trains/trips (Peak hr)	No of Coupled trains(peak hr)	No of trains/trips (Flat hr)	No of Coupled trains(flat hr)	No. Passenger (Total Ticket)	Avg. no of passengers per single train
12/1/2018	93	2	30	2	42,985	338
12/2/2018	93	3	30	2	40,743	318
12/3/2018	93	3	30	2	50,461	394
12/4/2018	92	3	30	2	46,609	367
12/5/2018	93	3	30	2	51,359	401
12/6/2018	93	3	30	2	50,620	395
12/7/2018	93	3	30	2	50,325	393
12/8/2018	93	3	30	1	49,686	391
12/9/2018	93	3	30	1	46,401	365
12/10/2018	92	3	30	1	52,884	420
12/11/2018	93	3	30	1	51,819	408
12/12/2018	93	3	30	1	51,725	407
12/13/2018	93	3	30	1	50,940	401
12/14/2018	93	3	30	1	52,641	414
12/15/2018	92	3	30	3	45,114	352
12/16/2018	98	3	32	3	40,641	299
12/17/2018	98	3	32	3	48,042	353
12/18/2018	98	3	32	3	48,701	358
12/19/2018	34	3	32	3	22,166	308
12/20/2018	98	3	32	3	48,666	358
12/21/2018	98	3	32	3	48,631	358
12/22/2018	96	3	32	2	47,974	361
12/23/2018	91	3	32	2	45,350	354
12/24/2018	86	3	32	3	49,190	397
12/25/2018	98	3	32	3	48,090	354
12/26/2018	98	3	32	3	50,843	374
12/27/2018	98	3	32	3	47,150	347
12/28/2018	98	3	32	3	43,328	319
12/29/2018	98	3	32	3	46,943	345
12/30/2018	98	3	32	3	43,661	321
12/31/2018	98	3	32	2	51,803	384
1/1/2019	93	3	30	3	54,236	420
1/2/2019	37	3	32	3	49,946	666
1/3/2019	98	4	32	2	46,620	343
1/4/2019	86	4	32	4	52,786	419
1/5/2019	98	4	28	4	48,571	362
1/6/2019	98	4	32	4	31,810	231

1/7/2019	98	4	32	3	29,426	215
1/8/2019	98	3	32	3	46,073	339
1/9/2019	98	4	32	4	51,539	373
1/10/2019	98	4	32	4	50,444	366
1/11/2019	94	4	32	4	48,774	364
1/12/2019	98	4	32	3	44,589	325
1/13/2019	98	4	32	4	46,261	335
1/14/2019	98	4	32	4	53,174	385
1/15/2019	98	4	32	4	51,996	377
1/16/2019	98	4	32	3	54,775	400
1/17/2019	92	4	32	4	50,658	384
1/18/2019	92	4	32	4	41,682	316
1/19/2019	98	4	32	4	37,402	271
1/20/2019	98	4	32	3	40,350	295
1/21/2019	98	4	32	4	48,660	353
1/22/2019	96	4	32	4	49,685	365
1/23/2019	98	4	32	4	49,483	359
1/24/2019	69	4	32	3	46,491	430
1/25/2019	69	4	32	4	48,931	449
1/26/2019	69	4	32	4	46,662	428
1/27/2019	89	4	32	4	35,171	273
1/28/2019	98	3	32	2	52,017	385
1/29/2019	90	3	32	3	47,241	369
1/30/2019	62	3	32	3	46,336	463
1/31/2019	98	3	32	3	49,993	368
						22,783
						367.462336

APPENDIX B

Intervals with a grade of 30‰ or above on the main track of the north-south line

Interval	Track distinction	Grade (‰)	Length of grade section (m)
NS27～NS26	Right	-50	225
	Left	-50.427	223
NS26～NS25	Right	47	295
	Left	47	295
NS25～NS24	Right	55	150
	Left	55	150
NS24～NS23	Right	-54	370
	Left	-54	370
NS23～NS22	Right	-46	420.171
	Left	-45.88	421.269
NS23～NS22	Right	55	326
	Left	55	326
NS22～NS21	Right	-46	615
	Left	-45.993	615.105
NS21～EW20	Right	-48.866	107
	Left	-49.136	107.225
NS20～NS19	Right	-55	280
	Left	-55	280
NS20～NS19	Right	46	165
	Left	46	165
	Right	-46	155

Interval	Track distinction	Grade (‰)	Length of grade section (m)
EW17～EW16	Left	-46	155
EW16～NS15	Right	-47	160
	Left	-46.886	160.388
NS15～NS14	Right	-43	72
	Left	-43	72
NS14～NS13	Right	-55	142
	Left	-55	142
NS12～NS11	Right	50	185
	Left	50	185
NS12～NS11	Right	45	185
	Left	45	185
NS12～NS11	Right	42	155
	Left	42	155
NS12～NS11	Right	-40	130
	Left	-40	130
NS12～NS11	Right	-50	110
	Left	-50	110
NS10～NS9	Right	-47	103
	Left	-47	103
NS10～NS9	Right	-44	258
	Left	-44	258
NS9～NS8	Right	-50	130
	Left	-50	130
	Right	-40	115

Interval	Track distinction	Grade (‰)	Length of grade section (m)
NS8～NS7	Left	-40.798	112.751

Mileages with curve radius less than 400m in the north-south line

Interval	Track	Distance between stations	Curve radius (m)	Length(m)	Speed restriction of curve
NS27～NS26	Right	741	304.5	95.55	45
	Left	747.538	304	94.359	
NS27～NS26	Right	741	65	137.366	20
	Left	747.538	70	124.163	
NS27～NS26	Right	741	305	195.606	65
	Left	747.538	300	218.383	
NS25～NS24	Right	608	304	182.652	65
	Left	605.983	300	206.038	

NS24～NS23	Right	612	54	97.403	20
	Left	604.346	50	111.299	
NS22～NS21	Right	739	104	162.891	35
	Left	739.106	100	173.165	
NS22～NS21	Right	739	100	175.318	35
	Left	739.106	104	165.131	
NS22～NS21	Right	591	55	98.183	20
	Left	583.225	50	94.536	
NS21～NS20	Left	583.225	300	20.765	35
EW19～EW18	Right	688	204	131.43	45

	Left	685.124	200	149.637	
EW18～EW17	Right	571.965	200	150.783	45
	Left	571.965	204	127.499	
EW17～EW16	Right	435	250	140.66	55
	Left	436.224	254	127.03	
EW16～EW15	Right	908	300	19.821	35
EW16～EW15	Right	908	50	93.48	20
	Left	915.388	55	97.194	
NS14～NS13	Right	610	290	201.946	
	Left	609.179	286	219.988	65

NS13～NS12	Right	555	290	238.746	65
	Left	554.963	294	220.936	
NS13～NS12	Right	555	240	177.116	60
	Left	554.963	236	195.164	
NS12～NS11	Right	1971.64	200	143.223	55
	Left	1971.16	204	124.888	45
NS12～NS11	Right	1971.64	354	86.434	60
	Left	1971.16	350	85.796	
NS12～NS11	Right	1971.64	300	105.27	55
	Left	1971.16	304	106.207	

NS8～NS7	Right	840	234	172.524	55
	Left	837.751	230	190.429	
NS7～NS6	Right	951	146	232.569	45
	Left	949.808	150	222.434	
NS7～NS6	Right	951	150	247.468	40
	Left	949.808	146	256.936	

Distance between stations of each inter - station of the north-south line.

Station name	Distance between stations (meter)	Station type
Origin		
NS27	196	Underground station

	743	
NS26		Ground station
	945	
NS25		Ground station
	604.88	
NS24		Elevated station
	667	
NS23		Ground station
	812.71	
NS22		Elevated station
	739	
NS21		Elevated station
	591	
EW20		Elevated common rail station

EW19	735	Elevated common rail station
EW18	688	Elevated common rail station
EW17	560	Elevated common rail station
EW16	445	Elevated common rail station
NS15	908	Ground station
NS14	481.12	Ground station
	610	

NS13		Ground station
	555	
NS12		Ground station
	1971.66	
NS11		Ground station
	861	
NS10		Ground station
	995	
NS9		Ground station
	535	
NS8		Ground station
	845	
NS7		Ground station

	950	
NS6		Ground station
	269	
Terminal		

APPENDIX C

Speed restriction used for simulation of traction drive when travelling across various interstation in North to South line of AA-LRT, according to the company's working document.

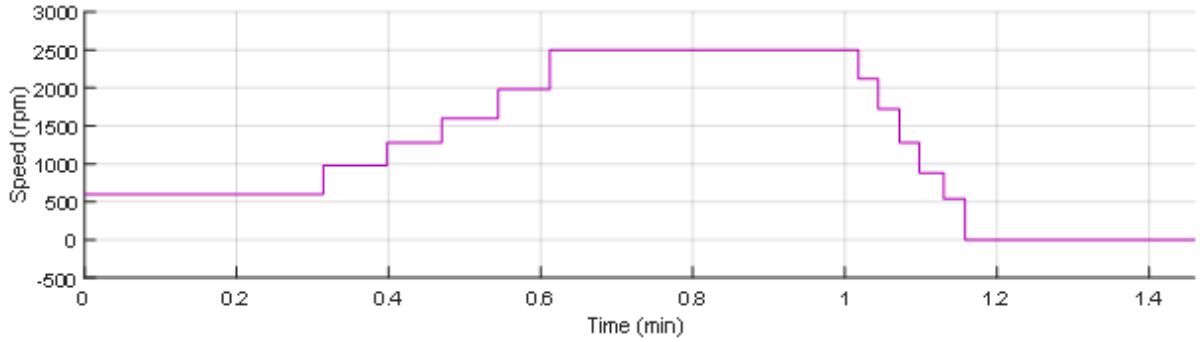

NS22 (Abnet) to NS23 (Sebategna)

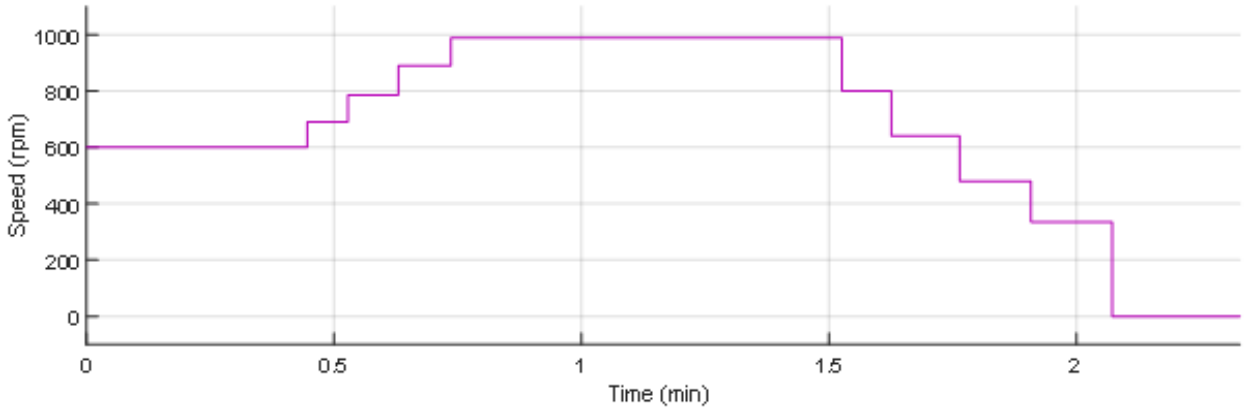

NS23(Sebategna) to NS24(Autobus Tera)

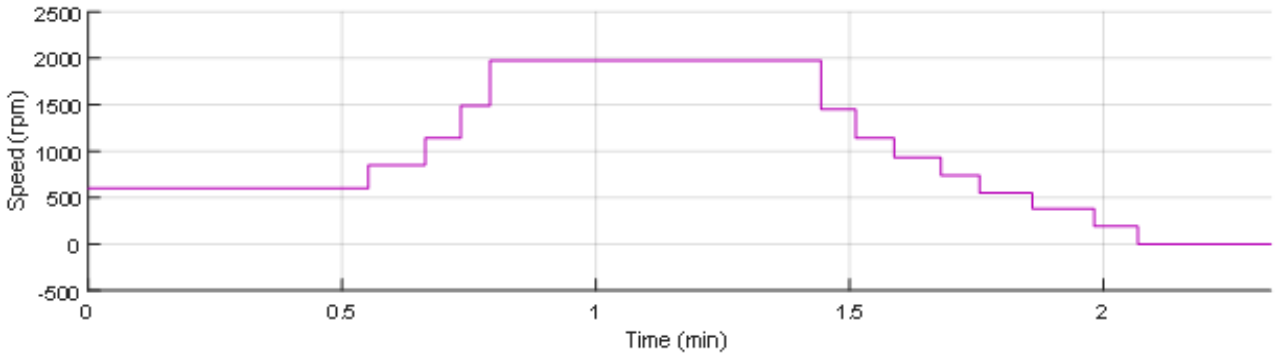

NS21 (Darmar) to NS22 (Abnet)

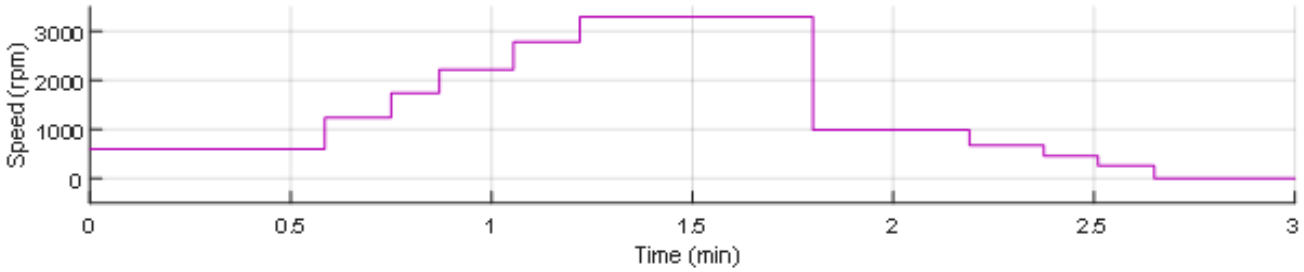

NS15 (Meshwalekia) to EW16 (Stadium)

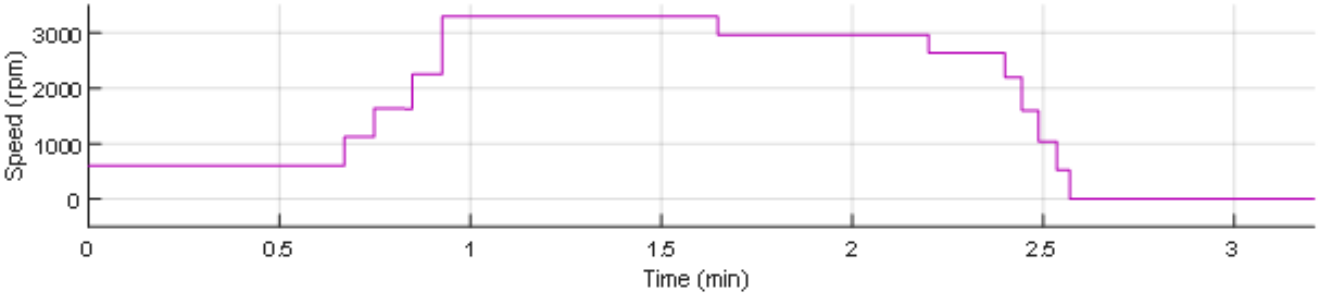

NS11 (Nefas silk2) to NS12 (Lancha)